

NORTHWESTERN UNIVERSITY

Foxp3-specific Deubiquitinase Modules Enhance T_{reg} Fitness

A DISSERTATION

SUBMITTED TO THE GRADUATE SCHOOL
IN PARTIAL FULFILLMENT OF THE REQUIREMENTS

for the degree
DOCTOR OF PHILOSOPHY

Field of Immunology

By
Elena Montauti

EVANSTON, ILLINOIS

December 2021

Abstract

Regulatory T (Treg) cells are required to control immune responses and maintain homeostasis, but are a significant barrier to antitumor immunity. Conversely, T_{reg} instability, characterized by loss of the master transcription factor Foxp3 and acquisition of proinflammatory properties, can promote autoimmunity and/or facilitate more effective tumor immunity. A comprehensive understanding of the pathways that regulate Foxp3 could lead to more effective T_{reg} therapies for autoimmune disease and cancer. The availability of new functional genetic tools has enabled the possibility of systematic dissection of the gene regulatory programs that modulate Foxp3 expression. In collaboration with the Marson Lab at UCSF, my thesis identifies several modulators of Foxp3 expression, using a CRISPR-based pooled screening platform for phenotypes in primary mouse T_{reg} cells including ubiquitin-specific peptidase 22 (Usp22). Usp22, a member of the deubiquitination module of the SAGA chromatin-modifying complex, was revealed to be a positive regulator that stabilized Foxp3 expression. T_{reg}-specific ablation of Usp22 in mice reduced Foxp3 protein levels and caused defects in their suppressive function that led to spontaneous autoimmunity but protected against tumor growth in multiple cancer models. These results reveal previously unknown modulator of Foxp3 and demonstrate a screening method that can be broadly applied to discover new targets for Treg immunotherapies for cancer and autoimmune disease.

The highly immunosuppressive tumor microenvironment (TME) favors T regulatory (T_{reg}) cell stability and function, while diminishing the anti-tumor activity of effector T cells. Here, we characterized previously unknown TME-specific cellular and molecular mechanisms that promote intratumoral T_{reg} adaptation through Foxp3. We uncovered the critical role of FOXP3-targeting deubiquitinases, ubiquitin specific peptidase 22 (Usp22) and 21 (Usp21) in T_{reg} stabilization under TME-specific environmental stressors including TGF-beta, hypoxia, and nutrient deprivation.

Specifically, Usp22 and Usp21 maintain optimal Foxp3 expression in response to alterations in HIF, AMPK and mTOR activity. The simultaneous loss of both USPs synergizes to alter T_{reg} metabolic signatures and impair suppressive mechanisms, resulting in enhanced anti-tumor activity. Finally, we developed the first Usp22-specific small molecule inhibitor, which significantly reduced intratumoral Treg cells and consequently enhanced anti-tumor immunity. My thesis unveils new mechanisms underlying the functional uniqueness of intratumoral T_{reg} cells, and identify Usp22 as an antitumor therapeutic target that inhibits T_{reg} adaptability in the TME.

Acknowledgements

In totality, this dissertation is a love letter to so many incredible individuals for all the encouragement, support, and mentorship I have received throughout my scientific journey.

To the inspiring and intelligent individuals who I have had the pleasure to work with and learn from, my journey continues thanks to you:

Although my love for biology began as a child, watching in awe at David Attenborough's nature documentaries about the ocean, it solidified as a career path thanks to an infectiously energetic woman who taught me how to balance a centrifuge, Mrs. Lata Mistry, and to a most inspiring educator, Erik Thiel, whose life I celebrate through these pages.

To my first real biology experience: I am incredibly grateful for my opportunity to work in Dr. Joseph Mougous' Lab under the careful mentorship of Dr. Michele LeRoux at University of Washington. As my first opportunity to master the use of the pipet, this lab taught me the basics of being a scientist: resilience, planning, and how to make a stellar PowerPoint.

To my Northwestern family: I am truly honored to have spent my doctorate surrounded by so many talented scientists. I give ultimate thanks to my Northwestern mentor and PI Dr. Deyu Fang for the opportunity to work on a dream project. Thank you for believing in me, for encouraging me, and for expecting so much of me. To my committee for their strong scientific advice. To Dr. Samuel Weinberg, my scientific inspiration, thank you for your knowledge, your encouragement, and for responding to my never-ending emails and text messages. To the Fang Gang: Nikita, Shana, Shuvam, Radhika and Amy, you all made lab life something to look forward to. Thanks for the (loud) conversation, great laughs, and relevant memes. And to my fellow PhD candidates, thank you for making Chicago home.

To the pillars of my life, for giving me all I could ever hope for:

To my family: I owe you everything. My parents, who have been with me through it all, thank you for your unwavering love and support. To my brilliant mother, for being my inspiration and my guide, and my father, who's passions instilled in me wonder and curiosity, thank you for always reminding me to look up at the stars.

To my adopted family, the Amemiya's: To Jackie and Kenji, for helping me grow a backbone. To Jamie, who has an unparalleled dedication and love for her work, for your sweet authenticity and great conversation. To Haley, a constant inspiration to young women scientists everywhere, for being a ray of sunshine on any cloudy day.

To my love, Sean MacDonald, who through both humor and wisdom supports and pushes me to be my best self every day, thank you for all the adventures. To my beautiful other half, (Dr.) Megan Nas, for your unyielding support and oat milk latte "incubation time" dates, thank you for being my rock, I wouldn't have made it without you. To my childhood best friend, Abbie Read, for being an inspiration of self-acceptance and determination. To Jen Jelincic, for being my conservation inspiration and emotional twin, thank you for truly understanding me. And to Matthew Mullen for always being thoughtful, kind, and above all else, truthful.

Showing the immense gratitude I have for each individual that has left a mark on my life is a feat I one day hope to achieve. Without you all, this journey would have been impossible, and I would not be who I am today, because "life is not what you alone make it. Life is the input of everyone who touched your life and every experience that entered it. We are all part of one another."

-Yuri Kochiyama

List of Abbreviations

AMPK: Adenosine Monophosphate Activated Protein Kinase

APC: Antigen Presenting Cell

B16: B16 Melanoma

B6: C57BL/6

CCL: C-C Motif Chemokine Ligand

CD: Cluster of Differentiation

CTL: Cytotoxic Lymphocytes

CTLA-4: Cytotoxic T-Lymphocyte-Associated Protein-4

CXCL: C-X-C Motif Ligand

dKO: Double Knock Out

DUB: Deubiquitinase

EAE: Experimental autoimmune encephalomyelitis

EG7: EG7 Lymphoma

FACS/Flow Cytometry: Fluorescence Activated Cell Sorting

Foxp3: Forkhead Box P3

GITR: glucocorticoid-induced TNF receptor family related protein

H&E: Hematoxylin and eosin

HIF: Hypoxia Inducible Factor

IFN: Interferon

IL-: Interleukin

KO: Knock Out

LLC1: Lewis Lung Carcinoma

LN: Lymph Node

MFI: Mean Fluorescent Intensity

mRNA: Messenger RNA

mTOR: Mechanistic Target of Rapamycin

PBMC: Peripheral Blood Mononuclear Cell

PBS: Phosphate Buffered Saline

PD-1: Programmed Cell Death Receptor 1

qPCR: Quantitative Polymerase Chain Reaction

RNAseq: RNA sequencing

RT: Room Temperature

SAGA: Spt-Ada-Gen5 Acetyl transferase

SMAD: *Caenorhabditis elegans* protein (Sma) and mothers against decapentaplegic (Mad)

Sp: Spleen

TCM: Tumor Conditioned Media

TGF: Transforming Growth Factor

Th: T Helper

TME: Tumor Microenvironment

TNF: Tumor Necrosis Factor

T_{reg} Cells: T Regulatory

iT_{reg}: induced T_{reg}

itTreg: intratumoral T_{reg}

nT_{reg}: Natural T_{reg}

Tu: Tumor

Ub: Ubiquitin

Usp: Ubiquitin Specific Peptidase

Usp22i-S02: Structure of compound CS30 / Usp22 specific inhibitor

WT: Wild Type

YFP: Yellow Fluorescent Protein

Table of Contents

ABSTRACT.....	3
ACKNOWLEDGEMENTS	5
ABBREVIATIONS.....	7
TABLE OF CONTENTS.....	9
LIST OF FIGURES.....	14
LIST OF TABLES	15
CHAPTER 1: INTRODUCTION.....	16
1.1 T Regulatory Cells.....	16
1.1.1 Overview of Adaptive Immunity.....	16
1.1.2 <i>T_{reg}</i> Generation and Function	17
1.1.3 <i>T_{reg}</i> Cell Markers and <i>Foxp3</i>	18
1.2 Tumor Immunology.....	20
1.2.1 Immunity in the Tumor Microenvironment	20
1.2.2 Current Cancer Immunotherapies.....	21
1.3 Treg Cells in Cancer	24
1.3.2 Treg Recruitment to the Tumor Microenvironment.....	25
1.3.2 Treg Conversion in the Tumor Microenvironment	26
1.3.3 Hypoxia.....	28
1.3.4 Nutrient Starvation	29
1.3.5 Lactate.....	31
1.3.6 TGF-beta	32
1.4 Treg Functional Regulation Through Ubiquitination	33
1.4.1 SAGA DUB Module Usp22.....	34

	10
1.4.2 <i>Usp21 prevents generation of Th1-like T_{reg} Cells</i>	34
1.4.3 <i>Usp7 inhibition results in severe T_{reg} instability</i>	36
CHAPTER 2: USP22 REGULATES T_{REG} FUNCTION THROUGH FOXP3 STABILIZATION	37
2.1 Rationale	37
2.2 Results	38
2.2.1 <i>CRISPR screen in T_{reg} cells reveals Usp22 as a modulator of Foxp3</i>	38
2.2.2 <i>Usp22 is required for Foxp3 expression and T_{reg} lineage stability</i>	41
2.2.3 <i>Usp22 transcriptionally regulates Foxp3 through Histone H2B deubiquitination</i>	42
2.2.4 <i>Usp22 and Rnf20 reciprocally regulate Foxp3</i>	46
2.2.5 <i>Usp22 is a DUB of Foxp3</i>	49
2.2.6 <i>T_{reg}-specific ablation of Usp22 results in age-related spontaneous autoimmunity</i>	51
2.2.7 <i>T_{reg}-specific ablation of Usp22 results in enhanced severity of EAE and colitis</i>	52
2.2.8 <i>T_{reg}-specific Usp22 ablation enhances antitumor immunity</i>	55
2.3 Conclusion	57
CHAPTER 3: THE TUMOR MICROENVIRONMENT ENHANCES T_{REG} FITNESS THROUGH UPREGULATION	
OF A FOXP3-SPECIFIC DEUBIQUITINASE MODULE	59
3.1 Rationale	59
3.2 Results	60
3.2.1 <i>Selective upregulation of Foxp3 deubiquitinases in iT_{reg} cells</i>	60
3.2.2 <i>Tumor-derived TGF-beta selectively induces Usp22 and Usp21 in T_{reg} cells</i>	64
3.2.3 <i>TGF-beta and Usp22 amplify canonical TGF-beta signaling through Usp22-SMAD positive feedback loop</i>	68
3.2.4 <i>Hypoxia selectively induces T_{reg} Usp22, which supports Foxp3 expression</i>	72
3.2.5 <i>Metabolic alterations in the tumor microenvironment induce Usp22 and Usp21 to promote Foxp3 stability</i>	73
3.2.6 <i>Usp22 and Usp21 modulate T_{reg} fitness through distinct pathways</i>	77

	11
3.2.7 <i>Usp22 and Usp21 deletion in T_{reg} cells synergize to enhance anti-tumor immunity</i>	82
3.2.8 <i>Identification of Usp22-specific small molecule inhibitors</i>	85
3.2.9 <i>Usp22i-S02 holds great preclinical efficacy in enhancing anti-tumor immunity</i>	90
3.3 Conclusion.....	94
CHAPTER 4: DISCUSSION	96
4.1 Innovation	96
4.1.1 <i>Addressing T_{reg} cells in Tumor Immunity</i>	97
4.1.2 <i>Importance of an Intratumoral T_{reg}-Specific Target</i>	98
4.2 TME Factors and Usps.....	99
4.2.1 <i>Tumor Produced TGF-beta</i>	100
4.2.2 <i>Hypoxia in the TME</i>	101
4.2.3 <i>AMPK and mTOR: Upstream Signaling</i>	102
4.2.4 <i>AMPK and mTOR: Downstream Signaling</i>	105
4.3 <i>Usp22 and Usp21 on Treg Stability in the TME</i>	106
4.3.1 <i>Cell Cycle Progression</i>	106
4.3.2 <i>Autophagy</i>	107
4.4 <i>Usp22 as the Ideal Antitumor Treg Target</i>	108
4.4.1 <i>Usp22 as an ideal Target for iT_{reg} cells</i>	108
CHAPTER 5: MATERIALS AND METHODS	110
5.1 Cell Lines, Plasmids, Antibodies, and Reagents	110
5.2 Animal Models	110
5.3 Pooled sgRNA Library Design and Construction	112
5.4 CRISPR Screen	113
5.5 Arrayed Cas9 RNP Preparation and Electroporation	114
5.6 Retroviral Transduction and Foxp3 Rescue Experiment.....	115

	12
5.7 Isolation of Genomic DNA from Fixed Cells	117
5.8 Preparation of Genomic DNA for Next Generation Sequencing.....	117
5.9 <i>In Vitro</i> Suppressive Assay	118
5.10 Tumor Models.....	118
5.11 Adoptive Transfer Model of Colitis	118
5.12 Induced Experimental Autoimmune Encephalomyelitis.....	119
5.13 Histology	119
5.14 Cell Isolation and Flow Cytometry for Analysis of Splenic and Intratumoral Treg cells	119
5.15 RNA Extraction for RNA Sequencing and qPCR.....	120
5.16 <i>In Vitro</i> iTreg Cell Generation	121
5.17 ChIP-qPCR Sample Preparation.....	121
5.18 ChIP-Seq Sample Preparation and Analysis	122
5.19 Ubiquitination Assay	124
5.20 <i>Ex-Vivo</i> nTreg Cell Culture Conditions	124
5.21 <i>In Vitro</i> Treg Cell Hypoxia Culture	125
5.22 Glucose and Amino Acid Restriction Assays	125
5.23 <i>In Vitro</i> Inhibitor Assays	126
5.24 Assessment of Cellular Metabolism.....	126
5.25 Homology Modeling of Human USP22	126
5.26 Virtual Screening.....	127
5.27 Molecular Docking Mechanism.....	127
5.28 Molecular Dynamics Simulation	128
5.29 Statistics and Data Availability	128
5.30 TABLES	129

	13
5.30.1 Structure and Chemical Names of Usp22 Inhibitors	129
5.30.2 FACS Antibodies	133
5.30.3 Western Antibodies	134
5.30.4 Primers	135
REFERENCES	136

List of Figures

Figure 2.1 Discovery and validation of Foxp3 regulators in primary mouse Treg cells using a targeted pooled CRISPR screen	40
Figure 2.2 Design and validation of Treg-specific Usp22-knockout mice	42
Figure 2.3 Usp22 is required for Foxp3 maintenance and Treg suppressive function	45
Figure 2.4 Usp22 regulates Foxp3 Through transcriptional mechanisms.....	48
Figure 2.5 Usp22 acts as a deubiquitinase to control post-translational Foxp3 expression	50
Figure 2.6 Autoimmune inflammation in Treg-specific Usp22 knockout mice	51
Figure 2.7 Treg-specific ablation of Usp33 results in autoimmunity and enhances antitumor immunity .	53
Figure 2.8 Tumor growth is inhibited in Treg-specific Usp22 knockout mice in multiple cancer models..	56
Figure 3.1 Intratumoral Treg cells have increased Foxp3 and activation markers.....	61
Figure 3.2 Intratumoral Treg cells have increased mRNA expression of Usp22 and Usp21.....	63
Figure 3.3 TGF-beta induces expression of Usp22 and Usp21 in Treg cells.....	66
Figure 3.4 Tumor cell secreted TGF-beta increases Usp22 and Usp21 levels in iTreg cells.....	67
Figure 3.5 Smad3 and Smad4 bind to conserved SBE on the Usp22 promoter.....	70
Figure 3.6 Usp22 reciprocally enhances TGF-beta signaling through Smad protein stabilization in positive feedback loop.....	71
Figure 3.7 Usp22 and Usp21 are required for Foxp3 stability in nTreg cells under environmental and metabolic stress found in the TME	75
Figure 3.8 HIF-alpha and the AMPK/mTOR balance modulates Treg cell Foxp3 stability through Usp22 and Usp21	76
Figure 3.9 Loss of Usp22 and Usp21 in Treg cells differentially impairs Foxp3 expression and cell function	79

Figure 3.10 Loss of Usp22 and Usp21 in Treg cells differentially alter Treg metabolic Pathways.....	81
Figure 3.11 Deletion of Usp22 and Usp21 in Treg cells synergize to enhance antitumor immunity	84
Figure 3.12 Development and validation of Usp22-specific inhibitor through structure-based hierarchical screening.....	89
Figure 3.13 Usp22i-S02 halts Usp22-mediated Foxp3 deubiquitination	92
Figure 3.14 Usp22i-S02 administration enhances antitumor immunity.....	93

List of Tables

Table 1: Structure and Chemical Names of Usp22 Inhibitors	129
Table 2: FACS Antibodies	133
Table 3: Western Antibodies.....	134
Table 4: PRIMERS	135

CHAPTER 1: Introduction

1.1 Regulatory T Cells

1.1.1 Overview of Adaptive Immunity

For protection against the high antigenic variability and mutation potential of pathogens, vertebrates have developed two highly interconnected branches of immunity: the innate and adaptive immune systems^{1,2}. While the innate immune system is a fast, nonspecific defense mechanism that occurs immediately after infection, the adaptive immune system is much more precise. Composed of specialized cells that recognize specific antigens, the adaptive immune system can mount an attack to the precise pathogen causing the infection. Furthermore, the adaptive immune system has the power to create immunological memory, leading to prompt and enhanced responses to subsequent re-infections³. Thus, the adaptive immune system is pivotal in prolonged resistance to future challenges by acquainted pathogens.

The cells that make up the adaptive immune system are known as B and T lymphocytes, which are derived from hematopoietic stem cells in the bone marrow. While B cells play an important role in the humoral response, T cells are more intimately involved in cell-mediated immune responses⁴. The cells that make up the T cell compartment are the cytotoxic CD8⁺ lymphocytes (CTL), and the CD4⁺ T cells. CD8⁺ T cells induce cell death of infected cells through the secretion of cytotoxins and granzymes, while CD4⁺ T cells function as immune mediators to maximize and tailor the immune response⁴. The specificity of the CD4⁺ T cell immune response depends on the pathogen that is encountered. Particularly, the type of pathogen encountered will elicit a response from one of the many types of CD4⁺ T cells. For example, T Helper 1 (Th1) cells, which are characterized by the production of interferon gamma (IFN-gamma), aid in activating the bactericidal activities of macrophages and function to eliminate intracellular pathogens such as

bacteria and viruses. Conversely, T Helper 2 (Th2) cells, characterized by the release of interleukin 4 and 5 (IL-4 and IL-5)⁵, are more specific to extracellular parasites including helminths and toxins. More recently, evidence for additional Th groups have arisen, such as Th17 cells, which secrete interleukin-17 (IL-17) capable of both driving granulocyte recruitment and stimulating interleukin-6 (IL-6) and tumor necrosis factor (TNF) production⁶. Broadly, the cytokines secreted by the various Th cells can activate certain cells of the innate immune system as well as facilitate the proper humoral response in B cells to the encountered pathogen⁷. This is just one method by which the cells of the adaptive immune system work closely with one another as well as with the innate immune system to fine-tune the immune response to any specific pathogen^{7,8}.

Occasionally, the mounted response could result in excessive inflammation resulting in tissue damage and loss of organ function. To tolerize this possible erratic immune response, both the innate and adaptive immune systems have regulatory components such as myeloid derived suppressor cells (MDSCs), regulatory dendritic cells, and the CD4⁺ subgroup called T Regulatory (T_{reg}) cells⁹.

1.1.2 T_{reg} Generation and Function

A highly important characteristic of the vertebrate immune system is the maintenance of peripheral tolerance through the function of T_{reg} cells. Distinct from the effector CD4⁺ T (T_{eff}) cells, T_{reg} cells are a highly immunosuppressive cell and represent 5-10% of the total CD4⁺ T cell population¹⁰. Although epigenetically distinct, there are two main types of T_{reg} cells that have complementary and overlapping regulatory functions¹¹. Natural (n) T_{reg} cells develop in response to self-antigen stimulation in the thymus, while induced (i)T_{reg} cells develop in the peripheral organs in response to cytokine stimulation and environmental antigen presentation^{11,12}.

Both nT_{reg} and iT_{reg} cells can control the immune system in an antigen-dependent manner, though the antigen specificity is a subject of continuous debate¹³. Naturally, T cells with a highly self-reactive TCR are depleted from the T cell repertoire to prevent auto-immunity. However, T_{reg} cells function in maintaining self-tolerance and therefore could be self-reactive, a characteristic which has been observed in various mouse models of autoimmune disease^{14,15}. This notion has been challenged by more recent studies analyzing hundreds of T_{reg} TCRs finding little evidence of preference to self-reactivity¹⁶. Furthermore, T_{reg} *in vivo* suppression studies present increasing evidence that T_{reg} cells exert their suppressive function in a more antigen-*restricted* manner, rather than an antigen-*specific* manner^{14,17}. Regardless, once activated through their TCR, suppressive capabilities of T_{reg} cells are enabled through the high expression of multiple inhibitory surface molecules, such as cytotoxic T-lymphocyte-associated protein-4 (CTLA-4)^{18,19} and programmed cell death receptor-1 (PD-1)²⁰, and through the secretion of anti-inflammatory cytokines such as interleukin-10 (IL-10) and TGF- β ^{13,21}.

1.1.3 T_{reg} Cell Markers and Foxp3

T_{reg} cells were first identified as a naturally occurring subset of CD4⁺ cells constitutively expressing the α -chain of the interleukin 2 (IL-2) receptor, CD25²². Since then, identification of additional surface molecules, including CTLA-4¹⁸, glucocorticoid-induced tumor necrosis factor receptor (TNFR) family related protein (GITR)²³, and inducible co-stimulator (ICOS)²⁴, began to paint a canonical T_{reg} cell surface signature. However, the distinction of T_{reg} cells by these surface markers remains challenging, as they are frequently upregulated in T_{eff} cells upon activation²⁵. Currently, the most definitive T_{reg} marker is forkhead box P3 (Foxp3). Uniquely important for T_{reg} identity and function, Foxp3 functions as the lineage-defining T_{reg} transcription factor²⁶. Although it has been documented that FoxP3 is transiently expressed in most human CD4⁺ and CD8⁺ T

cells⁷¹, levels are significantly higher in the CD4⁺CD25⁺ suppressor cells characterized by *Sakaguchi et al*, 1995, defining FoxP3 as the most specific marker to date²⁶.

The importance of identifying any targetable cell marker lies in the desire to control cellular function as it pertains to human disease. As T_{reg} cells are required to control immune responses and maintain homeostasis, modulating their function through specific markers can aid in immunotherapies for cancer and autoimmune disease. Particularly, the inhibitory function of T_{reg} cells is often hijacked by tumors, creating a highly suppressive tumor microenvironment (TME)²⁷. Targeting T_{reg} suppressive function was originally thought to be done through Foxp3. Noticeably, reduction or ablation of Foxp3 results in attenuation of T_{reg} suppressive function and a shift towards T_{eff}-like characteristics, including the production of inflammatory cytokines^{28,29}. Furthermore, the lethal autoimmune syndrome observed upon the global or Treg-restricted loss of Foxp3 results from CD4⁺CD25⁺ Treg deficiency²⁶. The plasticity resulting from FoxP3 downregulation could be used to shift the lymphocyte repertoire within the TME, potentially increasing the anti-tumor immune response by reducing the number of actively suppressive T_{reg} cells³⁰. However, human patients with Foxp3 dysregulation in T_{reg} cells develop a severe autoimmunity called immune dysregulation, polyendocrinopathy, enteropathy, X-linked (IPEX) syndrome³¹. Therefore, while Foxp3 is uniquely important for T_{reg} identify and function, targeting it would require great care as complete inhibition would likely drive significant autoimmunity²⁶. As such, likely therapeutic candidates will be those that control the expression and stability of Foxp3, rather than Foxp3 itself, to more carefully regulate Foxp3 levels.

1.2 Tumor Immunology

1.2.1 Immunity in the Tumor Microenvironment

Cancer arises through unrepaired genetic and epigenetic mutations resulting in aberrant cellular proliferation and eventual cellular immortality. This consistent proliferation paired with DNA repair dysfunction results in the expression of mutated proteins³². Once processed, these mutated proteins form neo-antigens that can be recognized as foreign by the hosts immune system². Neo-antigens can be presented on the surface of the tumor cells directly or on the surface of tumor-infiltrating immune cells, both of which act as antigen presenting cells (APC), through the major histocompatibility complexes (MHC)¹. The adaptive immune system, mainly through the functions of CD8⁺ CTLs and CD4⁺ Th cells, recognizes the neo-antigens as foreign, and mounts an immune response against the tumor^{1,2}. Ultimately, the immune system has the ability to recognize and eliminate malignant cells during their initial establishment, a process called immunosurveillance³⁷.

While neoplastic cells have sufficient antigenicity to promote an anti-tumor immune response, there has been growing evidence to support that immunosurveillance represents only a fraction of the relationship between cancer and the immune system³³. Particularly, even if immunosurveillance can eradicate the majority of transformed cells, some tumor cells can succeed in escaping this immune assault through multiple mechanisms including the production of immune suppressive mediators and cytokines, and defective antigen presentation^{27,34}. Therefore, tumor growth is sustained and unrestrained by the immune system. From here, vascular disorganization owing to tumor the enhanced rate of cellular proliferation and growth factor secretion creates a hostile TME depleted of oxygen, glucose, and amino acids while enriched with cytokines and lactic acid³². Many, if not all, of these alterations in the TME are known to inhibit anti-tumor

immune responses, including the disruption of T_{eff} cell function^{35,36}. Furthermore, recruitment of immune regulatory cells such as MDSCs and T_{reg} cells further diminish the anti-tumor effects of T_{eff} cells. Therefore, utilizing the natural cancer-fighting power of the immune system, while circumventing immune tolerance cause by the tumor, is a promising strategy for cancer therapies.

1.2.2 Current Cancer Immunotherapies

The first attempts at using the endogenous immune system to combat cancer was through therapeutic cancer vaccines, where the tumor-specific T cells within the patient would be primed by an administration of a vaccine containing the tumor antigen. However, a general lack of understanding about the tumor-immune system interplay resulted in little therapeutic potency³⁷. Further research resulted in vaccines capable of breaking immune tolerance through priming of tumor-antigen specific dendritic cells (DCs). These efforts, however, have not shown durable clinical responses or tumor regression^{37,38}.

Another promising form of immunotherapy, called Adoptive Cell Therapy (ACT), exploits the antitumor properties of lymphocytes. In ACT, lymphocytes are isolated from patients and expanded *ex vivo*, then re-administered to the patient with the intention of eradicating primary and metastatic tumors. ACT attempts to reverse the functional impairment of exhausted intratumoral T_{eff} cells, caused by both functional overexertion and immune impairment within TME^{39,40}. Often, following a lymphodepleting regimen to eliminate intratumoral immunosuppressive cells, ATC has resulted in multiple, durable tumor responses against melanoma⁴¹. Despite these optimistic outcomes, ACTs are not cost or time effective, and the pairing with lymphodepletion has resulted in many cases of severe autoimmunity^{37,39,40,42}. Furthermore, unlike the highly immunogenic melanoma, many tumors actively downregulate MHC expression to prevent anti-tumor T_{eff} cell activation⁴³. Advances in T cell engineering have addressed this by fusing an Ig variable domain

to the T cell receptor (TCR). These chimeric antigen receptor (CAR) T cells can by-pass the need for tumors to express a functional antigen processing machinery by binding directly to any tumor cell surface antigen⁴⁴. Administration of CAR T cells yielded remarkable efficacy in B-cell malignancies, with close to 70-90% complete remission in patients^{45,46}. Unfortunately, the effectiveness of CAR T cell therapy in solid tumors are less promising. Furthermore, simply administering high amounts of activated T_{eff} cells does not evade the immunoinhibitory conditions created by the TME that downregulates their function.

To circumvent immunosuppression within the tumor, alternative immunotherapeutic approaches focus on targeting the mechanisms by which tumor cells inhibit antitumor properties of T_{eff} cells. Upon normal T cell activation, checkpoint receptors are naturally upregulated to mitigate excessive immune responses. Particularly, cytotoxic lymphocyte antigen (CTLA-4)¹⁹, capable of blocking T cell co-stimulation, and programmed death-1 (PD-1)²⁰, which promotes T cell anergy, reduction of cytokine production, and apoptosis, follow this pattern. Tumors can exploit these natural checkpoints by expressing ligands to these inhibitory receptors, inducing immune tolerance³⁸. Promising new therapies use monoclonal antibodies to block the immune-inhibitory pathway cancer cells activate in order to unleash the pre-existing antitumor response of the T_{eff} cells, termed “checkpoint blockade” therapy^{37,38}. CTLA-4 was the initial target for checkpoint blockade immunotherapy and resulted in anti-tumor responses in multiple murine tumor models⁴⁷⁻⁴⁹. The therapy was then translated into the clinic with the first FDA-approved immune checkpoint blockade antibody, ipilimumab, for patients with melanoma^{50,51}. Although therapeutic responses were less durable in human patients, these trials ignited interest in other immune checkpoint blockade therapies, pioneering the field of cancer immunotherapy^{37,38}. Shortly thereafter, anti-PD-1 checkpoint blockade monoclonal antibodies, nivolumab and pembrolizumab,

were developed^{52–56}. Either PD-1 monoclonal antibody had less autoimmune related side effects, and more durable responses, than the previous anti-CTLA-4 treatments⁵⁷.

Unfortunately, neither therapeutic regimen resulted in a 6-month progression free survival rate over 50%, prompting for research into combinational therapies⁵⁸. Additionally, combinational therapies would account for the independent roles of CTLA-4 and PD-1 modulation of T cell signaling. Therefore, synergy was expected upon therapy combination. Indeed, the preclinical model of B16 melanoma showed an improved antitumor response upon dual-therapy administration⁵⁹. Clinically, administration of both ipilimumab and nivolumab reported an increase in durable responses to various cancers^{60–62}. Although dual administration of checkpoint therapy may increase in the magnitude, frequency, and onset of side effects, the promising responses of many patients indicates the importance and strength of combinational therapies.

Importantly, currently administered immunotherapies focus primarily on enhancing the immune system by augmenting lymphocyte effector function through either vaccination-mediated T cell priming, T cell *ex-vivo* expansion, or checkpoint inhibition. Problematically, these therapies address only one aspect of the immunosuppressive niche that accounts for tumor immune escape. Particularly, one major impediment to successful immunotherapy is T_{reg} cell mediated immunosuppression in the TME^{63–65}. Although T_{reg} cells are critical for the maintenance of peripheral tolerance, their function can be sequestered by the tumor to help overcome the inherent antigenicity of tumor cells. This accumulation of T_{reg} cells within the tumor is correlated with poor prognosis in many solid tumors, making T_{reg} cells an important target for future therapies^{65–68}.

1.3 Treg Cells in Cancer

The presence of intratumoral T_{reg} cells within the TME play a pivotal role in inhibiting anti-tumor immunity, and are a major hurdle for current tumor-targeting immunotherapies. The

exact composition of intratumoral (it) T_{reg} cells, and whether the majority of this population consists of n T_{reg} or tumor-induced i T_{reg} cells, remains unknown and may differ between tumor types⁶⁹. However, it is likely that both populations, although epigenetically distinct, thrive in the TME and further aid in dampening anti-tumor immunity.

As T_{reg} depletion through a T_{reg} -specific marker remains challenging^{30,70}, the particular pathways that enhance T_{reg} suppressive capabilities within the TME are attractive candidates for new therapeutic targets to diminish it T_{reg} suppressive function. Although Foxp3 is uniquely important for T_{reg} identify and function, it is an intracellular protein whose targeting would require great care as complete inhibition would likely drive significant autoimmunity²⁶. In addition, specifically targeting a transcription factor like Foxp3 remains technically challenging. Therefore, likely therapeutic candidates will be those that control the expression and stability of Foxp3 *specifically in the TME*.

The disorganized vascular system and enhanced rate of proliferation observed in tumors creates a hostile microenvironment depleted of oxygen, glucose, and amino acids while enriched with cytokines and lactic acid³². Many, if not all, of these alterations in the TME are known to inhibit anti-tumor immune responses through a variety of mechanisms. Particularly, these TME-derived pressures favorably alter it T_{reg} cells, resulting in heightened proliferative and suppressive abilities, while diminishing the anti-tumor effects of T_{eff} cells^{35,74,100,101}.

Interestingly, it T_{reg} cells display upregulated expression of the lineage-defining Treg transcription factor Foxp3^{72,102}, which functions to enhance T_{reg} fitness by augmenting T_{reg} cell stability and suppressive molecular function. Importantly, Foxp3 expression is essential for proper T_{reg} development and function²⁶. Although the molecular mechanisms underlying how and which

TME factors upregulate Foxp3 expression to potentiate iT_{reg} suppressive function remain an immunological mystery, many TME factors have known effects on T_{reg} cells.

1.3.1 T_{reg} Recruitment to the Tumor Microenvironment

T_{reg} homing to the TME is a critical step in the initiation and continuance of tumor-mediated immunosuppression^{63,71-74}. The ability of tumor conditioned media (TCM) to attract T_{reg} cells in migration assays demonstrates the importance of soluble factors in T_{reg} trafficking⁷⁵. Explicitly, various chemokines have been implicated in T_{reg} recruitment, and are generally dependent on tumor type.

Glioblastoma, as well as ovarian, breast, lung, and esophageal cancer all produce large quantities of CCL22, and its ligand CCR4 has been implicated in nT_{reg} function^{67,75-79}. Interestingly, the level of CCL22 production positively correlates with the n T_{reg} frequency within breast and gastric cancer, denoting the CCL22-CCR4 axis as a plausible nT_{reg}-attracting mechanism^{67,76}. Indeed, malignant pleural fluid from lung cancer patients as well as glioblastoma TCM, which contain high levels of CCL22, were preferentially chemotactic for nT_{reg} cells⁷⁸. Furthermore, *in vitro* incubation of CD4⁺ T cells with CCL22 showed preferential migration of T_{reg} over T_{eff} cells^{67,75-78}. The administration of antibodies blocking the CCL22-CCR4 axis demonstrated a significant decrease in nT_{reg} chemoattraction^{27,77,78}. Although CC17 can also interact with CCR4 to recruit nT_{reg} cells, the administration of a blocking antibody for CCL17 to lung cancer pleural fluid did not alter their migration, suggesting CCL22 to be the dominant chemoattractant⁷⁸.

Similarly, pancreatic, breast, and colon cancer can recruit high amounts of nT_{reg} cells through the CCL5-CCR5 axis⁸⁰⁻⁸². Knockdown of CCL5 in both murine pancreatic and colon cancer decreased nT_{reg} recruitment and significantly slowed tumor growth, as did systemic CCR5

antagonist administration^{80,82}. Interestingly, CT26 murine colon cancer deficient in CCL5 secretion reduced the T_{reg}-mediated apoptosis of CD8⁺ cytotoxic T cells, suggesting the importance of the CCL5-CCR5 axis on T_{reg} function. Correspondingly, CCR5-deficient mice had less T_{reg}-mediated killing ability and delayed tumor growth⁸⁰. Similarly, tumor-secreted CXCL12 preferentially recruits T_{reg} cells. Additionally, treatment of mice inoculated with BR%-1 ovarian cancer with a CXCR4 antagonist results in decreased T_{reg} recruitment, increased T_{eff} cells recruitment, and decreased tumor burden⁸³. Similar findings along the Sphingosine-1-Phosphate (S1P), CCL20-CCR6, CCL9/10/11-CXCR3, and CCL2-CCR4 axes demonstrate diminished recruitment of nT_{reg} cells upon neutralization antibody administration^{66,84-86}.

Interestingly, tumor cells are not unique in chemokine expression within the TME. Myeloid derived suppressor cells (MDSCs) found in tumor tissues also upregulate expression of CCL22 and CCL5, and induce nT_{reg} migration^{27,87}. Although this adds another level of complexity in discovering the primary mechanism for TME-mediated T_{reg} cell trafficking, it supports clear mechanisms for which T_{reg} are preferentially recruited to the TME. As T_{reg} infiltration in the TME is commonly associated with poor prognosis, future research will have to be conducted to determine the most likely targets to inhibit T_{reg} migration and diminish immunoregulation on the anti-tumor response.

1.3.2 Treg Conversion in the Tumor Microenvironment

Along with T_{reg} migration, multiple tumor stimuli can further promote an immunosuppressive environment by deriving iT_{reg} cells from naïve CD4⁺ T cells or converting them from T_{eff} cells. In non-Hodgkin lymphoma, tumor cells were capable of inducing T_{reg} cells from CD25⁻ PBMCs *in vitro*⁸⁸. Similarly, follicular lymphoma malignant B cells were capable of converting T_{eff} cells from both patient and normal blood into suppressive iT_{reg} cells⁸⁹. In another

blood cancer, acute myeloid leukemia (AML), IDO-expressing tumor cells could directly convert CD4⁺CD25⁻ cells into Foxp3⁺ T_{reg} cells expressing surface CTLA-4, a crucial step in T_{reg} development^{90,91}. This effect was abrogated upon IDO inhibition. Finally, a recent study in ovarian and colorectal cancer bearing mice discovered that IL-17A⁺FoxP3⁻ cells can convert to IL-17⁻Foxp3⁺ (ex-Th17) cells, and that these cells are a major source of tumor infiltrating T_{reg} cells in a solid tumor *in vivo*⁹².

Although cell-cell contact plays a role in tumor-driven iT_{reg} formation, many studies have pointed to the importance tumor derived soluble factors. Upon incubation with TCM derived from Glioblastoma cell line, CD4⁺ T_{eff} cells transiently increased expression of Foxp3 and TGF-beta , and became functionally suppressive⁷⁵. Furthermore, TCM from human lung cancer was able to maintain high levels of Foxp3 expression in ex-vivo tumor infiltrating T_{reg} cells, while normal T cell media could not. To determine the tumor-secreted factors important for iT_{reg} generation, it is important to consider pathways that generate iT_{reg} cells under non-malignant conditions. Induction and conversion to iT_{reg} cells both *in vitro* and *in vivo* require specific cytokine profiles, particularly IL-10 and TGF-beta ,^{93,94}. Tumors tissues ranging from ovarian, breast, renal, lung, and skin cancer have all shown expression of IL-10 mRNA transcripts⁹⁵. Likewise, as tumors grow, they secrete an increasing amount of TGF-beta , which is correlated with poorer prognosis⁹⁶. Although it has not been shown that TGF-beta , specifically from TCM is capable of generating iT_{reg} cells, tumor-secreted TGF-beta , has been shown to enhance iTreg FoxP3 levels and suppressive capabilities.

Induction and conversion of iT_{reg} cells in the TME increases the pool of T_{reg} cells within the TME, enhancing immunosuppression and driving tumor growth. Importantly though, the ability to convert and induce T_{reg} cells in the TME is reversible. A handful of studies show the

importance of certain genes in determining T_{reg} lineage stability. For example, GITR, Helios, and nrp1 deficiency in CD4⁺ Treg cells resulted in T_{reg} cell instability, converting these cells to a more effector-like phenotype and enhancing anti-tumor immunity^{97–99}. Whether it is the direct conversion to a more effector-like phenotype or a relief of suppression on existing T_{eff} cells, the manipulation of T_{reg} stability could uncover more potential therapeutic interventions for tumor immunotherapy.

1.3.3 Hypoxia

Unchecked proliferation of cancerous cells results in an insufficient blood supply tissue within the TME. The resulting hypoxia has been identified as a negative prognostic factor in human solid tumors^{32,103–107}. In low-oxygen conditions, the oxygen-sensing prolyl-hydroxylase (PHD) no longer catalyzes post-translational hydroxylation of hypoxia-inducible factors HIF-1 α and HIF-2 α , leading to their stabilization^{108,109}. The transcription factors HIF-1 α and HIF-2 α , collectively HIF- α , can then transcriptionally reprogram cells in response to the low oxygen levels^{109–111}. Transcriptional alterations due to hypoxia have many effects on cellular functions, and are usually unique to the cell type in question¹¹². Thus, certain cells are more adapted to functioning under low oxygen conditions, and can have many implications in tumor progression¹¹³.

Apart from contributing to chemoresistance, angiogenesis, and genomic instability, intratumoral hypoxia also alters immune cell function^{114–119}. As aerobic respiration is required for optimal T_{eff} cell function, hypoxic conditions downregulate T cell proliferation, receptor signal transduction, and effector function^{106,112,115,120}. Additionally, hypoxia impairs CD4⁺ Th1 differentiation *in vitro*. Conversely, nT_{reg} cells cultured in hypoxic conditions became more proliferative and suppressive than their normoxic counterparts, suggesting that hypoxia strengthens T_{reg} function¹¹⁵. A portion of this functional increase could be due to hypoxia

selectively inducing Foxp3 transcription, seemingly through HIF-1 α binding on to the Foxp3 promoter in a TGF-beta dependent manner¹¹⁶. Although, this phenotype is lost under Th17 skewing conditions, possibly because HIF-1 α is important in Th17 development through STAT3 activation of ROR γ ¹¹⁷. Furthermore, HIF-1 α has been shown to bind Foxp3 and aid in its degradation during development, further skewing differentiation towards Th17¹²¹. However, T_{reg} differentiation may not be highly important within TME, and the presence of hypoxia can have differing effects on cell function verses differentiation. Clever *et al.* demonstrated that a T_{reg}-specific deletion of PHD proteins, resulting in HIF- α stability, promoted T_{reg} induction while limiting Th1 responses in pulmonary metastases¹⁰⁸. Alternatively, Hsiao *et al.* demonstrated that a T_{reg}-specific loss of Deltex (DTX1), a promoter of HIF- α degradation, resulted in loss of suppressive function and Foxp3 levels in both *in vivo* models of airway inflammation and colitis¹²². Therefore, DTX1-null T_{reg} cells has reduced levels of Foxp3 even though HIF- α degradation was decreased, countering the co-degradation model demonstrated by Dang *et al.*

Ultimately, there is more to dissect about the relationship between Fox3 and HIF- α , but it is clear that T_{reg} cells under hypoxic conditions have enhanced proliferative and suppressive capabilities. These enhancements no doubt weaken anti-tumor immunity, and block current immune therapies.

1.3.4 Nutrient Starvation

As tumors grow, the fierce competition for nutrients within the TME influences immune cell growth, survival, and function. Particularly, glucose and amino acid restriction alters T_{eff} cell function by dampening proliferative abilities, cytokine production, and inducing antigen hyporesponsiveness^{36,101,123,124}. Unlike T_{eff} cells, which classically display a predominantly glycolytic metabolic program, T_{reg} cells utilize higher levels of oxidative phosphorylation,

potentially giving T_{reg} cells an advantage under glucose starvation^{125,126}. Mechanistically, this metabolic preference partially functions through Foxp3, which can reprogram T cell metabolism to favor oxidative phosphorylation over glycolysis^{35,125}. Importantly, as stated above, Foxp3 is upregulated in T_{reg} cells, potentially resulting in a functional advantage within the TME^{72,127}.

Similar to glucose, amino acid deficiency within the TME can further restrict the anti-tumor response of T_{eff} cells³⁶. For example, T cells deficient in glutamine and neutral amino acid transporters are protected by inflammatory diseases due to lack of functional T_{eff} cells¹²⁸. Furthermore, deprivation of certain amino acids promotes naive T cell differentiation into T_{reg} cells *in vitro*¹²⁹. On the contrary to T_{eff} cells, T_{reg} cells exhibit increased oxidation of fatty acids compared with T_{eff} cells and are not dependent on fatty acid synthesis, suggesting that amino acid starvation negatively impacts T_{eff} cells over T_{reg} cells^{130,131}.

T cell activation and effector function depend on cellular reprogramming to activate anabolic pathways^{124,132,133}. In environments deplete of both glucose and amino acids, activation of adenosine monophosphate-activated protein kinase (AMPK) suppresses anabolic metabolism while upregulating oxidative metabolism to promote cellular survival¹³⁴. As such, T_{eff} cell generation was severely impaired upon AMPK activation. On the contrary, AMPK activation strongly enhances T_{reg} expansion¹³⁵. Furthermore, T_{reg} induction by AMPK activation is accompanied by a shift towards oxidative metabolism, which may further enhance T_{reg} survival in the TME¹³⁵. These data suggest that nutrient starvation partially functions through activation of AMPK to differentially alter immune cell function¹³⁵.

AMPK functions in balance with mammalian target of rapamycin (mTOR) signaling to regulate the cellular metabolic state. For example, in response to energy stress, AMPK activation increases catabolic metabolism in part due to mTOR inhibition¹³⁴. As the AMPK/mTOR

equilibrium functions as an environmental sensor for nutrient availability, starvation conditions in the TME disrupt T cell activation and T cell induce anergy through mTOR inhibition¹³⁶. Consistently, T cells deficient in mTOR preferentially induce into iTreg cells rather than T_{eff} populations *in vitro*¹³⁷. Furthermore, inhibition of mTOR through rapamycin treatment enhances Treg proliferation both *in vitro* and *in vivo*.

Together, these data suggest that a shift towards catabolic and oxidative metabolism that occurs due to nutrient restriction within the TME has profoundly different effects on T_{eff} cells versus T_{reg} cells. As such, T_{reg} ability to adapt better to low-nutrient conditions gives them a metabolic and functional advantage over T_{eff} cells, and further capitulates immunosuppression within the TME. Therefore, understanding the molecular mechanisms behind Treg adaptation to nutrient starvation can lead to the discovery of new molecular targets for potential therapeutics.

1.3.5 Lactate

A side-effect of the enhanced glycolytic nature of tumor cells is the secretion of lactate as a byproduct, and lactate accumulation itself is instrumental for the promotion of tumor growth and angiogenesis^{138,139}. High extracellular accumulation of lactate in the TME disturbs the gradient between cytoplasmic and extracellular lactate, reversing its necessary export in T_{eff} cells. High influx of lactate disturbs T_{eff} cell metabolism by shunting glycolysis, resulting in impaired T_{eff} cell proliferation and cytokine production^{35,133}. Conversely, T_{reg} cells can withstand the suppressive effects of lactate through Foxp3-mediated metabolic reprogramming. Particularly, Foxp3 suppresses Myc and glycolysis while favoring oxidative and increasing nicotinamide adenine dinucleotide (NAD) oxidation. This metabolic shift favors lactate turnover to pyruvate, thus making Treg cells resistant to lactate-mediated cell suppression. These adaptations allow T_{reg} cells

a metabolic advantage in environments rich in lactate, and provides another mechanism of selective immune modulation in the TME to drive cancer progression³⁵.

1.3.6 TGF-beta

Soluble factors secreted by tumors are known to enhance tumorigenicity as well as alter immune cell function^{75,140}. One such factor is TGF-beta. Although TGF-beta is a potent down-regulator of cellular proliferation and activation, tumors become unresponsive to the suppressive effects of TGF-beta through loss of TGF-beta receptor and loss of TGF-beta signal transduction^{141,142}. Furthermore, TGF-beta promotes epithelial-to-mesenchymal transition as well as increased tumor burden and vascularity, factors associated with high grade malignancy and metastasis¹⁴³⁻¹⁴⁵. As tumors overcome TGF-beta -mediated suppression, high levels of production can be advantageous through immunosuppression. Particularly, TGF-beta aids in dampening anti-tumor immunity within the TME by preventing T_{eff} cell migration to the tumor site as well as interfering with the generation of tumor specific T_{eff} cells¹⁴⁶. Furthermore, TGF-beta is implicated in cycle arrest and inhibition of effector molecules of T_{eff} cells through downregulation of IL-2 and upregulation of cell cycle inhibitors¹⁴⁷. Conversely, as described in section 1.3.2, TGF-beta induces the formation of iT_{reg} cells from either naïve T cells or from T_{eff} cell skewing⁹³. Additionally, TGF-beta signaling within the TME is necessary for T_{reg}-mediated immunosuppression on T_{eff} cells¹⁴⁸. T_{reg} cells also suppress T_{eff} cells through TGF-beta secretion^{149,150}, and that secretion can enforce T_{reg} stability and function. This secretion creates a feedback loop of TGF-beta mediated suppression, and firmly links TGF-beta to tumor immune evasion.

1.4 T_{reg} Functional Regulation Through Deubiquitination

As one of the most conserved mechanisms in all biology, ubiquitination is one of the most intensely studied of the posttranslational modifications. A pathway with many end goals, ubiquitination refers to the sequential three-step cascade initiated by ubiquitin activation by ubiquitin activating enzymes (E1s), followed by conjugation by ubiquitin conjugating enzymes (E2s), and culminated with covalent ligation of ubiquitin to the target protein by ubiquitin ligases (E3s)^{151,152}. Whether it be protein degradation, transcription, activation, or cellular localization the particular lysine residue by which the ubiquitin is attached, and the length of the ubiquitin chain, determines the fate of the target protein^{153–158}. Ligation of polyubiquitin chains can occur at one of seven lysine residues on the ubiquitin protein: K6, K11, K27, K29, K33, K48, and K63. K48 and K63 modifications are the best understood. K63-ubiquitin chains result in the association of the target protein with proteins involved in DNA repair, endocytic trafficking, and signal transduction¹⁵⁹. Contrarily, K48 polyubiquitination culminates in the degradation of target proteins by the 26S proteasome¹⁵⁵. Furthermore, mono-ubiquitination on key histone lysine residues can regulate transcriptional accessibility.

Appropriately, the process of ubiquitination is dynamic and reversible. The highly regulated removal of ubiquitin, termed deubiquitination, has been implicated in numerous cellular functions, including cell cycle regulation¹⁶⁰, proteasome-dependent degradation¹⁶¹, and gene expression¹⁶². Deubiquitination is catalyzed by a group of cysteine proteases called deubiquitinases (DUBS), that encompass more than 100 proteins shown to regulate p53 activity, WNT, NF- κ B pathways, EGFR, cell cycle progression, apoptosis and response to DNA damage^{161,163}. Clearly, ubiquitination mediates many diverse cellular processes, and their dysregulation has been specifically implicated in cancer and autoimmunity. Importantly, ubiquitination

facilitates both immune activation and restraint, particularly through the ubiquitin specific pathways that modulate T_{reg} generation, stability, and function.

Since understanding the fundamental regulators of T_{reg} cells is critical, scientists have sought to identify novel regulators of Foxp3 in the hopes of finding potential therapeutic targets. Observations that post-translational modifications of Foxp3, including ubiquitination, result in protein destabilization have attracted a lot of recent attention^{121,164,165}. Since direct ubiquitination of Foxp3 can drive its degradation, it stands to reason that counteracting this process should preserve levels of this important regulatory hub of the T_{reg} phenotype. Three novel DUBs of FoxP3 have been identified in the past 7 years, all of which belong to the ubiquitin-specific peptidase (USP) family^{166–168}.

1.4.1 SAGA DUB module: Usp22

Ubiquitin-specific peptidase 22 (Usp22) is a highly conserved member of the USP family, and is known for its importance in transcription through histone de-ubiquitination as part of the Spt-Ada-Gen5 Acetyl transferase (SAGA) complex¹⁶⁹. In addition, Usp22 has been implicated in cancer through its involvement in regulating genes involved in cell cycle progression, apoptosis, and development, and has been identified as one of 11 “death from cancer” signature genes^{170–173}. The silencing of Usp22 in many cancer types results in the cessation of proliferation. In Chapters 2 and 3, I will describe new and exciting discoveries on Usp22 importance in T_{reg} function, particularly on Usp22 as an environmentally-sensitive factor that regulates T_{reg} cell identity, metabolism and function through Foxp3 stabilization.

1.4.2 Usp21 prevents generation of Th1-like T_{reg} cells

Another USP family member has been established as a Foxp3 regulator, ubiquitin-specific peptidase 21 (Usp21). Usp21 was first discovered through a human placenta cDNA library as a

novel regulator of cell growth through both as a DUB and as a NEDD8-specific isopeptidase¹⁷⁴. More recently, Usp21 was implicated in T_{reg} phenotypic stability and Foxp3 expression through the deubiquitination of GATA3¹⁷⁵. Although GATA3 is the master regulator for Th2 cell differentiation and function, it also plays a major role in nT_{reg} development and function^{176,177}. Specifically, T_{reg} specific loss of GATA3 results in spontaneous autoimmunity through defective T_{reg} suppressive capabilities¹⁷⁶. Therefore, by stabilizing GATA3 levels through its DUB function, Usp21 indirectly supports Foxp3 expression and T_{reg} function¹⁷⁵.

Directly, Usp21 prevents the generation of T helper-1-like T_{reg} cells through the deubiquitination of Foxp3 itself¹⁶⁷. Aged mice with Usp21 ablation in T_{reg} cells displayed autoimmune symptoms such as lymphocytic infiltration into peripheral organs as well as spontaneous T cell activation. Particularly, these mice demonstrated excessive Th1 skewing of T_{reg} cells through both heightened T_{reg} expression of IFN-gamma and lower expression of FoxP3. RNAseq of the skewed T_{reg} cells displayed impaired transcriptional ability of T_{reg} signature genes, with a trend towards expression of genes controlling T_{eff} cell fate. Furthermore, about 35% were direct Foxp3 targets, suggesting that Usp21 regulates the function of T_{reg} cells mainly through Foxp3¹⁶⁷. This finding, however, could likely be due to the fact that the aged mice are already highly inflamed, creating an optimal environment for Foxp3 loss. Functionally, Usp21-null T_{reg} cells had a significantly impaired suppressive capacity both *in vitro* on T_{eff} cell proliferation and *in vivo* in an EAE model of multiple sclerosis. Furthermore, when transferred into EAE-bearing mice, the Usp21-null T_{reg} cells quickly began to lose Foxp3, suggesting that Usp21 is important for T_{reg} stability as well as function. Although the authors demonstrate Usp21 DUB function on Foxp3, all experiments were done in an overexpression system. To further cement Usp21 as an important Foxp3 regulator, investigation of the acute loss of Usp21 on Foxp3 protein stability on

endogenous T_{reg} cells should be explored. Furthermore, to state that Usp21 loss functions primarily through Foxp3, the consequence of the re-introduction of Foxp3 through retroviral transduction in the Usp21-null T_{reg} cells would have to be tested.

1.4.3 Usp7 inhibition results severe T_{reg} instability

Ubiquitin-specific peptidase 7 (Usp7) was the first DUB implicated in T_{reg} suppressive function. Although not highly expressed in T_{reg} cells, USP7 was found to regulate T_{reg} function through direct interaction and deubiquitination of Foxp3¹⁶⁷. In co-ordinance with the other DUBs of Foxp3, the loss of Usp7 in T_{reg} cells resulted in a loss of suppressive function *in vitro* and *in vivo*. Strikingly, both a pan-DUB inhibitor and shRNA against Usp7 significantly reduced T_{reg} function both in colitis and tumor models *in vivo*, suggesting that DUB targeting is an effective strategy to break T_{reg}-enforced tolerance in the cancer setting^{168,178}. Singularly, Usp7 resulted in both a drop in Foxp3 MFI as well as a decrease in T_{reg} cell percentage, resulting in severe autoimmunity and premature death in the USP7f/fFoxp3YFP-Cre inducible mice. Therefore, many of the experiments were conducted in a tamoxifen inducible model, speaking to the severity of Usp7 deletion and its importance in T_{reg} function. It is important to note, that therapeutic inhibition of Usp7 may result in extremely high levels of autoimmunity in cancer patients upon administration. So, although Usp7 is an important regulator of Foxp3 and therefore T_{reg} function, its inhibition may have too strong of adverse effects for it to be an attractive potential therapeutic.

CHAPTER 2: Usp22 Regulates T_{reg} function through Foxp3 stabilization

2.1 Rationale

Aggressive cancers are less sensitive to standard cancer treatments available, such as chemotherapy and radiotherapy, reducing prolonged survival rates and increasing relapse percentage in affected individual¹⁷⁹. As a result, there is an increasing need for alternative therapeutics that will prolong the survival of affected patients. Tumors have long been recognized as having distinctive properties of growth, invasion, and metastasis, but their ability to evade immune destruction has recently attracted attention^{34,38}. As stated in section 1.2.1, tumors have sufficient antigenicity to promote anti-tumor immune responses, however multiple mechanisms of immunosuppression diminish the natural or immunotherapeutic response against the tumors^{1,2}. Particularly, the accumulation of T_{reg} can promote tumor progression through the suppression of tumor immune invasion, creating a major hurdle when targeting tumors for immunotherapy¹⁸⁰⁻¹⁸².

Current immunotherapies targeting inhibitory molecules expressed by immune cells, such as CTLA-4 and PD-1 provide notable clinical effectiveness in melanoma, but not all cancers respond equally well⁶⁰⁻⁶². Recently, new studies using the CD25-IL-2 axis for T_{reg} specific depletion through antibody-dependent cell-mediated toxicity show promising results against many murine cancer types, including B16 melanoma and MCA205 sarcoma^{183,184}. However, using CD25 and IL-2 therapies for T_{reg} depletions also have the ability to target activated T_{eff} cells, possibly lessening therapeutic benefit. This indicates a need for new therapeutic targets and identification of prognosis predicting clinical biomarkers. Depletion of T_{regs} in these highly immunogenic cancers through T_{reg}-specific markers is a promising strategy for the enhancement of tumor immunotherapy. Unfortunately, as stated in section 1.1.3, most T_{reg} markers are non-specific or could result in severe autoimmunity in patients. Therefore, a promising new strategy of tumor

immunotherapy is through regulation of FoxP3 expression, resulting in the attenuation of Treg suppressive function.

Since T_{reg} cells are pinnacle for maintaining immune homeostasis, and Foxp3 is central to T_{reg} function, diminishing Foxp3 intracellular levels without reducing T_{reg} numbers can dampen T_{reg}-mediated tumor-immune suppression without causing auto-immunity. Here, we uncovered Usp22 as an important regulator of T_{reg} function through Foxp3 upregulation and stabilization, and demonstrate its importance in tumor immunity. Furthermore, as Usp22 is implicated in both oncogenic c-Myc activation as well as indirectly antagonizing the tumor suppressive abilities of p53, it is identified as a cancer stem cell marker^{170,171}. Therefore, **Usp22 is a promising therapeutic against highly immunogenic cancers** because its suppression not only induces tumor cell death, but also boosts antitumor immunity through T_{reg} impairment.

2.2 Results

2.2.1 CRISPR screen in T_{reg} cells reveals Usp22 as modulator of Foxp3

To identify potential regulators of Foxp3 stability, we developed a pooled CRISPR-screening platform in primary mouse T_{reg} cells (**Fig. 2.1a**). We first designed a targeted library of 489 nuclear factors on the basis of optimized single guide RNA (sgRNA) sequences from the Brie library and used a retroviral vector to introduce this library into T_{reg} cells isolated from *Foxp3^{GFP-cre}Rosa26^{LSL-RFP}Cas9* mice. We then stained the cells for endogenous Foxp3 protein and sorted the highest (Foxp3^{high}) and lowest (Foxp3^{low}) Foxp3-expressing cells. MAGeCK software systematically identified sgRNAs that were enriched or depleted in Foxp3^{low} cells relative to Foxp3^{high} cells.

Our screen revealed many Foxp3 regulators, with a bias towards identifying positive regulators over negative regulators (**Fig. 2.1b and c**). sgRNAs enriched in the Foxp3^{low} population

reflect positive regulators (blue) that promote Foxp3 expression, whereas sgRNAs depleted in the Foxp3^{low} population reflect negative regulators (red) that inhibit Foxp3 expression. As expected, sgRNAs targeting *Foxp3* were enriched in the Foxp3^{low} population. We also identified many established regulators known to be important for maintenance of Foxp3 expression, including Cbfb, Runx1 and Stat5b¹⁸⁵⁻¹⁸⁷ as positive regulators, and Sp3 and Satb1 as negative regulators¹⁸⁸ providing further confidence in our hits. Of note, several previously unknown factors and complexes that modulate Foxp3 were identified, including the positive regulators Usp22 and the negative regulator Rnf20. The deubiquitinase (DUB) Usp22 is a member of deubiquitination module of the SAGA chromatin modifying complex¹⁶⁹. To validate the effects of our screen hits on Foxp3 levels, we assessed five of the top-ranking positive regulators by individual CRISPR knockout with Cas9 ribonucleoproteins (RNPs). The effects on Foxp3 levels were consistent across multiple guide RNAs (gRNAs) targeting the key candidate regulators (**Fig. 2.1 d**)

As our screen indicated that Usp22 is a positive regulator of Foxp3, we used RNPs to knock out *USP22* in human T_{reg} cells. We observed a significant decrease in FOXP3 mean fluorescence intensity (MFI) (**Fig. 2.1e and f**). These findings confirm critical regulation of Foxp3 by Usp22.

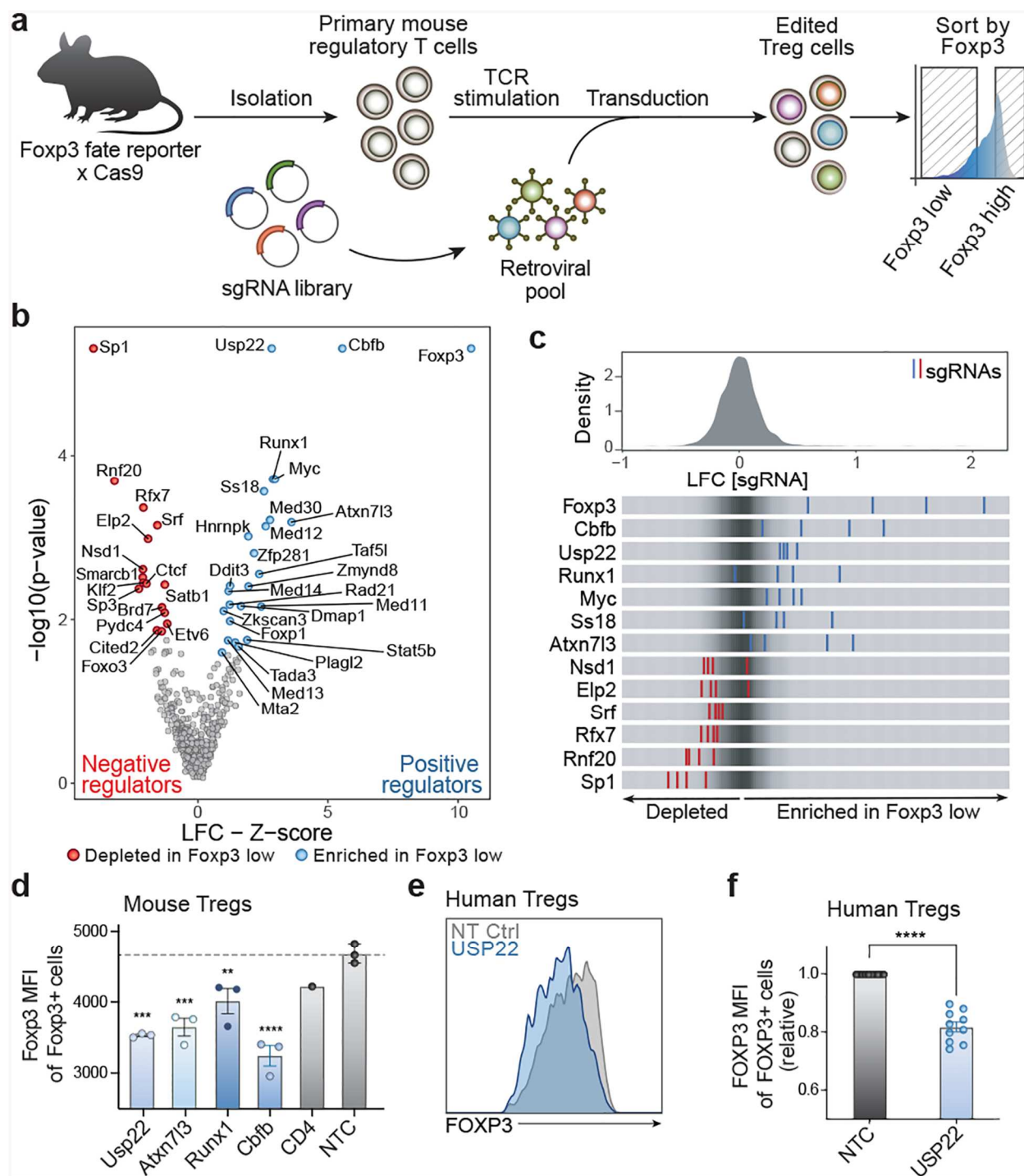


Figure 2.1 Discovery and validation of *Foxp3* regulators in primary mouse T_{reg} cells using a targeted pooled CRISPR screen. **a**, Schematic of pooled CRISPR screening platform in primary mouse T_{reg} cells. **b**, Volcano plot for hits from the screen. The *x*-axis shows *z*-score for gene-level \log_2 fold change (LFC); median of LFC for all sgRNAs per gene, scaled. The *y*-axis shows the *P* value as calculated by MAGeCK. Red indicates negative regulators (depleted in $Foxp3^{low}$ cells), whereas blue dots show positive regulators (enriched in $Foxp3^{low}$ cells) defined by false discovery rate (FDR) < 0.5 and *z* score > 0.5 . **c**, Top, distribution of sgRNA-level LFC values of $Foxp3^{low}$ cells over $Foxp3^{high}$ cells for 2,000 guides. Bottom, LFC for all four individual sgRNAs targeting genes enriched in $Foxp3^{low}$ cells (blue lines) and depleted genes (red lines), overlaid on grey gradient depicting the overall distribution. **d**, MFI of Foxp3 in $Foxp3^+$ cells. Each data point represents effects of an

independent gRNA for each target gene. Statistics are based on comparison with NTC. **e**, Representative histogram showing FOXP3 MFI (pre-gated on live cells) from human T_{reg} cells electroporated with NTC or USP22 RNPs. **f**, Statistical analysis of FOXP3 MFI in human T_{reg} cells from ten biological replicates. T_{reg} cells from each donor here were targeted with the same high efficiency gRNA (USP22-2). **g**, All data are presented as mean ± s.e.m. NS, not significant. **P* < 0.05, ***P* < 0.01, ****P* < 0.001, *****P* < 0.0001.

2.2.2 Usp22 is required for Foxp3 expression and T_{reg} lineage stability

To understand the in vivo significance of Usp22 in T_{reg} cells, we generated mice with T_{reg}-specific ablation of Usp22 by creating *Usp22^{fl/fl}* mice (**Fig. 2.2a and b**) and crossing them with *Foxp3^{YFP-cre}* mice¹⁸⁹. Western blot analysis confirmed specific deletion of Usp22 in T_{reg} cells, but not in CD4⁺ conventional T_{eff} cells (**Fig. 2.2c**). *Usp22^{fl/fl}Foxp3^{YFP-cre}* and *Usp22^{+/+}Foxp3^{YFP-cre}* are referred to as Usp22-knockout (22KO) or wild-type (WT) mice, respectively, indicating their *Usp22* status in T_{reg} cells. *Usp22^{+/+}Foxp3^{YFP-cre}* mice were used to control for possible confounding effects of *Foxp3^{YFP-cre}*. *Usp22^{fl/fl}Foxp3^{YFP-cre}* KO mice showed a marked decrease in Foxp3 MFI in T_{reg} cells isolated from spleens, thymus and peripheral lymph nodes (pLN) (**Fig. 2.3a-c**) compared with *Usp22^{+/+}Foxp3^{YFP-cre}* WT mice, as well as decreased T_{reg} cell frequencies (**Fig. 2.2d**). Western blot analysis confirmed a significant reduction in Foxp3 protein in *Usp22*-KO T_{reg} cells (**Fig. 2.2e**). A decrease in Foxp3⁺ cells was also seen in induced T_{reg} (iT_{reg}) cells, although the decrease was less pronounced with increasing levels of TGF-β (**Fig. 2.2f and g**). Given the diminished Foxp3 levels in *Usp22*-KO T_{reg} cells, we reasoned that these cells may exhibit defects in suppressive function. Indeed, *Usp22*-KO T_{reg} cells were less able to suppress T effector cells than WT T_{reg} cells from *Usp22^{+/+}Foxp3^{YFP-cre}* mice (**Fig. 2.2h, Fig. 2.3d**), and this defect could be rescued by heterologous expression of Foxp3 (**Fig. 2.2i and j**). These data substantiate the results of our screen and suggest that Usp22 promotes Foxp3 levels and is critical for T_{reg} function.

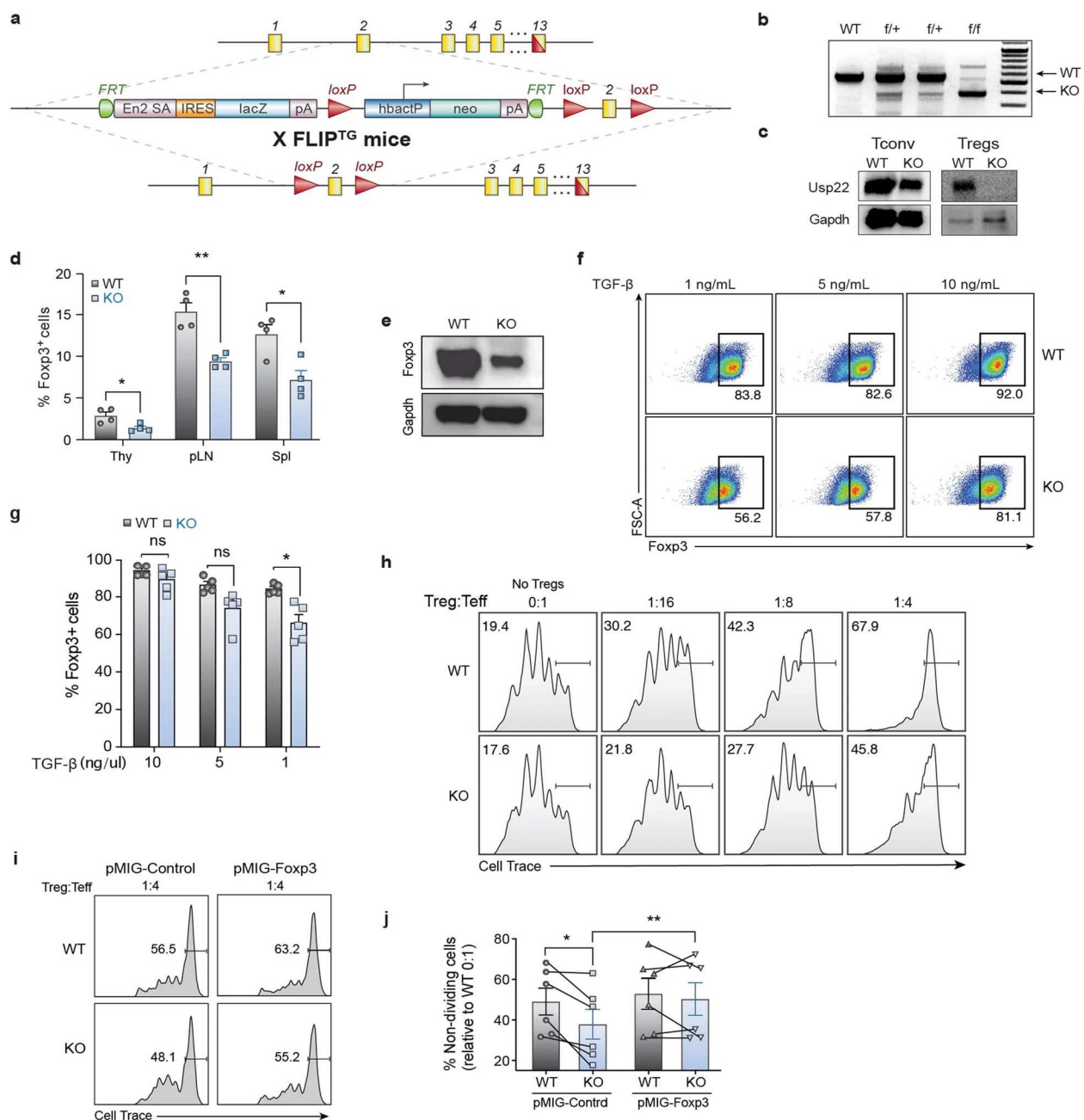


Figure 2.2 Design and validation of T_{reg}-specific *Usp22*-knockout mice. **a**, Schematic of the mouse *Usp22* locus. Targeting vector contains IRES-lacZ and a neo cassette inserted into exon 2. **b**, Genotyping by PCR showed a 600-bp band for the WT allele and a 400-bp band for mutant allele, simultaneously in the homozygous floxed (*f/f*) mice. **c**, Western blot analysis of *Usp22* in CD4⁺CD25⁻ conventional T cells (T_{conv}) and CD4⁺CD25⁺ T_{reg} cells isolated from *Usp22*^{+/+}*Foxp3*^{YFP-cre} WT and *Usp22*^{f/f}*Foxp3*^{YFP-cre} KO mice. GAPDH was used as a loading control. **d**, Statistical analysis of CD4⁺Foxp3⁺ T_{reg} frequencies, corresponding to Fig. 2.3. **e**, Western blot analysis of Foxp3 protein from T_{reg} cells isolated from spleen and lymph nodes of *Usp22*^{+/+}*Foxp3*^{YFP-cre} WT or *Usp22*^{f/f}*Foxp3*^{YFP-cre} KO mice. GAPDH was used as a loading control. **f**, iT_{reg} differentiation of naive CD4⁺ T cells from *Usp22*^{+/+}*Foxp3*^{YFP-cre} WT or *Usp22*^{f/f}*Foxp3*^{YFP-cre} KO mice with titration of TGF- β (as indicated). **g**, Summary of iT_{reg} differentiation of naive CD4⁺ T cells from *Usp22*^{+/+}*Foxp3*^{YFP-cre} WT or *Usp22*^{f/f}*Foxp3*^{YFP-cre} KO mice with titration of TGF- β (as indicated). **h**, In vitro suppressive activity of T_{reg} cells assessed by the division of naive CD4⁺CD25⁻ T cells. Naive T cells were labelled with cytosolic cell proliferation dye and activated by anti-CD3 and antigen-presenting cells (irradiated

splenocytes from WT mice, depleted of CD3⁺ T cells), then cocultured at various ratios (as indicated above) with YFP⁺ T_{reg} cells sorted from eight-week-old *Usp22*^{+/+}*Foxp3*^{YFP-cre} WT or *Usp22*^{fl/fl}*Foxp3*^{YFP-cre} KO mice. Numbers indicate the percentage of non-dividing cells for each ratio. **i**, In vitro suppressive activity of control (pMIG-Control) or Foxp3⁺ (pMIG-Foxp3) transduced YFP⁺ T_{reg} cells sorted from *Usp22*^{+/+}*Foxp3*^{YFP-cre} WT or *Usp22*^{fl/fl}*Foxp3*^{YFP-cre} KO mice. Naive T cells were labelled with cytosolic cell proliferation dye and activated then cocultured at 1:4 transduced YFP⁺ T_{reg} cells to naive T effectors (T_{eff}). Numbers indicate the percentage of non-dividing cells for each ratio. **j**, Summary of in vitro suppression experiments, corresponding to **i**. Lines connect paired samples. Ratios indicate the proportion of T_{reg} cells to naive T effectors (T_{eff}). Data are presented as the frequency of non-dividing cells relative to the corresponding WT 0:1 T_{reg}:T_{eff} control.

2.2.3 *Usp22* transcriptionally regulates Foxp3 through histone H2B deubiquitination

Control of Foxp3 stability, and thus T_{reg} function, can occur at the transcriptional and/or post-transcriptional level^{157,164,165,167}. Chromatin modifications at the *Foxp3* locus and other key loci can affect *Foxp3* transcription^{190–192}. As *Usp22* is a component of the chromatin-modifying SAGA complex, we hypothesized that *Usp22* controls Foxp3 expression through transcriptional regulation. IRES–YFP knock-in at the *Foxp3* locus of *Usp22*^{fl/fl}*Foxp3*^{YFP-cre} mice enabled us to use YFP as a reporter to assess the effect of *Usp22* on *Foxp3* transcript levels. Similar to endogenous Foxp3 protein, YFP MFI was significantly decreased in *Usp22*-null T_{reg} cells isolated from the thymus, pLN and spleen in *Usp22*^{fl/fl}*Foxp3*^{YFP-cre} mice compared with *Usp22*^{+/+}*Foxp3*^{YFP-cre} mice, despite normal T_{reg} frequencies (**Fig. 2.3e**; **Fig. 2.4a-c**). Furthermore, analysis by quantitative PCR with reverse transcription (RT–qPCR) showed that *Foxp3* transcripts were significantly reduced in splenic T_{reg} cells from *Usp22*^{fl/fl}*Foxp3*^{YFP-cre} compared with *Usp22*^{+/+}*Foxp3*^{YFP-cre} mice (**Fig. 2.3f**). RNA sequencing confirmed that *Foxp3* transcripts are significantly reduced in T_{reg} cells from *Usp22*^{fl/fl}*Foxp3*^{YFP-cre} mice relative to those from WT mice (**Fig. 2.3g**). *Foxp3* transcript levels were also lower as a result of acute targeting by *Usp22* RNPs in mouse and human T_{reg} cells, although these results were less consistent, perhaps owing to variability in knockout efficiency and/or other experimental factors (**Fig. 2.4d-f**).

Usp22 is required for SAGA-mediated deubiquitination of histones, which regulates transcriptional activity¹⁶⁹. We therefore tested whether histone ubiquitination was altered

in *Usp22*-KO T_{reg} cells. Western blot analysis confirmed that *Usp22^{fl/fl}Foxp3^{YFP-cre}* mice had increased levels of ubiquitinated histones 2A and 2B (H2AK119Ub and H2BK120Ub, respectively) in iT_{reg} cells compared with *Usp22^{+/+}Foxp3^{YFP-cre}* mice (**Fig. 2.4g**). Chromatin immunoprecipitation followed by quantitative PCR (ChIP–qPCR) showed increased H2BK120Ub in the conserved non-coding sequence 1 (CNS1) region of the *Foxp3* locus in *Usp22^{fl/fl}Foxp3^{YFP-cre}* T_{reg} cells, whereas effects on H2AK119Ub levels at the locus were not significant (**Fig. 2.4h-j**). Further interrogation with chromatin precipitation followed by genome-wide sequencing (ChIP–seq) revealed significant increases in H2BK120Ub levels across the *Foxp3* locus in *Usp22^{fl/fl}Foxp3^{YFP-cre}* T_{reg} cells compared with control T_{reg} cells. A significant accumulation of H2BK120Ub at the locus also was observed in T_{reg} cells electroporated with *Usp22* RNPs compared with those treated with NTC RNPs (**Fig. 2.3h**). These findings demonstrated that *Usp22* is essential for chromatin regulation at the *Foxp3* locus.

We next analyzed effects of *Usp22* loss on chromatin states across the T_{reg} genome. First, we found evidence that *Usp22* can co-occupy many *Foxp3*-bound regions in T_{reg} cells (**Fig. 2.5k**). *Foxp3*-bound regions tended to gain H2BK120Ub in *Usp22*-deficient cells compared with control cells, and increases in H2BK120Ub were more pronounced than effects on H2AK119Ub, suggesting that H2KB120Ub is probably the more relevant chromatin target of *Usp22* in T_{reg} cells (**Fig. 2.3h; Fig. 2.4k**). Considering the genome more broadly, we found that sites that significantly gained H2BK120Ub in both 22-KO and *Usp22* RNP-targeted T_{reg} cells were enriched for activating histone modifications (H3K4me3, H3K4me and H3K27ac), suggesting that changes occurred at gene regulatory elements, including at T_{reg} superenhancers (**Fig. 2.4l and m**). These data revealed a critical role for *Usp22* in control of H2KB120Ub across the T_{reg} chromatin landscape.

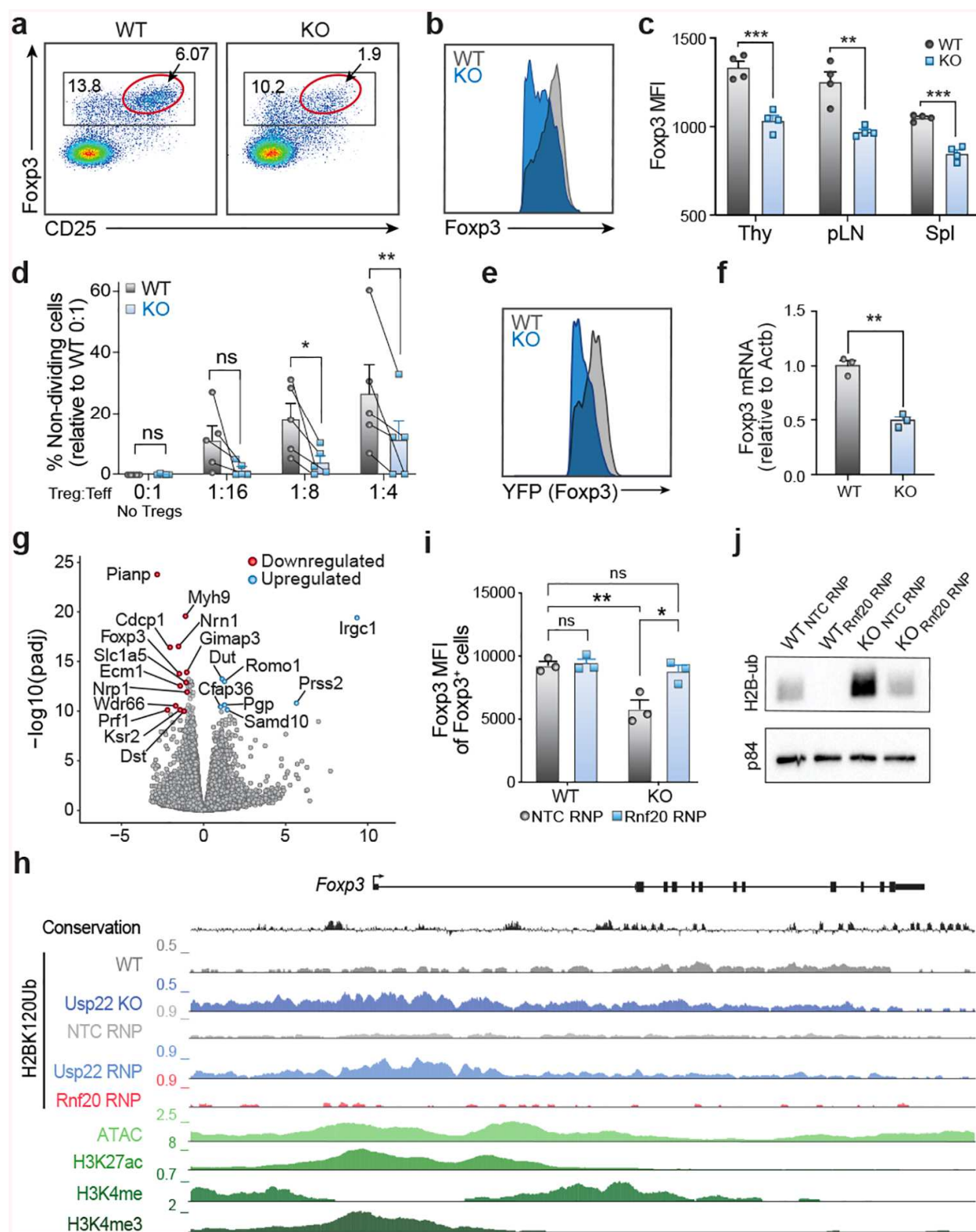


Figure 2.3 *Usp22* is required for *Foxp3* maintenance and *Treg* suppressive function. **a**, Representative flow cytometry analysis of the *Treg* population (gated on CD4⁺ cells) from the spleens of *Usp22*^{+/+}*Foxp3*^{YFP-cre} WT (*Usp22*^{+/+}) or *Usp22*^{fl/fl}*Foxp3*^{YFP-cre} KO (*Usp22*^{Treg-KO}) mice. A subset of *Treg* cells with the highest expression

of Foxp3 and CD25 is highlighted with a red gate. **b**, Histogram of Foxp3 expression in Foxp3⁺ T_{reg} cells from spleens of *Usp22*^{+/+}*Foxp3*^{YFP-cre} WT or *Usp22*^{fl/fl}*Foxp3*^{YFP-cre} KO mice from **a**. **c**, Statistical analysis of Foxp3 MFI from CD4⁺Foxp3⁺ T_{reg} cells in thymus (Thy), peripheral lymph nodes (pLN) and spleen (Spl) of *Usp22*^{+/+}*Foxp3*^{YFP-cre} WT or *Usp22*^{fl/fl}*Foxp3*^{YFP-cre} KO mice. **d**, Summary of in vitro suppression experiments, corresponding to Fig. 2.2h. Lines connect paired samples. Ratios indicate the proportion of T_{reg} cells to naive T_{eff} cells. Data are presented as the frequency of non-dividing cells relative to the corresponding WT 0:1 T_{reg}:T_{eff} control, with any negative values after normalization replaced with 0. **e**, Histogram of YFP expression in T_{reg} cells from the spleen and lymph nodes of *Usp22*^{+/+}*Foxp3*^{YFP-cre} WT or *Usp22*^{fl/fl}*Foxp3*^{YFP-cre} KO mice from Fig. 2.4a. **f**, RT-qPCR analysis of *Foxp3* mRNA levels in sorted YFP⁺ cells of spleen from *Usp22*^{+/+}*Foxp3*^{YFP-cre} WT or *Usp22*^{fl/fl}*Foxp3*^{YFP-cre} KO mice. **g**, Volcano plot for RNA sequencing of YFP⁺ T_{reg} cells sorted from *Usp22*^{+/+}*Foxp3*^{YFP-cre} WT or *Usp22*^{fl/fl}*Foxp3*^{YFP-cre} KO mice. The *x*-axis shows LFC and the *y*-axis shows $-\log_{10}$ of the adjusted *P* value (adj. *P*) as calculated by DESeq2. Genes downregulated in the KO are shown in red and genes upregulated are shown in blue defined by adjusted *P* < 1×10^{-10} and LFC > 1. **h**, Genome tracks of CHIP-seq for H2BK120Ub at the *Foxp3* locus in WT (*Usp22*^{+/+}), *Usp22*^{Treg-KO}, NTC RNP, *Usp22* RNP and *Rnf20* RNP treated T_{reg} cells. Evolutionary conservation, ATAC-seq, and CHIP-seq for H3K27ac, H3K4me3 and H3K4me in WT T_{reg} cells are also shown. **i**, Analysis of reciprocal regulation of Foxp3 by the deubiquitinase *Usp22* and E3 ubiquitin ligase *Rnf20*. Foxp3 MFI of T_{reg} cells sorted from *Usp22*^{+/+}*Foxp3*^{YFP-cre} WT or *Usp22*^{fl/fl}*Foxp3*^{YFP-cre} KO mice and then electroporated with either NTC RNP or *Rnf20* RNP. **j**, Western blot analysis of H2BK120Ub (H2B-ub) levels in T_{reg} cells sorted from *Usp22*^{+/+}*Foxp3*^{YFP-cre} WT or *Usp22*^{fl/fl}*Foxp3*^{YFP-cre} KO mice and then electroporated with either NTC RNP or *Rnf20* RNP; corresponding to **i**. p84 was used as a loading control.

2.2.4 *Usp22* and *Rnf20* reciprocally regulate Foxp3 transcription

Our screen nominated E3 ubiquitin ligase *Rnf20* as a candidate negative regulator of Foxp3. We hypothesized that the DUB *Usp22* and E3 ubiquitin ligase *Rnf20* might have an epistatic relationship, given their reciprocal effects on histone ubiquitination. To test this, we used RNPs to knock out *Rnf20* in 22KO or WT T_{reg} cells. Although Cas9 RNP-mediated loss of *Rnf20* alone did not significantly increase Foxp3 levels in WT T_{reg} cells (Extended Data **Fig. 2.3d and h**), RNP knockout of *Rnf20* was able to rescue the impairment in *Foxp3* transcript levels (assessed by YFP levels) in 22KO T_{reg} cells (**Fig. 2.4n**). Double RNP knockout of both *USP22* and *RNF20* in mouse and human T_{reg} cells also rescued FOXP3 protein levels relative to RNP knockout of *USP22* alone, although effects on transcript levels were less consistent (**Fig. 2.3i**; **Fig. 2.4e and f**). Consistent with a model in which the ubiquitin ligase *Rnf20* and DUB *Usp22* have reciprocal functional roles, we found that *Rnf20* co-occupies Foxp3-bound regions (**Fig. 2.4k**). Although *Rnf20* ablation did not affect already-low levels of H2BK120Ub at the *Foxp3* locus, targeting *Rnf20* tended to reduce H2BK120Ub levels at these Foxp3-bound

regions genome-wide, whereas Usp22 deficiency increased them (**Fig. 2.3h**, **Fig. 2.4k**). Western blot analysis confirmed that targeting Rnf20 in Usp22-deficient cells restored H2BK120Ub levels back to those of control T_{reg} cells (**Fig. 2.3j**). Together, these results show reciprocal regulation of Foxp3 and key chromatin regions in T_{reg} cells by Usp22 and Rnf20.

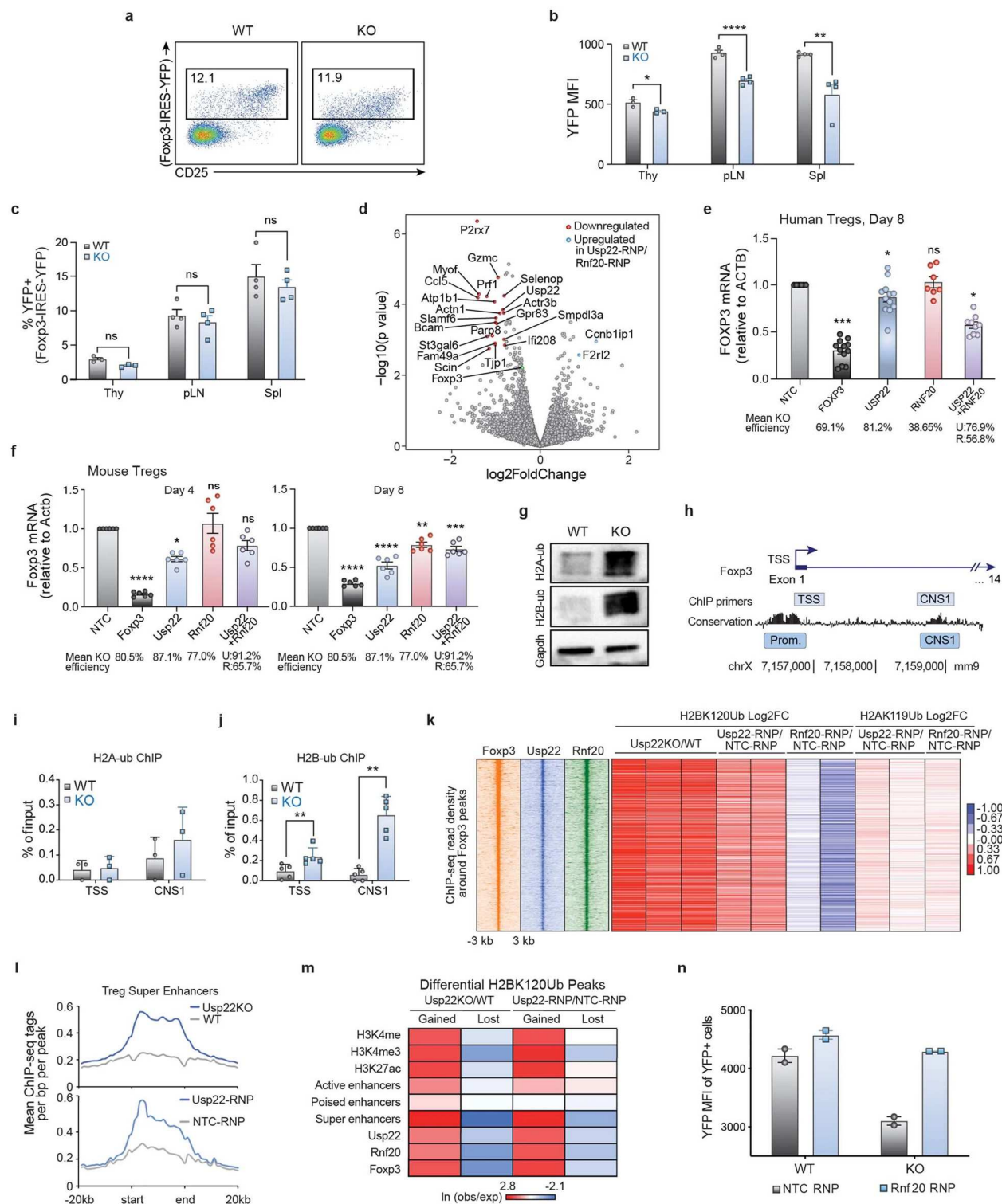


Figure 2.4 *Usp22* regulates *Foxp3* through transcriptional mechanisms. **a**, Representative flow cytometry analysis of the YFP⁺ T_{reg} population (gated on CD4⁺ cells) from the spleen and lymph nodes of *Usp22*^{+/+}*Foxp3*^{YFP-cre} WT or *Usp22*^{fl/fl}*Foxp3*^{YFP-cre} KO mice. **b**, Statistical analysis of YFP MFI in CD4⁺YFP⁺ T_{reg} cells from the thymus (Thy), peripheral lymph nodes (pLN) and spleen (Spl) of *Usp22*^{+/+}*Foxp3*^{YFP-cre} WT or *Usp22*^{fl/fl}*Foxp3*^{YFP-cre} KO mice. **c**, Statistical analysis of CD4⁺YFP⁺ T_{reg} frequencies in *Usp22*^{+/+}*Foxp3*^{YFP-cre} WT or *Usp22*^{fl/fl}*Foxp3*^{YFP-cre} KO mice, corresponding to **b**.

d, Volcano plot for RNA sequencing of *Usp22* RNP KO T_{reg} cells vs *Rnf20* RNP KO T_{reg} cells. The x axis shows LFC; the y axis shows $-\log_{10}$ of the P value as calculated by DESeq2. Genes downregulated in the *Usp22* RNP KO compared with *Rnf20* RNP KO are shown in red and upregulated genes are shown in blue, defined by $P < 5 \times 10^{-3}$ and LFC > 0.8 . Foxp3 (shown in green) trended down but did not reach significance. **e**, qPCR analysis of *FOXP3* mRNA in human T_{reg} cells from 2 donors 8 days post-electroporation with Cas9 RNPs targeting NTC, *FOXP3*, *USP22*, *RNF20* or both *USP22* and *RNF20*; normalized to the expression of *ACTB* transcripts. Data are mean \pm s.e.m. and are representative of at least two independent experiments. **f**, qPCR analysis of *Foxp3* mRNA levels in mouse T_{reg} cells 4- and 8-days post-electroporation with Cas9 RNPs targeting NTC, *Foxp3*, *Usp22*, *Rnf20* or both *Usp22* and *Rnf20*; normalized to the expression of *Actb* transcripts. **g**, Western blot analysis of ubiquitinated histone 2A (H2AK119Ub; H2A-ub) and ubiquitinated histone 2B (H2BK120Ub; H2B-ub) from iT_{reg} cells from *Usp22*^{+/+}*Foxp3*^{YFP-cre} WT or *Usp22*^{fl/fl}*Foxp3*^{YFP-cre} KO mice. GAPDH was used as a loading control. **h**, Schematic of *Foxp3* locus depicting PCR products used for ChIP-qPCR in **i** and **j**. **i**, ChIP-qPCR analysis of H2AK119Ub (H2A-ub), where primers amplified across the TSS and the CNS1 enhancer region of the *Foxp3* locus. Data are normalized to the input and are presented as mean \pm s.d. **j**, ChIP-qPCR data analysis for H2BK120Ub (H2B-ub) for PCR across the TSS and across the CNS1 enhancer region of the *Foxp3* locus. Data are normalized to the input and are presented as mean \pm s.d. **k**, Heat map of ChIP-seq read density for *Foxp3*, *Usp22* and *Rnf20* at sites bound by Foxp3 ranked by highest to lowest Foxp3-binding signal. The corresponding LFC for either H2BK120Ub or H2AK119Ub upon *Usp22* or *Rnf20* deletion at these sites are plotted on the right, with each biological replicate shown as an individual column. **l**, Average ChIP-seq read density of H2BK120Ub at T_{reg} superenhancers in control versus *Usp22*-deficient T_{reg} cells. **m**, Co-occurrence analysis showing the natural log of the ratio of the observed number of overlapping regions over the expected values for sites that either gain or lose H2BK120Ub in *Usp22*-deficient T_{reg} cells against publicly available histone modification data for H3K4me, H3K4me3 and H3K27ac as well as enhancer classes. **n**, Analysis of reciprocal regulation of Foxp3 by deubiquitinase *Usp22* and E3 ubiquitin ligase *Rnf20*. YFP MFI of T_{reg} cells sorted from *Usp22*^{+/+}*Foxp3*^{YFP-cre} WT or *Usp22*^{fl/fl}*Foxp3*^{YFP-cre} KO mice and then electroporated with either NTC or *Rnf20* RNP, corresponding with Figure 2.3j, where Foxp3 MFI from the same experiment is shown.

2.2.5 *Usp22* is a DUB of Foxp3

Foxp3 protein can also be dynamically controlled post-translationally by DUBs or ubiquitin ligases in response to proinflammatory signals^{193–195}. Since FOXP3 protein level decreased in the *Usp22*-deficient T_{reg} cells, we hypothesized that Foxp3 could be a substrate of *Usp22*. To test this hypothesis, we used co-immunoprecipitation (co-IP) and western blot analysis. *USP22* bound to Foxp3 in iT_{reg} cells, indicating that *Usp22* interacts endogenously to FOXP3 (**Fig. 2.5a**). Furthermore, ectopic expression of *USP22* largely diminished FOXP3 ubiquitination, indicating that *Usp22* is a DUB of Foxp3. In contrast, when the C19 ubiquitin-specific peptidase-inactive mutant of *USP22* was co-expressed, FoxP3 ubiquitination was less affected (**Fig. 2.5b**). Since *Usp22* functions as a specific DUB of Foxp3, it is possible that *USP22* could stabilize FOXP3 protein in T_{reg} cells. Indeed, when *USP22* was co-expressed, the degradation of FOXP3 was largely

blocked. Conversely, loss of USP22 in Tregs significantly facilitated FoxP3 protein degradation in primary Tregs (**Fig. 2.5c and d**). Collectively, these results demonstrated that Usp22 is a DUB that protects Foxp3 from ubiquitination-mediated degradation in T_{reg} cells.

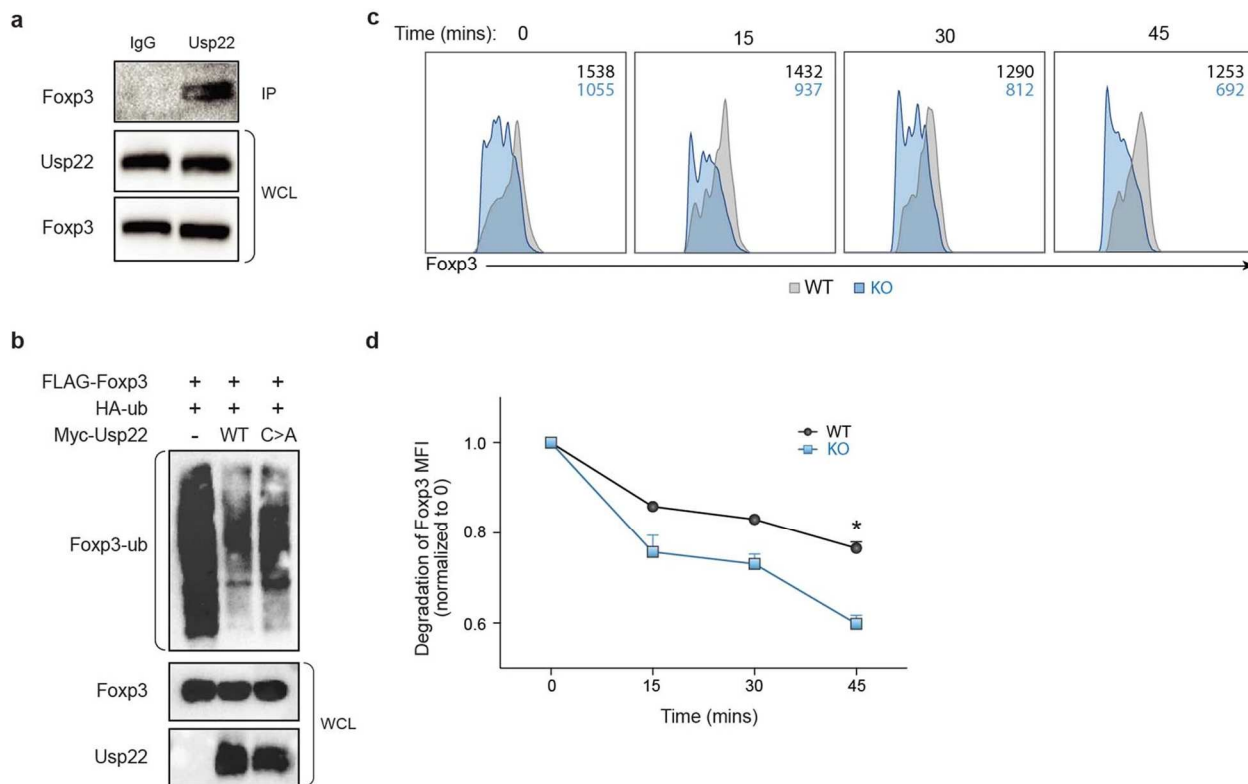


Figure 2.5 *Usp22* acts as a deubiquitinase to control post-translational Foxp3 expression. **a**, Endogenous interaction of Usp22 and Foxp3 in mouse iT_{reg} cells from WT mice. Rabbit Usp22 antibody was used to perform the immunoprecipitation and mouse Foxp3 antibody was used to detect the bound Foxp3. Normal rabbit IgG was used as control. Whole-cell lysates (WCL) were used as sample processing controls. **b**, Ubiquitination assay of Foxp3. HEK293 cells were cotransfected with Flag-Foxp3 and HA-ubiquitin (HA-ub) and either Myc-empty vector, Myc-Usp22, or the catalytically inactive mutant Myc-Usp22(C185A) (C>A), and then immunoprecipitated with anti-Flag and immunoblotted for HA-ubiquitin (Foxp3-ub). Whole-cell lysates were used as sample processing controls. **c**, Splenocytes isolated from *Usp22*^{+/-}*Foxp3*^{YFP-cre} WT or *Usp22*^{fl/fl}*Foxp3*^{YFP-cre} KO mice were treated with 200 $\mu\text{g ml}^{-1}$ cycloheximide for the indicated times. Inset numbers for each histogram indicate the MFI of Foxp3 in T_{reg} cells (black, WT; blue, KO). **d**, Foxp3 MFI from splenic $CD4^+CD25^+Foxp3^+$ T_{reg} population treated with 200 $\mu\text{g ml}^{-1}$ cycloheximide for the indicated time course ($n = 3$), corresponding to **c**.

2.2.6 T_{reg} -specific ablation of *Usp22* results in age-related spontaneous autoimmunity

To determine the *in vivo* functional relevance of *Usp22* deficiency in T_{reg} cells, we characterized the spontaneous autoimmune symptoms of *Usp22^{fl/fl}Foxp3^{YFP-cre}* mice. *Usp22^{fl/fl}Foxp3^{YFP-cre}* mice were born at normal size, but their body weights were lower than those of age- and sex-matched *Usp22^{+/+}Foxp3^{YFP-cre}* mice after five weeks of age (**Fig. 2.6a**, **Fig. 2.7a**). We next assessed whether this reduction in body weight might be a result of chronic inflammation, as is observed with impaired T_{reg} function¹⁶⁸. Indeed, flow cytometry analysis detected higher frequencies of $CD4^+$ and $CD8^+$ effector memory T cells ($CD44^{\text{high}}CD62L^{\text{low}}$) and corresponding lower percentages of naive T cells ($CD44^{\text{low}}CD62L^{\text{high}}$) in seven-month-old KO mice compared with WT mice (**Fig. 2.6b and c**). Additionally, histological analysis of aged mice detected lymphocyte infiltration in multiple organs, including kidney, lung, colon and liver (**Fig. 2.7b**). These findings underscore the importance of *Usp22* in T_{reg} function in age-related autoimmunity.

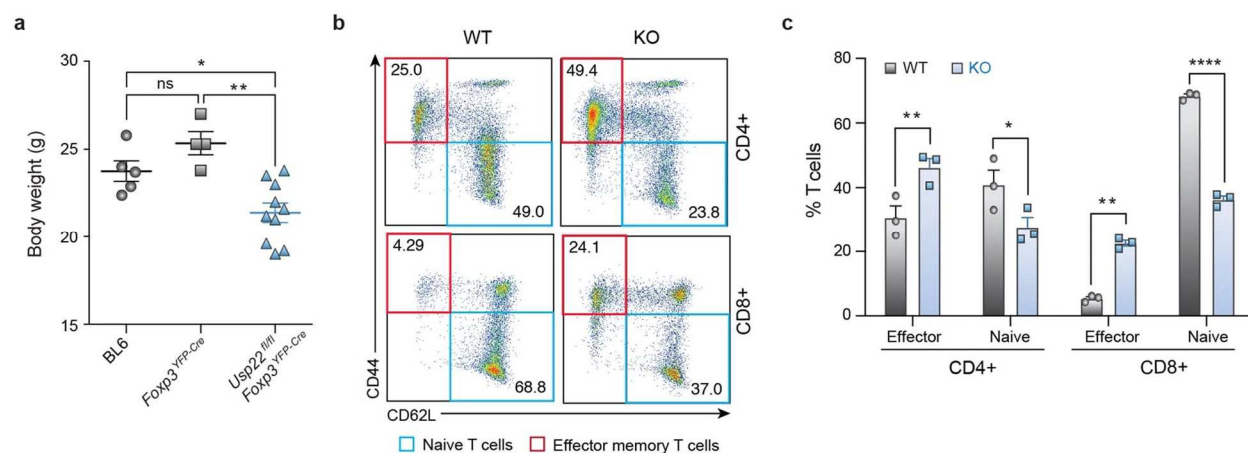


Figure 2.6 Autoimmune inflammation in T_{reg} -specific *Usp22* knockout mice. **a**, Body weight differences between 8-week-old, sex-matched C57BL/6 WT (BL/6), *Usp22^{+/+}Foxp3^{YFP-cre}* WT or *Usp22^{fl/fl}Foxp3^{YFP-cre}* KO mice. **b**, Representative flow cytometry analysis of CD44 and CD62L expression in splenic $CD4^+$ and $CD8^+$ T cells from aged seven-month-old *Usp22^{+/+}Foxp3^{YFP-cre}* WT and *Usp22^{fl/fl}Foxp3^{YFP-cre}* KO mice. Numbers in quadrants indicate percentage of each cell population. **c**, The frequency of splenic $CD4^+$ and $CD8^+$ effector T cells ($CD44^{\text{high}}CD62L^{\text{low}}$) and naive T cells ($CD44^{\text{low}}CD62L^{\text{high}}$) of aged seven-month-old *Usp22^{+/+}Foxp3^{YFP-cre}* WT and *Usp22^{fl/fl}Foxp3^{YFP-cre}* KO mice summarized, corresponding to **b**.

2.2.7 Treg-specific ablation of Usp22 results in enhanced severity of EAE and colitis

We further validated the *in vivo* requirements for Usp22 in T_{reg} suppressive function using multiple models of autoimmune disease. We assessed T_{reg} suppressive activity *in vivo* using an adoptive transfer model of colitis and a MOG-induced experimental autoimmune encephalomyelitis (EAE) model. In the colitis model, mice that received defective 22KO T_{reg} cells were not protected against colitis, in contrast to those that received WT T_{reg} cells (**Fig. 2.7c and d**). Similarly, in the EAE model, *Usp22^{fl/fl}Foxp3^{YFP-cre}* mice exhibited worse clinical scores compared with WT mice, suggesting an inability of the Usp22-deficient T_{reg} cells to limit autoimmunity (**Fig. 2.7e**).

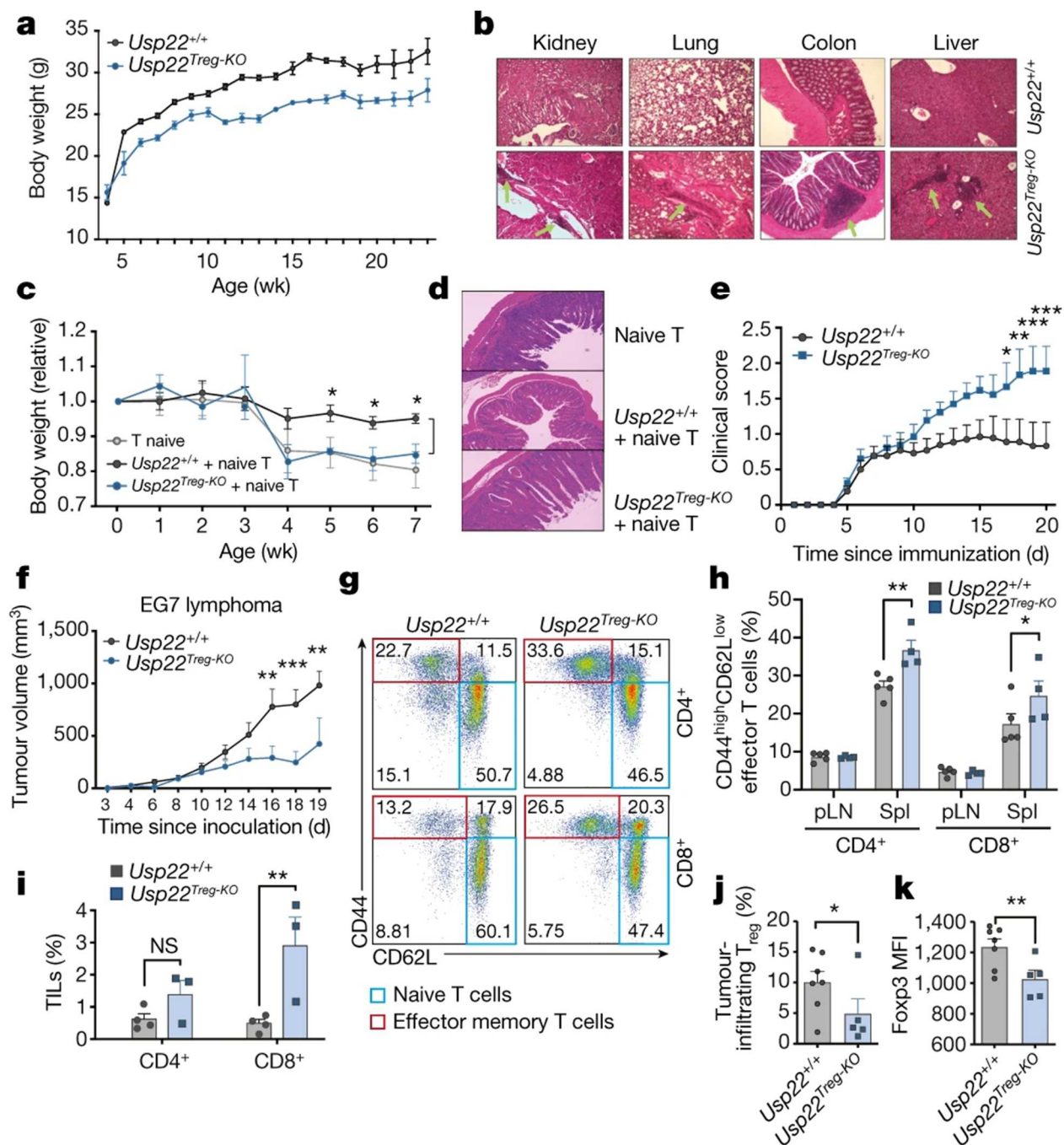


Figure 2.7 *T_{reg}*-specific ablation of *Usp22* results in autoimmunity and enhances antitumor immunity. **a**, Body weight differences between *Usp22*^{+/+}*Foxp3*^{YFP-cre} WT (*Usp22*^{+/+}) or *Usp22*^{fl/fl}*Foxp3*^{YFP-cre} KO (*Usp22*^{Treg-KO}) littermate mice. **b**, Hematoxylin and eosin (H&E) staining of kidney, lung, colon and liver sections from seven-month-old *Usp22*^{+/+}*Foxp3*^{YFP-cre} WT or *Usp22*^{fl/fl}*Foxp3*^{YFP-cre} KO mice. Original magnification, 100×. **c**, Body weight of *Rag*^{-/-} recipient mice over time after adoptive transfer of CD4⁺CD25⁻CD44^{low}CD62^{high} (CD45.1⁺) naive T cells sorted from SJL mice, alone or together with CD4⁺YFP⁺ (CD45.2⁺) T_{reg} cells from nine-week-old *Usp22*^{+/+}*Foxp3*^{YFP-cre} WT or *Usp22*^{fl/fl}*Foxp3*^{YFP-cre} KO mice, relative to weight at day 0. **d**, H&E staining of colon tissues from the *Rag*^{-/-} recipient mice shown in **c**, seven weeks after transfer. Original magnification, 100×. **e**, Clinical severity of EAE in *Usp22*^{+/+}*Foxp3*^{YFP-cre} WT or *Usp22*^{fl/fl}*Foxp3*^{YFP-cre} KO mice was monitored for 20 days after immunization with MOG peptide. **f**, EG7 lymphoma tumor volume in *Usp22*^{+/+}*Foxp3*^{YFP-cre} WT or *Usp22*^{fl/fl}*Foxp3*^{YFP-cre} KO mice. Mice were

subcutaneously inoculated with 1×10^6 EG7 cells. Tumor volume was measured every 1–2 days by scaling along 3 orthogonal axes (x, y and z) and calculated as $(xyz)/2$. **g**, Representative flow cytometry analysis of the expression of CD44 and CD62L in CD4⁺ and CD8⁺ T cells of spleen from *Usp22*^{+/+}*Foxp3*^{YFP-cre} WT or *Usp22*^{fl/fl}*Foxp3*^{YFP-cre} KO EG7 tumor-bearing mice. **h**, Frequency of effector T cells (CD44^{high}CD62L^{low}) from *Usp22*^{+/+}*Foxp3*^{YFP-cre} WT or *Usp22*^{fl/fl}*Foxp3*^{YFP-cre} KO EG7 tumor-bearing mice summarized. **i**, Percentage of tumor-infiltrating lymphocytes (TILs) in EG7-bearing *Usp22*^{+/+}*Foxp3*^{YFP-cre} WT or *Usp22*^{fl/fl}*Foxp3*^{YFP-cre} KO mice collected 19 days after tumor inoculation. **j**, Percentage of tumor-infiltrating T_{reg} cells in EG7 tumor-bearing *Usp22*^{+/+}*Foxp3*^{YFP-cre} WT or *Usp22*^{fl/fl}*Foxp3*^{YFP-cre} KO mice collected 19 days after tumor inoculation. **k**, Foxp3 MFI of the CD4⁺Foxp3⁺ EG7 tumor-infiltrating T_{reg} population in *Usp22*^{+/+}*Foxp3*^{YFP-cre} WT or *Usp22*^{fl/fl}*Foxp3*^{YFP-cre} KO mice.

2.2.8 T_{reg}-specific Usp22 ablation enhances antitumor immunity

Since these data suggest that Usp22 deficiency reduces Foxp3 stability and impairs T_{reg} suppressive function, we next tested whether *Usp22^{fl/fl}Foxp3^{YFP-cre}* mice would exhibit increased antitumor immunity using syngeneic tumor models. As expected, growth of EG7 lymphoma tumors was significantly inhibited by T_{reg}-specific Usp22 gene deletion (**Fig. 2.7f**). We next examined the immune responses in these tumor-bearing mice and found greater proportions of effector memory CD4⁺ and CD8⁺ T cells in the spleens of *Usp22^{fl/fl}Foxp3^{YFP-cre}* mice compared with WT mice (**Fig. 2.7g and h**). We also found increased frequencies of interferon- γ (IFN- γ) and granzyme B producing CD8⁺ T cells, as well as increased mRNA levels of *Ifn-gamma*, *Gzmb* and *Cd8a* from tumor tissue (**Fig. 2.8d**), suggesting an increased cytotoxic lymphocyte response owing to impaired T_{reg} suppressive function. Splenic T_{reg} cells from these mice showed reduced MFIs of Foxp3-target genes important for T_{reg} function, including CD25 (**Fig. 2.8a-c**). Further analysis of tumor-infiltrating lymphocytes indicated a significant increase in CD8⁺ T cell frequencies and decreased percentages of intratumoral Foxp3⁺ T_{reg} cells in EG7 tumor-bearing *Usp22^{fl/fl}Foxp3^{YFP-cre}* mice (**Fig. 2.7i and j**). Consistent with the lymphoid organs, we found that the Foxp3 MFI was significantly decreased in the intratumoral T_{reg} cells from EG7 tumor-bearing *Usp22^{fl/fl}Foxp3^{YFP-cre}* mice (**Fig. 2.7k**). Together, these data indicate that *Usp22* knockout impairs T_{reg} suppressive function and reduces T_{reg} abundance in EG7 tumors, consequently enhancing the antitumor immune response. We also showed that *Usp22^{fl/fl}Foxp3^{YFP-cre}* mice exhibit increased antitumor immunity in additional tumor models (**Fig. 2.8e-m**). These results highlight Usp22 in T_{reg} cells as a potential target for antitumor immunotherapies.

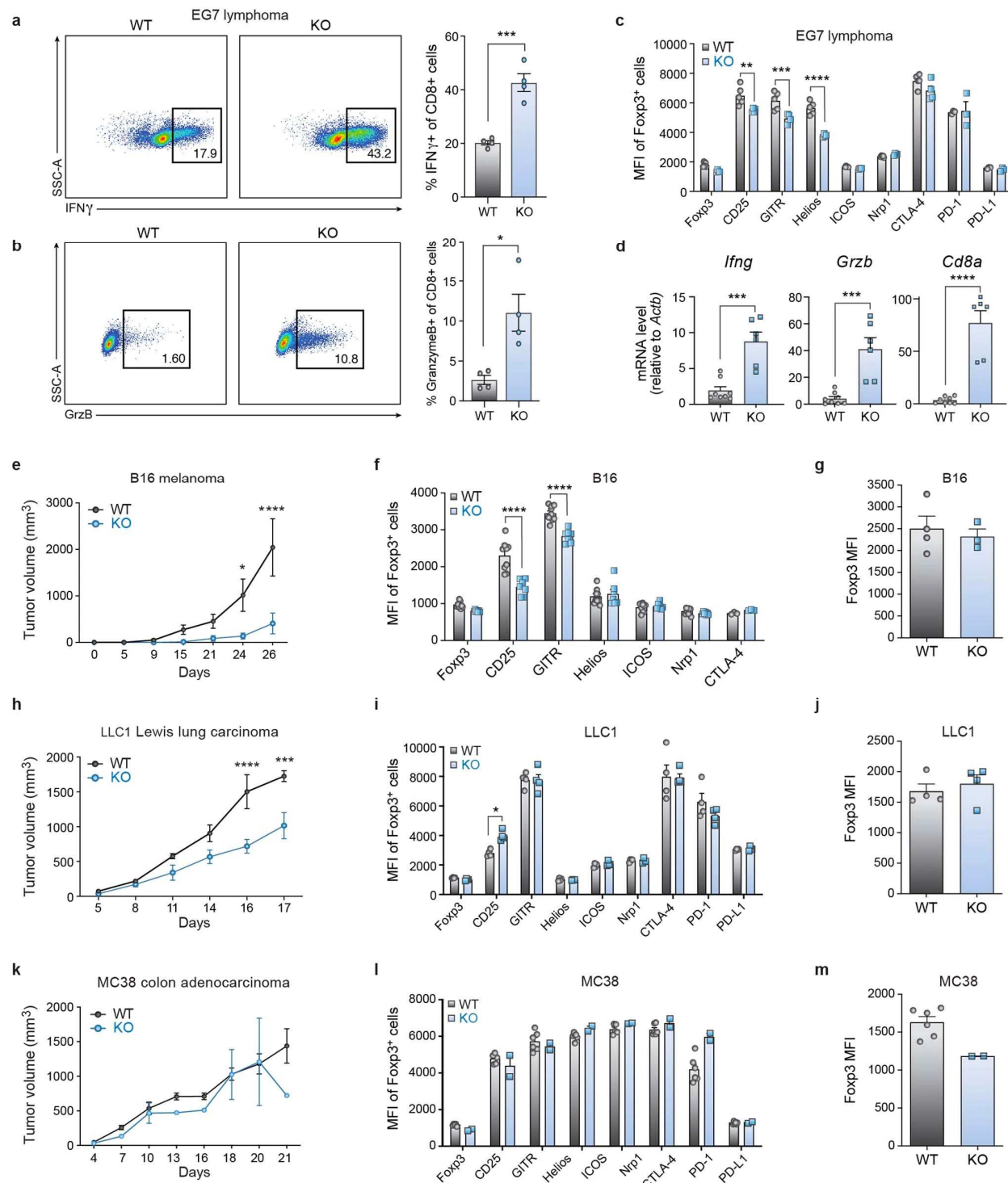


Figure 2.8 Tumor growth is inhibited in *Treg*-specific *Usp22* knockout mice in multiple cancer models. **a**, Left, representative flow cytometric analysis of splenic IFN-gamma in CD8 $^+$ T cells from EG7 tumor-bearing *Usp22* $^{+/+}$ *Foxp3* $^{YFP-cre}$ WT or *Usp22* $^{fl/fl}$ *Foxp3* $^{YFP-cre}$ KO mice. Right, statistical analysis of IFN-gamma production by splenic CD8 $^+$ T cells from EG7 tumor-bearing *Usp22* $^{+/+}$ *Foxp3* $^{YFP-cre}$ WT or *Usp22* $^{fl/fl}$ *Foxp3* $^{YFP-cre}$ KO. **b**, Left, representative flow cytometric analysis of splenic granzyme B (GrzB) in CD8 $^+$ T cells from EG7 tumor-bearing *Usp22* $^{+/+}$ *Foxp3* $^{YFP-cre}$ WT or *Usp22* $^{fl/fl}$ *Foxp3* $^{YFP-cre}$ KO mice. Right, statistical analysis of granzyme B production by splenic CD8 $^+$ T cells from EG7 tumor-bearing *Usp22* $^{+/+}$ *Foxp3* $^{YFP-cre}$ WT or *Usp22* $^{fl/fl}$ *Foxp3* $^{YFP-cre}$ KO mice. **c**, The MFI of various T_{reg} markers (as indicated) from splenic

CD4⁺Foxp3⁺ T_{reg} cells from *Usp22*^{+/+}*Foxp3*^{YFP-cre} WT or *Usp22*^{fl/fl}*Foxp3*^{YFP-cre} KO EG7 tumor-bearing mice, assessed by flow cytometry. **d**, qPCR analysis of *Ifng*, *Gzmb* and *Cd8a* mRNA levels in the tumor tissue of *Usp22*^{+/+}*Foxp3*^{YFP-cre} WT or *Usp22*^{fl/fl}*Foxp3*^{YFP-cre} KO EG7 tumor-bearing mice. **e**, Tumor volumes from *Usp22*^{+/+}*Foxp3*^{YFP-cre} WT or *Usp22*^{fl/fl}*Foxp3*^{YFP-cre} KO mice subcutaneously inoculated with 5×10^4 B16 melanoma cells. For **e**, **h**, **k**, tumor volumes were measured every 2–3 days by scaling along 3 orthogonal axes (*x*, *y* and *z*) and calculated as $(xyz)/2$. **f**, The MFI of various T_{reg} markers (as indicated) from splenic CD4⁺Foxp3⁺ T_{reg} cells in *Usp22*^{+/+}*Foxp3*^{YFP-cre} WT or *Usp22*^{fl/fl}*Foxp3*^{YFP-cre} KO B16 tumor-bearing mice, assessed by flow cytometry. **g**, Foxp3 MFI of Foxp3⁺ cells from tumor-infiltrating T_{reg} cells in *Usp22*^{+/+}*Foxp3*^{YFP-cre} WT or *Usp22*^{fl/fl}*Foxp3*^{YFP-cre} KO B16 tumor-bearing mice. **h**, Tumor volumes from *Usp22*^{+/+}*Foxp3*^{YFP-cre} WT or *Usp22*^{fl/fl}*Foxp3*^{YFP-cre} KO mice subcutaneously inoculated with 1×10^6 LLC1 Lewis lung carcinoma cells. **i**, The MFI of various T_{reg} markers (as indicated) from splenic CD4⁺Foxp3⁺ T_{reg} cells in *Usp22*^{+/+}*Foxp3*^{YFP-cre} WT or *Usp22*^{fl/fl}*Foxp3*^{YFP-cre} KO LLC1 tumor-bearing mice, assessed by flow cytometry. **j**, Foxp3 MFI of Foxp3⁺ cells from tumor-infiltrating T_{reg} cells in *Usp22*^{+/+}*Foxp3*^{YFP-cre} WT or *Usp22*^{fl/fl}*Foxp3*^{YFP-cre} KO LLC1 tumor-bearing mice. **k**, Tumor volumes from *Usp22*^{+/+}*Foxp3*^{YFP-cre} WT or *Usp22*^{fl/fl}*Foxp3*^{YFP-cre} KO mice subcutaneously inoculated with 1×10^6 MC38 colon adenocarcinoma cells. **l**, The MFI of various T_{reg} markers (as indicated) from splenic CD4⁺Foxp3⁺ T_{reg} cells in *Usp22*^{+/+}*Foxp3*^{YFP-cre} WT or *Usp22*^{fl/fl}*Foxp3*^{YFP-cre} KO MC38 tumor-bearing mice, assessed by flow cytometry. **m**, Foxp3 MFI of Foxp3⁺ cells from tumor-infiltrating T_{reg} cells in *Usp22*^{+/+}*Foxp3*^{YFP-cre} WT or *Usp22*^{fl/fl}*Foxp3*^{YFP-cre} KO MC38 tumor-bearing mice.

2.3 Conclusion

In this study, we developed a CRISPR-based pooled screening platform for primary mouse T_{reg} cells and applied this technology for systematic identification of gene modifications that control Foxp3 levels. We identified several regulators of Foxp3, including *Usp22* and *Rnf20*, developed a T_{reg}-specific *Usp22*-knockout mouse, and showed that *Usp22* is critical for stabilizing Foxp3 and maintaining T_{reg} suppressive functions in vivo. We demonstrated that *Usp22* is a regulator of *Foxp3* transcript levels, probably through deubiquitination of H2B at *Foxp3* and other key loci, and that *Usp22* can also regulate Foxp3 post-translationally. Mice with *Usp22*-null T_{reg} cells exhibited an impaired ability to resolve autoimmune inflammation and an enhanced antitumor immune response. This study identifies Foxp3 regulators that can be perturbed to fine tune T_{reg} function and specifically defines the function of *Usp22* and *Rnf20* as important modulators of Foxp3 and potential targets for T_{reg} immunotherapies.

Usp22 could be a particularly attractive target for cancer immunotherapy, because—in addition to its role in T_{reg} cells, which can limit antitumor immune responses—overexpression of

Usp22 in cancer cells is associated with poor prognosis in a variety of tumor types¹⁹⁶, and Usp22 knockdown in cancer cells can induce their apoptosis¹⁷¹. Furthermore, Usp22 impairs T_{reg} suppressive activity without affecting the functions of T_{eff} cells (data not shown). In summary, our findings further emphasize the importance of deubiquitinase in regulating immune system and state that Usp22 could not only be a tumorigenesis factor, but also be a positive regulator of T_{reg} cells, which provide another reason to choose Usp22 as a potential target in the cancer treatment.

The innovation of this proposed study is multiple folds: **(1)** This study defines the physiological role of Usp22 and Rnf20 on Foxp3 expression and T_{reg} suppressive function, which expands our knowledge on T_{reg} biology and immune regulation; **(2)** This study provides a rationale for the antitumor immune therapy against immunogenic, chemotherapy-resistant cancers such as melanoma by targeting Usp22; and **(3)** Our lab is the first to develop USP22 conditional knockout using the Cre-LoxP system to study USP22 function in the context of the immune system as well as other tissues and organs.

CHAPTER 3: The Tumor Microenvironment Enhances T_{reg} Fitness through Upregulation of a Foxp3-specific Deubiquitinase Module

3.1 Rationale

Interactions between malignant and non-transformed cells create the TME. TME factors, in addition to directly promote tumor cell growth, are also critical to reprogram immune response to evade antitumor immunity^{32,103,197–199}. For example, cytokines and chemokines produced by both infiltrated immune cells and tumor cells can induce and attract suppressive T_{reg} cells^{76,80,200}. As stated in section 1.3, iT_{reg} cells have the capability to adapt themselves to the harsh conditions found within the TME. Identifying the mechanisms of this adaptation can identify superior therapeutic candidates controlling the expression and stability of Foxp3 *specifically in the TME*.

While the exact composition of iT_{reg} cells, and whether the majority of this population consists of natural nT_{reg} or tumor-induced T_{reg} cells, remains unknown⁶⁹, it is likely that both populations, although epigenetically distinct, thrive in the TME and further aid in dampening anti-tumor immunity. Interestingly, iT_{reg} display upregulated expression of Foxp3^{72,102}, which functions to enhance T_{reg} fitness and adaptation in the TME. However, the molecular mechanisms underlying how and which TME factors upregulate Foxp3 expression to potentiate iT_{reg} suppressive function remains unknown.

Foxp3 expression and stability can be regulated from the transcriptional to the post-translational level, with each layer independently controlling the stability and overall function of T_{reg} cells. Particularly, a newly appreciated layer of Foxp3 regulation and T_{reg} functional modulation is through ubiquitination^{195,201}. Ubiquitination of histones on the Foxp3 promoter and conserved non-coding DNA sequence (CNS) regions via E3 ubiquitin ligases results in chromatin condensation and lack of Foxp3 transcription¹⁶⁶. Furthermore, direct ubiquitination of the FOXP3

protein can result in proteasomal degradation. Importantly, ubiquitin may be removed from these sites by deubiquitinating enzymes (DUBs), functioning to both open the chromatin at the transcriptional level, and to stabilize FOXP3 at the protein level ²⁰¹. The balance between E3 Ligases and DUBs on Foxp3 expression results in an equilibrium state that regulates Foxp3 levels within T_{reg} cells. We and others have discovered three members of the ubiquitin specific peptidase (USP) family as direct modulators of FOXP3 deubiquitination at the transcriptional and/or post-translational level: Usp7, Usp21, and Usp22 ^{167,168,201}. However, the broad environmental cues and cellular regulation of these deubiquitinases remain unknown. Here, we investigate the role of the TME on the USP-FOXP3 axis, and develop the first Usp22-specific inhibitor capable of antitumor activity.

3.2 Results

3.2.1 Selective upregulation of FoxP3 deubiquitinases in iT_{reg} cells

Since tumors create a hostile microenvironment where immune cell function is greatly altered, we began by characterizing the suppressive profiles of murine iT_{reg} cells (**Fig. 3.1**). Upon subcutaneous injection of B16 melanoma, LLC1 Lewis Lung Carcinoma, and EG7 Lymphoma into WT Foxp3^{YFP-cre} (WT) mice, iT_{reg} displayed both increased percentages of FOXP3⁺ cells and FOXP3 protein levels relative to splenic T_{reg} cells within the same mouse as well as against a non-challenged control mouse (**Fig. 3.1a-c**). Furthermore, iT_{reg} cells in each tumor type exhibited increased surface expression of multiple known T_{reg} suppressive markers including CTLA-4 and PD-1 (**Fig. 3.1d-g**). These data suggest that iT_{reg} cells have elevated immune suppressive functions through the upregulation of FOXP3 and surface inhibitory receptors, which is consistent with previous studies demonstrating that human intratumor T_{reg} cells display enhanced suppressive function ¹⁰⁰.

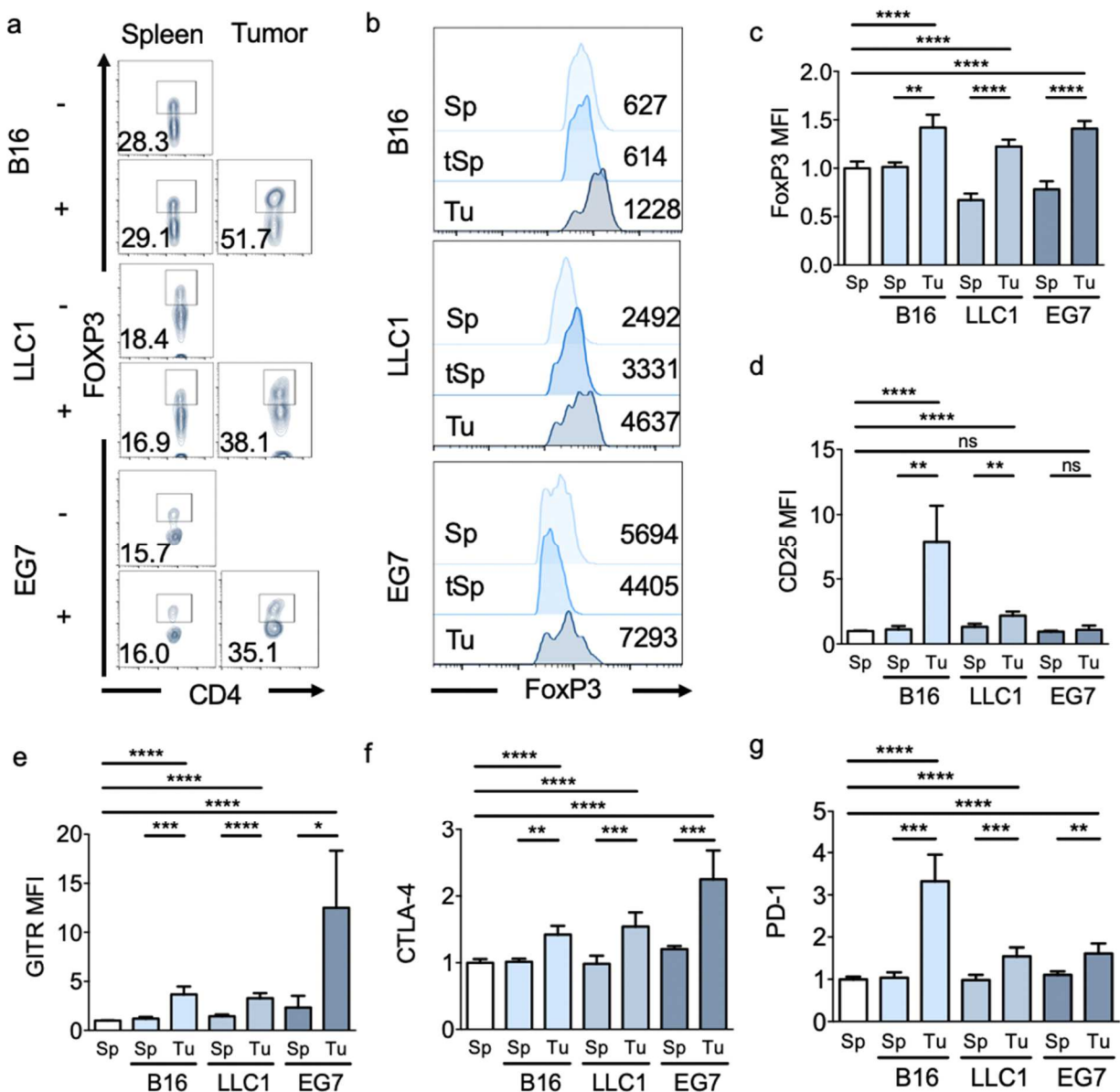


Figure 3.1 Intratumoral T_{reg} cells have increased *Foxp3* and activation markers. **a**, Representative CD4+ FOXP3+ percentage by flow cytometry of cells from non-tumor challenged controls and B16-, LLC1-, and EG7-challenged mice. B16: n=3-4, EG7: n=2-6, and LLC1: n=5-6. **b**, Representative overlay of FOXP3 MFI in tumor and spleen of CD45+ CD4+ FOXP3+ (Treg) cells of control and tumor-challenged mice. **c**, Quantification of FOXP3 MFI in control spleen and tumor-challenged spleen and tumor T_{reg} cells. n=4-11. **d-g**, MFI of Treg cell-associated markers under control T_{reg} cells isolated from the spleen and splenic and tumor T_{reg} cells from B16, EG7, or LLC1 challenged animals. CD25: n=4-11; GITR: n=3-11; CTLA-4: n=4-11; PD-1: n=4-11. All MFI values calculated relative to WT T_{reg} cell levels of non-challenged mice spleens. **c-g**, Two-tailed unpaired t-test was performed to determine statistical significance. All data are presented as mean \pm stdev. NS, not significant. * $P < 0.05$, ** $P < 0.01$, *** $P < 0.001$, **** $P < 0.0001$.

As the three FOXP3-targeting USPs aid in maintaining FOXP3 stability¹⁶⁶⁻¹⁶⁸, we hypothesized that modulation of their expression may drive the FOXP3 upregulation in iT_{reg} cells. Interestingly, the mRNA level of Usp22 was consistently increased within iT_{reg} cells in comparison to the peripheral T_{reg} cells harvested from same mouse or non-challenged controls, but Usp7 mRNA level was unchanged. In contrast, Usp21 mRNA level was only increased under B16 challenge, suggesting that Usp21 upregulation in T_{reg} cells occurs only under certain TME conditions (**Fig. 3.2a-c**). These data indicate that one or many factors in the TME upregulate both Usp22 and Usp21 transcription to potentially stabilize FOXP3, leading to enhanced iT_{reg} function. To support this notion, we further confirmed that Usp22 is upregulated in T_{reg} cells isolated from human tumor lung tissue patient samples (LTu) in comparison to adjacent healthy lung tissue (AHL) (**Fig. 3.2d**). This upregulation shows a strong positive correlation with FoxP3 upregulation within the LTu patient samples, suggesting Usp22 promotes Foxp3 expression in iT_{reg} cells in human tumors. Similar to our observation from the syngeneic lung cancer model, Usp21 was not increased in human lung tumor iT_{reg} cells nor did it have a significantly positive correlation with Foxp3 (**Fig. 3.2d**), suggesting that Usp22 is the more dominant USP in T_{reg} cells within the tumor at least in lung cancer.

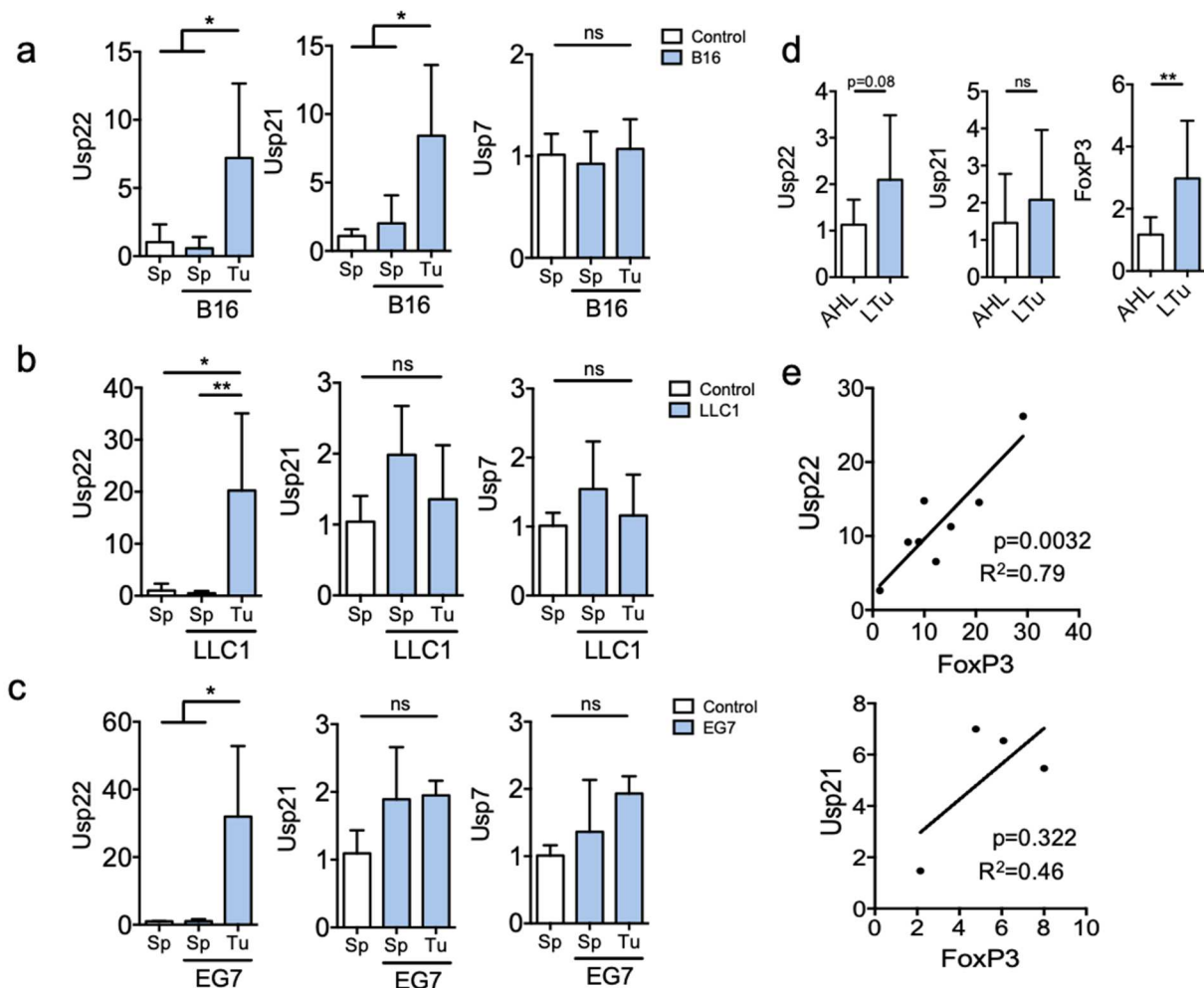


Figure 3.2. Intratumoral T_{reg} cells have increased mRNA expression of *Usp22* and *Usp21*. **a-c**, mRNA level of YFP⁺ sorted T_{reg} cells from control mice spleens, and tumor-challenged mice spleens and tumor cells. All mRNA values calculated relative to WT T_{reg} cell levels of unchallenged mice. spleens B16) *Usp22*: n=5-6, *Usp21*: n=3-5, *Usp7*: n=3-5. LLC1) *Usp22*: n=5-6, *Usp21*: n=3-6, *Usp7*: n=3-6. EG7) *Usp22*: n=4-5, *Usp21* n=3-4, *Usp7*: n=3-7. **d**, mRNA level of *Usp22*, *Usp21* and *Foxp3* in CD4⁺CD25⁺CD127⁻ T_{reg} cells isolated from human lung cancer patients relative to T_{reg} cells recovered from healthy lung tissue isolated from the same patient. AHL: adjacent healthy lung; LTu: lung tumor. *Usp22*: n=8, *Usp21*: n=3, *Foxp3*: n=11. **e**, mRNA level of *Usp21* and *Foxp3* in T_{reg} cells isolated from human lung cancer patients. AHL: adjacent healthy lung; LTu: lung tumor n=9. **a-c**, Two-tailed unpaired t-test was done to determine statistical significance. **d**, Two-tailed paired t-test was performed to determine statistical significance of *Foxp3* and *Usp22* in Ltu vs. AHL. **e**, Linear regression was calculated for the correlation between *Usp22* and *Foxp3* within Ltu. All data are presented as mean \pm stdev. NS, not significant. * $P < 0.05$, ** $P < 0.01$, *** $P < 0.001$, **** $P < 0.0001$.

3.2.2 Tumor-derived TGF-beta selectively induces Usp22 and Usp21 in T_{reg} cells

As soluble factors secreted by the tumors are known to alter immune cell function^{75,140}, we investigated the role of TME-soluble factors in regulating Usp22 and Usp21 in iT_{reg} cells. We exposed *in vitro* induced (i)T_{reg} cells to media obtained from cultured tumor cells (tumor conditioned media or TCM) (**Fig. 3.3a**). Interestingly, TCM from B16 and LLC1, but not EG7 cells, enhanced Usp22 and Usp21 mRNA levels (**Fig. 3.4a**). In contrast, the levels of Usp7 remained unchanged, recapitulating the results in Fig. 1. Similar to the mRNA levels, USP22 and USP21 protein levels were increased upon incubation with LLC1 TCM (**Fig. 3.4b**). Consistently, the addition of EG7 cultured media was not able to enhance any of the USPs at the protein level (**Fig. 3.4b**), indicating that specific tumor types selectively inducing Foxp3 deubiquitinases in T_{reg} cells.

Many types of tumors secrete large amounts of TGF-beta, which dampens immune responses and promotes metastasis^{143,144}. Together with the fact that TGF-beta is particularly important for iT_{reg} generation and stability⁹³, we speculated that TGF-beta could aid in enhancing Foxp3 expression in iT_{reg} cells through induction of Usp22 and Usp21. Indeed, mRNA levels of both Foxp3-targeting USPs were increased when TGF-beta was added to the media of iT_{reg} cells 3 days after polarization, while Usp7 showed no such increase (**Fig. 3.3b**). This increase of both Usp22 and Usp21 expression was largely diminished by the addition of a TGF-beta inhibitor (LY 3200882) (**Fig. 3.3c**). Importantly, the level of Foxp3 mRNA rose concurrently with the levels of Usp22 and Usp21 (**Fig. 3.3d**), demonstrating that the TGF-beta can further enhance FoxP3 expression through Usp22 and Usp21 induction.

To further determine if TGF-beta is implicated in TCM-driven Usp22 and Usp21 upregulation, we added the TGF-beta inhibitor to the TCM from each of the aforementioned tumor

cell lines. Indeed, the TGF-beta inhibitor completely diminished the mRNA enhancement of Usp22 (**Fig. 3.4c**), signifying that TGF-beta is the primary factor in the B16 and LLC1 TCM that enhances Usp22 expression. Interestingly, the Usp21 level was also diminished when the inhibitor was added to the LLC1 TCM, but was not under B16 TCM condition (**Fig. 3.4c**). It is possible that this difference could be due to the quantity of TGF-beta secreted by the tumor cell lines into the medias. Indeed, LLC1 cells secreted significantly higher amounts of TGF-beta than both B16 and EG7 cells (**Fig. 3.3e**), which positively correlates with observed increase in Usp22 and Usp21 mRNA expression (**Fig. 3.3f and g**). The levels of Usp7 remain unchanged under all treatment groups and displayed no correlation to the increasing level of TGF-beta in the various tumor types (**Fig. 3.3b-c and h; Fig. 3.4c**). Therefore, our data identify TGF-beta as a critical soluble factor to selectively induce Usp22 and Usp21 in T_{reg} cells.

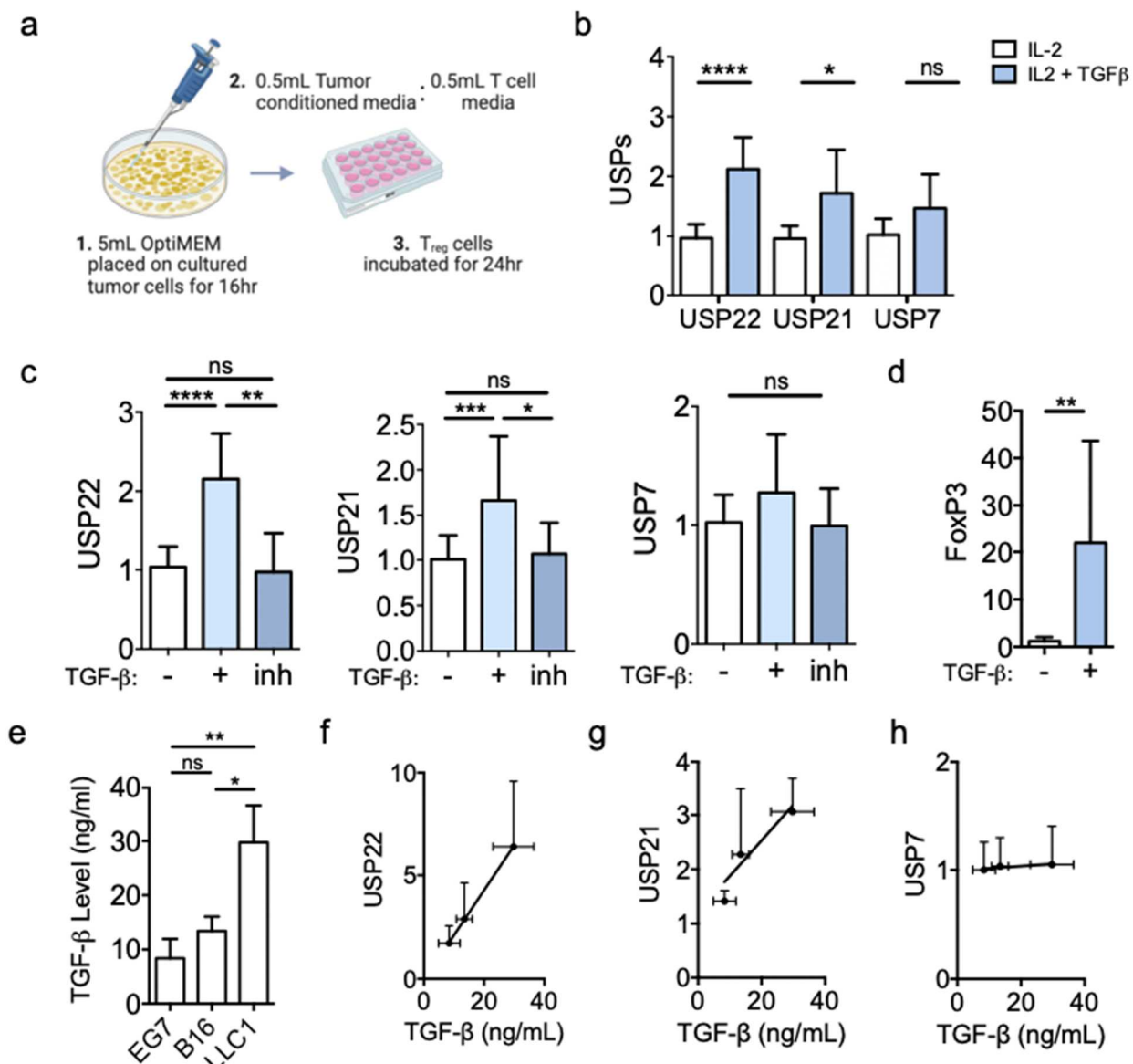


Figure 3.3 *TGF-beta* induces expression of *Usp22* and *Usp21* in T_{reg} cells. **a**, Visual representation of Tumor Conditioned Media (TCM) experiments. **b**, iT_{reg} USP mRNA level under $TGF-\beta$ induction post-polarization. Usp22: n=18-19; Usp21: n=7-8; Usp7: 4-5. **c**, iT_{reg} USP mRNA level under $TGF-\beta$ with and without a $TGF-\beta$ inhibitor. Usp22: n=3-11; Usp21: n=8-18; Usp7: 3-8. **d**, T_{reg} FoxP3 mRNA level with $TGF-\beta$ induction. n=10. **b-d**, All mRNA values calculated relative to WT untreated iT_{reg} cells. **e**, $TGF-\beta$ level in B16, LLC1 and EG7 tumor conditioned media n=3. **f-h**, Correlation between USP induction and $TGF-\beta$ level in the tumor conditioned media. Usp22: n=3-10; Usp21: n=3-8; Usp7: n=3-6. **b-e**, Two-tailed unpaired t-test was performed to determine statistical significance. All data are presented as mean \pm stdev. NS, not significant. * $P < 0.05$, ** $P < 0.01$, *** $P < 0.001$, **** $P < 0.0001$.

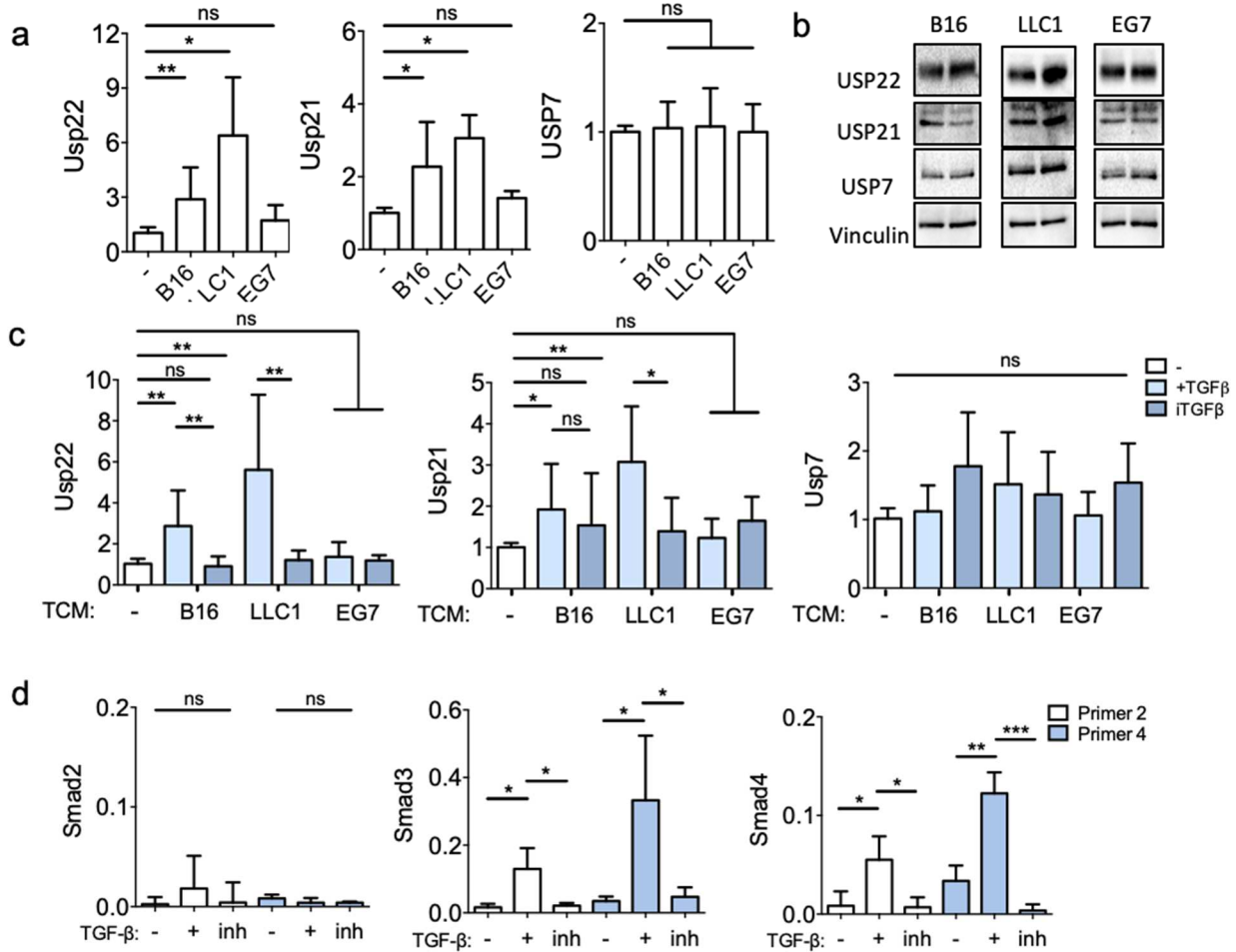


Figure 3.4 Tumor cell secreted TGF-beta increases *Usp22* and *Usp21* level in *iTreg* cells. **a**, USP mRNA level in *iTreg* cells in control T cell media compared to addition of tumor cell treated media at 50/50 with T cell media for 24 hours. Usp22) Control: n=14, B16: n=10, LLC1: n=5, EG7: n=4. Usp21) Control: n=12, B16: n=8, LLC1: n=3, EG7: n=3. Usp7) Control: n=10, B16: n=7, LLC1: n=4, EG7: n=5 **b**, USP protein level in *iTreg* cells in control T cell media compared to addition of tumor cell treated media at 50/50 with T cell media for 24 hours. **c**, USP mRNA level in *iTreg* cells with the addition of a TGF- β inhibitor in tumor cell media (Usp22) Control: n=22, B16: n=15, B16+Inh: n=5, LLC1: n=10, LLC1+inh: n=5, EG7: n=7, EG7+inh: n=5. Usp21) Control: n=20, B16: n=13, B16+Inh: n=5, LLC1: n=8, LLC1+inh: n=4, EG7: n=7, EG7+inh: n=5. Usp7) Control: n=14, B16: n=10, B16+Inh: n=5, LLC1: n=8, LLC1+inh: n=3, EG7: n=8, EG7+inh: n=6. **d**, SMAD2, SMAD3, and SMAD4 binding capacity along the *Usp22* promoter under TGF- β inhibition. SMAD2: n=4-5; SMAD3 n=3; SMAD4: n=3. **a-c**, All mRNA values calculated relative to untreated WT *iTreg* cells. **a-d**, Two-tailed unpaired t-test was performed to determine statistical significance. All data are presented as mean \pm stdev. NS, not significant. * $P < 0.05$, ** $P < 0.01$, *** $P < 0.001$, **** $P < 0.0001$.

3.2.3 TGF-beta and Usp22 amplify canonical TGF-beta signaling through Usp22-SMAD positive feedback loop

To uncover the mechanism by which TGF-beta acts on Usp22 and Usp21 transcription, we first investigated the canonical TGF-beta signaling pathway, which works through the co-activating Smad transcription factors (homologues of the *Drosophila* protein, mothers against decapentaplegic (Mad) and the *Caenorhabditis elegans* protein Sma): Smad2, Smad3 and Smad4 through specifically binding to the Smad-binding element (SBE)^{202,203}. We then scanned along the promoter regions of both Usp22 and Usp21 for sequences of conserved SBE. Along the Usp22 promoter, we found three promising regions for which we made primers and assessed the Smad binding capacity (**Fig. 3.5a and b**). Chromatin immunoprecipitation (ChIP) analysis detected that SMAD3 and SMAD4, but not SMAD2, bind to Usp22 promoter at around 1200 and 300 base pairs upstream of the transcription start site (**Fig. 3.5b**). Smad binding at both sites was ablated upon the addition of the TGF-beta inhibitor, demonstrating that Smad3 and Smad4 binding to the Usp22 promoter is due directly to TGF-beta signaling (**Fig. 3.4d**). Smad2 showed no binding capacity to any regions of the Usp22 promoter (**Fig. 3.4d; Fig. 3.5e-g**); likely due to steric hinderance blocking its direct DNA interaction²⁰⁴. Unlike with Usp22, no SBEs were found when scanning the Usp21 promoter, implying that TGF-beta induces Usp21 expression independent of Smads. Indeed, none of the regions showed binding capacity of any of the tested SMAD proteins, confirming that Usp21 expression is not induced through canonical TGF-beta signaling (**Fig. 3.5c**).

We have recently observed that, although Usp22-null iT_{reg} cells polarize normally with high levels of TGF-beta, sub-optimal polarization conditions resulted in a significant decrease in FOXP3 MFI and percentage relative to the WT iT_{reg} cells¹⁶⁶. This suggests an important function of Usp22 in perpetuating TGF-beta signaling within iT_{reg} polarization. Indeed, Usp22-null iT_{reg} cells display a significant deficiency in both SMAD2 and SMAD4 protein levels compared to WT

iT_{reg} cells, with no difference in their mRNA levels (**Fig. 3.6a and b**). This suggests Usp22 functions as a positive regulator for TGF-beta signaling pathway through stabilizing Smads at the protein level. As Usp22 is a DUB, this decrease is possibly due to enhanced SMAD ubiquitination and proteasomal degradation upon Usp22 deletion. Indeed, Usp22 interacts with and deubiquitinates both SMAD2 and SMAD4 (**Fig. 3.6c-d and f**). Although Usp22 interacts with SMAD3, it does not act as a DUB of SMAD3 (**Fig. 3.6c and f**), suggesting it acts specifically through stabilizing SMAD2 and SMAD4. Particularly, USP22-null iT_{reg} cells displayed enhanced degradation of SMAD2 and SMAD4 upon cycloheximide treatment relative to WT (**Fig. 3.6g**). Therefore, our data suggests that USP22 functions to reciprocally enhance TGF-beta signaling through SMAD2 and SMAD4 protein stabilization. This act ensures upregulation of itself through a positive feedback loop, further ensuring Foxp3 expression in iT_{reg} cells.

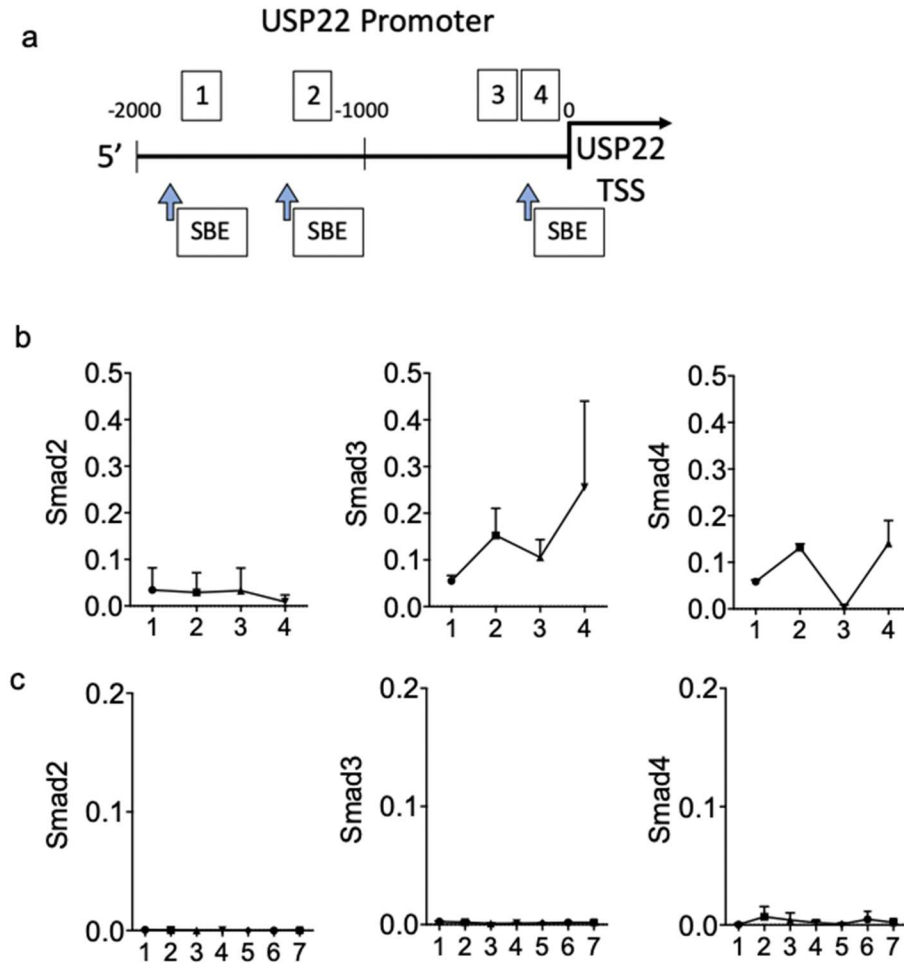


Figure 3.5 *Smad3* and *Smad4* bind to conserved SBE on the *Usp22* promoter. **a**, *Usp22* promoter region overlaid with plausible Smad binding elements (SBE) and placement of primers created for ChIP. **b-d**, Binding of Smad2, Smad3 and Smad4 along the *Usp22* promoter region using ChIP-qPCR n=2-7 **e-g**, Binding of Smad2, Smad3 and Smad4 along the *Usp21* promoter region using ChIP-qPCR n=1-2.

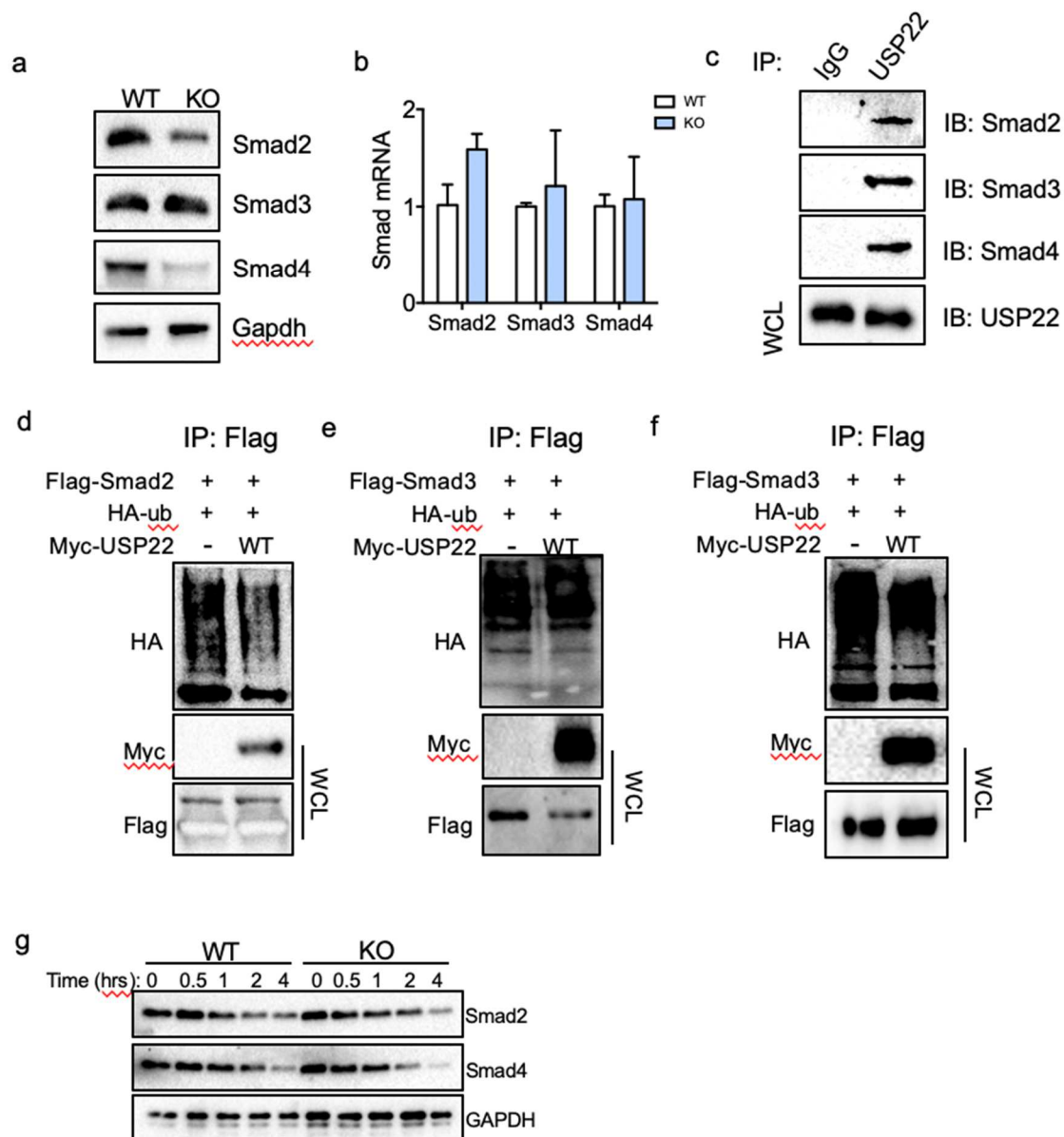


Figure 3.6 *USP22 reciprocally enhances TGF-beta signaling through Smad protein stabilization in positive feedback loop.* **a**, Representative protein level of SMAD2, SMAD3, and SMAD4 in USP22 WT and KO iT_{reg} cells. **b**, mRNA level of Smad2, Smad3, and Smad4 in USP22 WT and KO iT_{reg} cells (n=3). All mRNA values calculated relative to unchallenged WT iT_{reg} cells. Two-tailed unpaired t-test was performed to determine statistical significance. All data are presented as mean \pm stdev. NS, not significant. * $P < 0.05$, ** $P < 0.01$, *** $P < 0.001$, **** $P < 0.0001$. **c**, USP22 endogenous IP with SMAD 2, SMAD 3, and SMAD 4 proteins within iT_{reg} cells. **d-f**, Overexpression DUB assay IP in 293T cells of USP22 with SMAD2, SMAD3, and SMAD4. **g**, SMAD2 and SMAD4 protein degradation in WT and KO iT_{reg} cells under cycloheximide treatment.

3.2.4 Hypoxia selectively induces T_{reg} Usp22, which supports Foxp3 expression

Although iT_{reg} Usp22 levels were upregulated in the EG7 tumor model (**Fig. 3.1c**), levels of Usps remained unchanged in Tregs under culture with EG7 TCM (**Fig. 3.4a-c**), implying that additional TME factors may influence on iT_{reg} stability and function through USPs. In addition to tumor cell secreted factors, tumor-driven hypoxia has been repeatedly implicated in FOXP3 stability and T_{reg} cell function^{113,115}. A known negative prognostic factor in solid tumors^{32,103}, hypoxia preferentially downregulates T cell proliferation, receptor signal transduction, and effector function while increasing T_{reg} cell suppressive capabilities^{106,115,116}. We, therefore, investigated the effects of hypoxia on USP levels in T_{reg} cells. Surprisingly, only Usp22 expression was enhanced under hypoxic conditions at both the mRNA and protein levels (**Fig. 3.7a**; **Fig. 3.8a and b**). Therefore, we speculated that Usp22 could function as a stabilizer of FOXP3 under the hypoxic conditions in the TME. Indeed, Usp22-deficient nT_{reg} cells show a reduced ability to sustain FOXP3 expression under hypoxic conditions (**Fig. 3.7b**, **Fig. 3.8c**), signifying that Usp22 is required for FOXP3 stabilization under the hypoxic conditions found within the TME.

Under hypoxic conditions, hypoxia inducible factor α (HIF- α) are stabilized resulting in the activation of a transcriptional program that promotes cellular adaptation to low oxygen levels¹¹¹. HIFs are known to have two functional binding sites on the Usp22 promoter²⁰⁵, suggesting that hypoxic induction of Usp22 may be HIF- α -dependent. Indeed, incubation with hypoxia-independent HIF- α activator, dimethylxalylglycine (dMOG), increased Usp22 mRNA level in both nT_{reg} and iT_{reg} cells (**Fig. 3.7d**; **Fig. 3.8d**), indicating that hypoxia-induced Usp22 expression is involved in FoxP3 stabilization. To support this, we further showed that Usp22-deficient nT_{reg} cells displayed decreased stability of FOXP3 following treatment with dMOG, confirming that Usp22-dependent FOXP3 stabilization under hypoxic conditions is HIF- α dependent (**Fig. 3.8e**).

In contrast, this FOXP3 stabilization was not observed in iT_{reg} cells under hypoxic conditions or with DMOG treatment (**Fig. 3.8f and g**). This could be due to the lack of TGF-beta present in the experimental conditions, which is pivotal for Foxp3 expression stabilization in iT_{reg} cells. Regardless, these results demonstrate the importance of Usp22 in hypoxia-mediated T_{reg} cell FOXP3 expression within the TME.

3.2.5 Metabolic alterations in the tumor microenvironment induce Usp22 and Usp21 to promote Foxp3 stability

In addition to oxygen, glucose levels in the TME are often decreased in part through its enhanced uptake by tumor cells, competing with the glucose necessity of the highly glycolytic T_{eff} cells^{36,198}. Conversely, FOXP3 promotes oxidative phosphorylation over glycolysis in T_{reg} cells, potentially giving them a functional advantage within the TME^{35,125,126}. Therefore, we hypothesized the observed T_{reg} cell advantage in nutrient deprived environments could exist partially as a consequence of USPs mediated enhancement of Foxp3 expression and stability. Indeed, Usp22 mRNA and protein levels were increased in T_{reg} cells upon glucose deprivation (**Fig. 3.7d and Fig. 3.8h and i**). Additionally, Usp22-deficient T_{reg} cells have significantly lower FOXP3 expression under glucose deprivation compared to WT T_{reg} cells, demonstrating that Usp22 functions to stabilize FOXP3 under glucose-restricted conditions (**Fig. 3.7e and Fig. 3.8j**).

Along with the competition for glucose, a scarcity of amino acids within tumors may also alter immune cell function³⁶. Importantly, amino acid starvation is known to enhance T_{reg} cell induction¹²⁹. To investigate the role of USPs in amino acid starvation induced Foxp3 expression we cultured T_{reg} cells in media lacking amino acids. Indeed, amino acid starvation led to increased expression of Usp22 and Usp21, but not Usp7, in nT_{reg} and iT_{reg} cells (**Fig. 3.7f; Fig. 3.7k**). Furthermore, the stability of FOXP3 in amino acid starved iT_{reg} cells is reduced by the deficiency of Usp22 or Usp21 (**Fig. 3.7g**). In environments deplete of both glucose and amino acids,

activation of adenosine monophosphate-activated protein kinase (AMPK) suppresses anabolic metabolism while upregulating oxidative metabolism to promote cellular survival¹³⁴, suggesting AMPK activation is involved in Usp22 or Usp21 upregulation. We then treated T_{reg} cells with an inhibitor of mitochondrial ATP synthase, Oligomycin A, and measured USP mRNA levels. Indeed, oligomycin treatment increased both Usp22 and Usp21, but not Usp7, mRNA level in nT_{reg} cells (**Fig. 3.7h**), further supporting our observation that glucose deprivation and subsequent energy stress induces Usp22 expression in T_{reg} cells.

It is well known that AMPK functions in balance with mammalian target of rapamycin (mTOR) signaling to regulate the cellular metabolic state¹³⁴. Intriguingly, pharmacologic inhibition of mTOR also resulted in increased Usp22 and Usp21, but not Usp7, expression in nT_{reg} cells (**Fig. 3.7i**). In iT_{reg} cells, however, Usp21 was not upregulated at the mRNA level upon AMPK activation or mTOR inhibition (**Fig. 3.8l and m**), suggesting cell-type specificity of the response. Collectively, these findings suggest that the global metabolic state as determined by the balance of AMPK and mTOR activity, act to modulate Foxp3 expression and stability through Usp22, and to a lesser extent Usp21, in T_{reg} cells.

It has been proposed that iT_{reg} cells better adapt to the metabolically stressful conditions of the TME, which offers them a functional advantage over T_{eff} cells^{35,75}. Combined, our data suggests that alterations in the microenvironment can drive increased levels of Usp22 and Usp21 potentially through modulation of HIF- α , AMPK, and mTOR activity to enhance Treg stability in the tumor microenvironment.

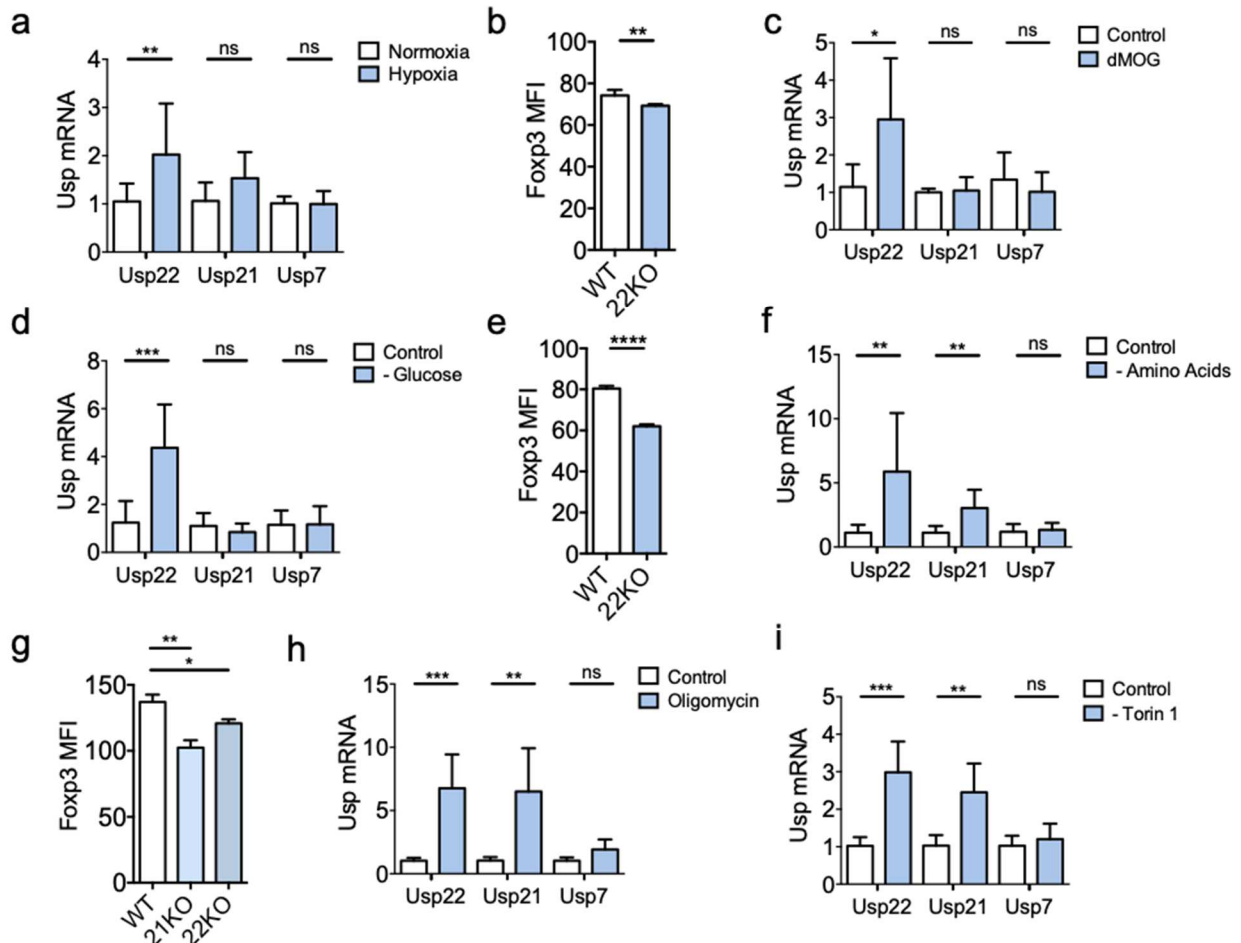


Figure 3.7 USP22 and USP21 are required for FOXP3 stability in nT_{reg} cells under environmental and metabolic stress found in the TME. All mRNA values calculated relative to unchallenged WT T_{reg} cells. **a**, nT_{reg} USP mRNA level in normoxic (21% O₂) versus hypoxic (1% O₂) conditions after 24 hours (n=6-13). **b**, FOXP3 MFI change in USP22 KO nT_{reg} cells relative to WT nT_{reg} cells after 72 hours (n=5). **c**, nT_{reg} USP mRNA level after treatment with dMOG for 24 hours (n=6). **d**, USP mRNA level in nT_{reg} cells after exposure to glucose-restricted (0.5mM) conditions after 24 hours relative to normal media (11mM glucose) (n=7-18). **e**, Relative FOXP3 MFI change in nT_{reg} cells from control and cells cultured under low glucose conditions after 48 hours (n=3). **f**, nT_{reg} USP mRNA level under amino acid starvation for 24 hours (n=7-9). **g**, FOXP3 MFI stability in USP22- or USP21-null nT_{reg} cells cultured in normal media conditions versus amino acid starvation after 48 hours in (n=3). **h**, nT_{reg} USP mRNA level after treatment with 1 μM oligomycin A for 24 hours (n=5-7). **i**, nT_{reg} USP mRNA level after treatment with 250nM Torin1 for 24 hours (n=5-7). **a-i**, Two-tailed unpaired t-test was performed to determine statistical significance. All data are presented as mean ± stdev. NS, not significant. **P* < 0.05, ***P* < 0.01, ****P* < 0.001, *****P* < 0.0001.

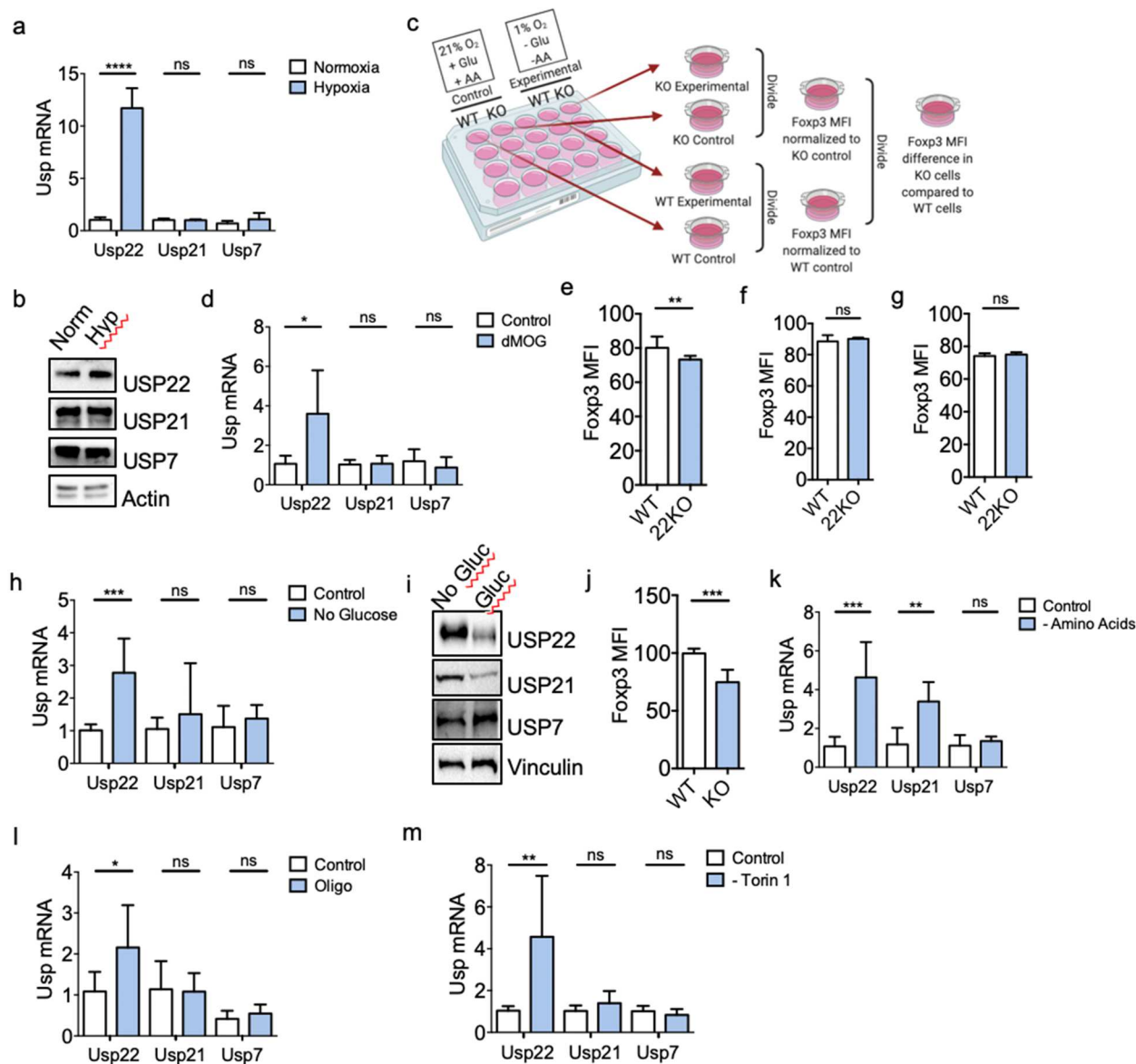


Figure 3.8 HIF- α and the AMPK/mTOR balance modulates T_{reg} cell FoxP3 stability through USP22 and USP21. All mRNA values calculated relative to unchallenged WT T_{reg} cells. **a**, iT_{reg} USP mRNA level in normoxic and hypoxic conditions after 4 hours (n=4-5). **c**, iT_{reg} USP protein level in normoxic and hypoxic conditions after 24 hours. **c**, Visual representation of stability assay calculations of Foxp3 MFI level. %O₂ is the percentage of oxygen, Glu is glucose, and AA is amino acids. **d**, iT_{reg} cell Foxp3 MFI change in hypoxia relative to normoxia or after 72 hours (n=3). **e**, iT_{reg} cell USP mRNA level after treatment with DMOG for 24 hours (n=6). **f-g**, Foxp3 MFI change after treatment with DMOG for 48 hours relative to untreated nTreg (E) (n=9-10) or iT_{reg} (F) (n=4) cells. **h**, iT_{reg} cell USP mRNA level under low glucose conditions after 24 hours (n=3-8). **i**, iT_{reg} cell USP protein level under low glucose conditions after 24 hours. **j**, iT_{reg} Foxp3 MFI change low glucose conditions after 72 hours relative to complete media (n=7). **k**, iT_{reg} cell USP mRNA level in amino acid starvation relative to complete media after 24 hours (n=6). **l**, iT_{reg} cell USP mRNA level after treatment with 1 μ M oligomycin for 24 hours (n=6). **m**, iT_{reg} USP mRNA level after treatment with 250nM Torin1 for 24 hours (n=5-9). **a-m**, Two-tailed unpaired t-test was performed to determine statistical significance. All data are presented as mean \pm stdev. NS, not significant. *P < 0.05, **P < 0.01, ***P < 0.001, ****P < 0.0001.

3.2.6 Usp22 and Usp21 modulate T_{reg} fitness through distinct pathways

Our discoveries thus far have suggested that Usp22, and to a lesser extent Usp21, are important in maintaining FOXP3 expression and thus T_{reg} fitness in the TME through multiple pathways. To study their combined functionality *in vivo*, we generated a strain of T_{reg}-specific Usp22 and Usp21 double knockout (dKO) mice by breeding Usp21^{f/f} mice with Usp22^{f/f}FoxP3^{YFPcre} single knockout mice. This breeding strategy gave us the T_{reg}-specific knockout of Usp22 (22KO), Usp21 (21KO), and the dKO, all of which were confirmed via qPCR (**Fig. 3.9a**). Deletion of either Usp22, Usp21, or both in T_{reg} cells did not alter the frequency of either B or T cells in the spleens of 6-week-old mice (**Fig. 3.10a and b**). Importantly, while the mice display similar weights early in life, by 24 weeks of age the 22KO and dKO animals are consistently smaller in size compared to WT (**Fig. 3.9b**).

Unsurprisingly, all three KO groups showed significant increase in CD44^{hi}CD62^{Lo} activated splenic T_{eff} cells in comparison to age matched WT mice, consistent with the development of low level, progressive inflammation with age (**Fig. 3.9c**). Importantly, only the 22KO and dKO mice showed decreases in Foxp3 expression and significant reductions in T_{reg} cell-associated suppressive markers (**Fig. 3.9d and e**). Although a previous study reported that the 21KO mice develop age-related impairments in T_{reg} cell function and number secondary to impaired Foxp3 expression¹⁶⁷, our 8-week-old mice showed no changes in FoxP3 expression, suggesting that Usp21 may be dispensable for Foxp3 expression early in life.

Interestingly, transcriptional profiling revealed more T_{reg} cell suppressive markers were differentially expressed in the dKO mice than in either single KO animal when compared to WT gene expression (**Fig. 3.9e**), suggesting a possible synergism between the loss Usp22 and Usp21 on T_{reg} cell stability and function. Furthermore, differentially expressed genes (DEGs) between the

21KO and the 22KO were relatively distinct (**Fig. 3.9f**). Although gene set enrichment analysis (GSEA) of both single KO mice showed changes in many cell cycle and proliferative pathways, such as G2M checkpoints and E2F targets, as well as changes in oxidative phosphorylation (Fig. 4G), there were only a total of 32 overlapping differentially expressed genes between the 21KO and the 22KO (**Fig. 3.9f**). Importantly, T_{reg} cells from the dKO animals displayed a GSEA and bulk gene expression signature that merged the changes found in each of the single KO mice, suggesting that the loss of both Usp22 and Usp21 synergize to diminish T_{reg} cell function.

As we demonstrated that both Usp22 and Usp21 are regulated by metabolic alterations in the TME, it was particularly interesting to identify disruption of multiple metabolic pathways in each of the KO animals. In fact, T_{reg} cells from dKO mice had profound changes in lipid metabolic processes, one carbon metabolism, and ribosomal biogenesis (**Fig. 3.10c-e**). Interestingly, Usp22-null T_{reg} cells, but not Usp21 deficient cells, displayed similar alterations in both lipid metabolism and one-carbon metabolism to the dKO T_{reg} cells (**Fig. 3.10c and d**). In contrast, T_{reg} cells from 21KO and dKO mice showed profound decreases in ribosomal gene expression, which was not identified in the Usp22-null T_{reg} cells (**Fig. 3.10e**), suggesting distinct pathways by which Usp22 and Usp21 modulate T_{reg} fitness. Our *in vitro* metabolic flux analysis further demonstrated that, unlike the 21KO, both 22KO and the dKO display enhanced mitochondrial oxygen consumption (OCR) and extracellular acidification rates (ECAR) (**Fig. 3.10f and g**), suggesting that Usp22 may play an essential role in modulating the metabolic state of regulatory T cells. Collectively, these data imply that both Usp22 and Usp21 modulate T_{reg} cell metabolism although seemingly through unique pathways.

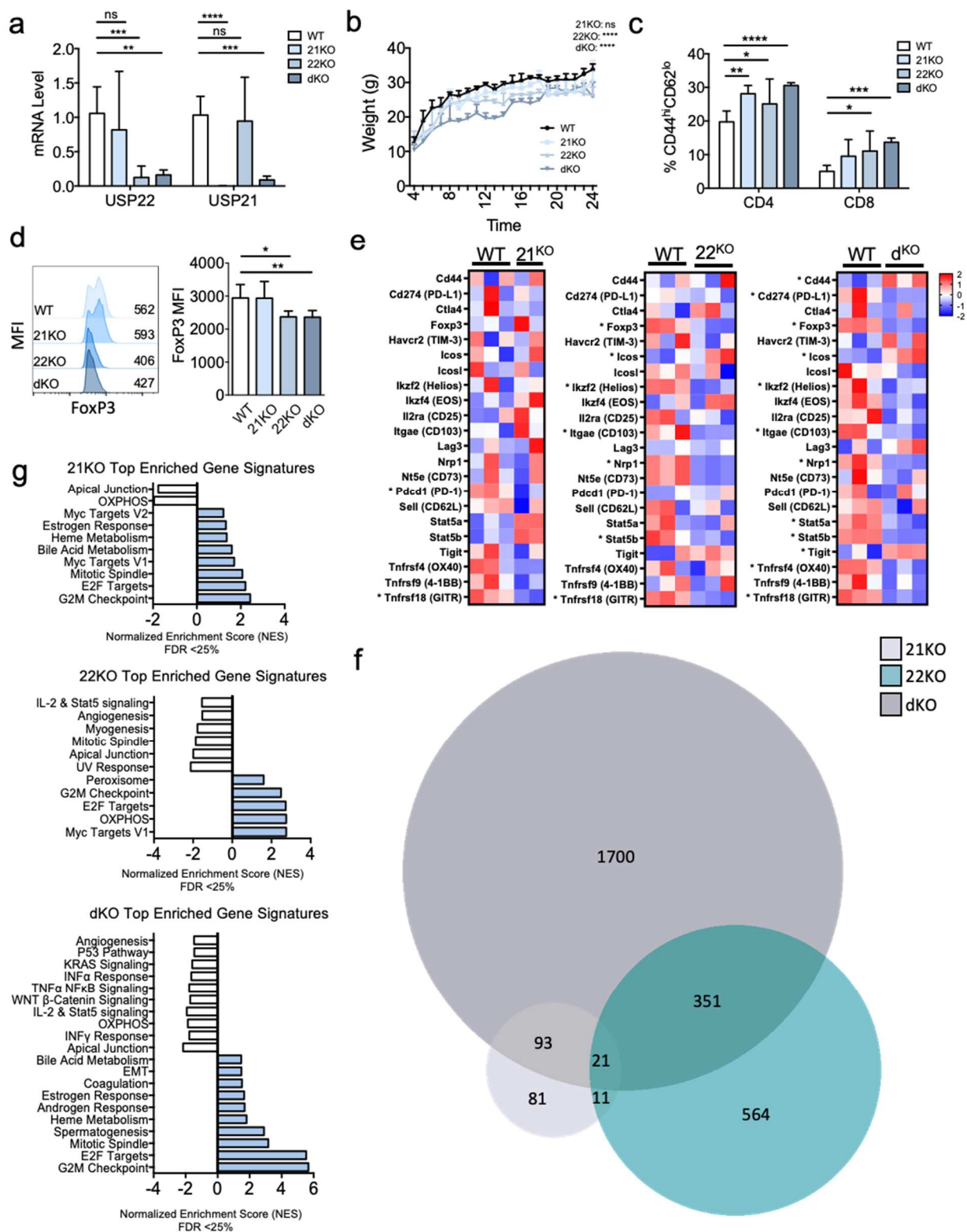


Figure 3.9 Loss of *Usp22* and *Usp21* in T_{reg} cells differentially impairs *FoxP3* expression and cell function. **a**, *Usp22* and *Usp21* levels in WT, USP21 KO, USP22 KO and dKO mice (n=5-8). All mRNA values calculated relative to WT T_{reg} cells. **b**, Mice weights over a 2-month period (n=2-9). **c**, Peripheral activation of CD4⁺ and CD8⁺ T cells as measured by CD44⁺ CD62L⁻ expression (n=7-9). **d**, Representative histogram (left) and

quantification (right) of FOXP3 MFI in splenic T_{reg} cells of WT and KO animals (n=6-8). **e**, Heat map of T_{reg} cell signature genes (*significance is adjusted $P < 0.01$) in USP21KO (n=2), USP22KO (n=3), and dKO (n = 3) versus WT (n=3) mice. **f**, Venn Diagram of DEGs (adj. $p < 0.01$) between 22KO, 21KO and dKO (n=2-3). **g**, Normalized enrichment scores from gene set enrichment analysis (False Discovery Rate, FDR<25%) from the hallmark gene set in the molecular signatures database comparing the gene set generated from RNA sequencing of Wt, 21KO, 22KO, and dKO mice (n=2-3). **a-c**, Two-way ANOVA with multiple comparisons between rows was performed to determine statistical significance. All data are presented as mean \pm stdev. NS, not significant. * $P < 0.05$, ** $P < 0.01$, *** $P < 0.001$, **** $P < 0.0001$. **d**, One-way ANOVA with multiple comparisons between rows was performed to determine statistical significance. All data are presented as mean \pm stdev. NS, not significant. * $P < 0.05$, ** $P < 0.01$, *** $P < 0.001$, **** $P < 0.0001$.

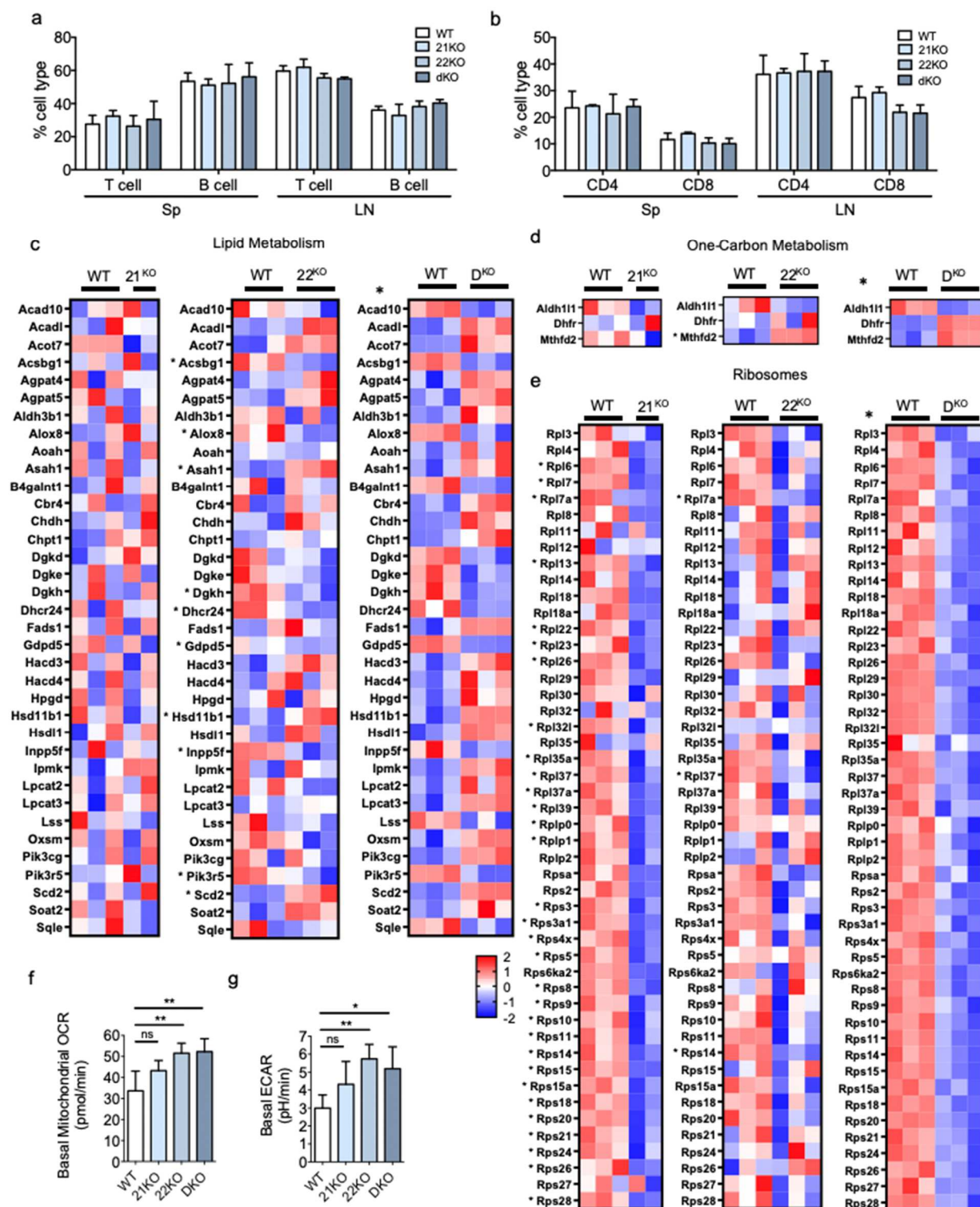


Figure 3.10 Loss of *Usp22* and *Usp21* in T_{reg} cells differentially alter T_{reg} metabolic pathways. **a**, T and B cell percentages in peripheral organs of KO and WT animals (n=5-9). **b**, Percent of CD4 and CD8 T cells in peripheral organs of CD45+ cells? (n=4-10). **c-e**, Heat map of metabolic pathways (significance is noted by * adjusted $P < 0.01$) in U21KO (n=2), U22KO (n=3), and dKO (n = 3) versus WT (n=3) mice. Genes chosen based on differential expression (adj. $p < 0.01$) in the dKO mice. **f**, Basal mitochondrial OCR and **g**, Basal ECAR of

21KO (n=5), 22KO (n=5) and dKO (n=4-5) relative to WT (n=5) nT_{reg} cells. **a-b**, Two-way ANOVA with multiple comparisons between rows was performed to determine statistical significance. All data are presented as mean \pm stdev. NS, not significant. *P < 0.05, **P < 0.01, ***P < 0.001, ****P < 0.0001. **f-g**, One-way ANOVA with multiple comparisons between rows was performed to determine statistical significance. All data are presented as mean \pm stdev. NS, not significant. *P < 0.05, **P < 0.01, ***P < 0.001, ****P < 0.0001.

3.2.7 Usp22 and Usp21 deletion in T_{reg} cells synergize to enhance anti-tumor immunity

To test the importance of T_{reg} cell Usp22 and Usp21 in tumor conditions *in vivo*, we used the B16 melanoma syngeneic tumor model. Mice with T_{reg}-specific ablation of Usp22 showed increased tumor rejection compared to the deletion of Usp21. Importantly, though, mice harboring the joint deletion of both Usp22 and Usp21 in T_{reg} cells grew the smallest tumors (**Fig. 3.11a**). Additionally, the dKO and 22KO animals showed greater proportions of effector memory CD8⁺ T cells in the spleens. In contrast, deletion of Usp21 in Tregs was insufficient to enhance the B16 tumor rejection (**Fig. 3.11b**). Consistently, 21KO mice cytokine levels were on par with WT mice, while the 22KO mice displayed an increase of CD8⁺ Granzyme B (GrzB) production. Notably, the tumor-bearing dKO mice had significant increases of both IFN-gamma and GrzB producing CD8⁺ T cells in the spleens, and each cytokine was enhanced even in comparison to single KO animals (**Fig. 3.11c**). Furthermore, both the 22KO and dKO had significant drops in FoxP3 and T_{reg} suppressive marker MFI in peripheral T_{reg} cells, which was not observed in 21KO T_{reg} cells (**Fig. 3.11d-g**). Collectively, these data suggest that the combined loss of Usp21 and Usp22 in T_{reg} cells results in enhanced activation of T_{eff} cells effect compared to individual loss of Usp21 or Usp22.

Further analysis of tumor infiltrating lymphocytes indicated a significant increase in CD4⁺ and CD8⁺ T cell frequencies in both the 22KO and the dKO mice, with each compartment in the dKO secreting higher amounts of both IFN-gamma and GrzB than WT mice (**Fig. 3.11h and i**). Notably, the dKO mice had significantly higher levels of T_{eff} cell infiltration even than the 22KO mice, as well as the having the highest levels of IFN-gammasecretion. Consistent with splenic T_{reg} cells, iT_{reg} cells in the 22KO and dKO mice had significantly lower T_{reg} infiltration and FOXP3

MFI than in the WT and 21KO (**Fig. 3.11k**). Although the loss of USP22 alone displayed significant anti-tumor immunity, the loss of both Usp22 and Usp21 in T_{reg} cells displayed a more vigorous anti-tumor response, as documented by the dKO mice having a dramatically increased cytokine production, the highest infiltrating T cell number, and the smallest tumor sizes. Collectively, this data suggests that Usp21 and Usp22 cooperate to maintain Foxp3 expression and T_{reg} cell function in the TME.

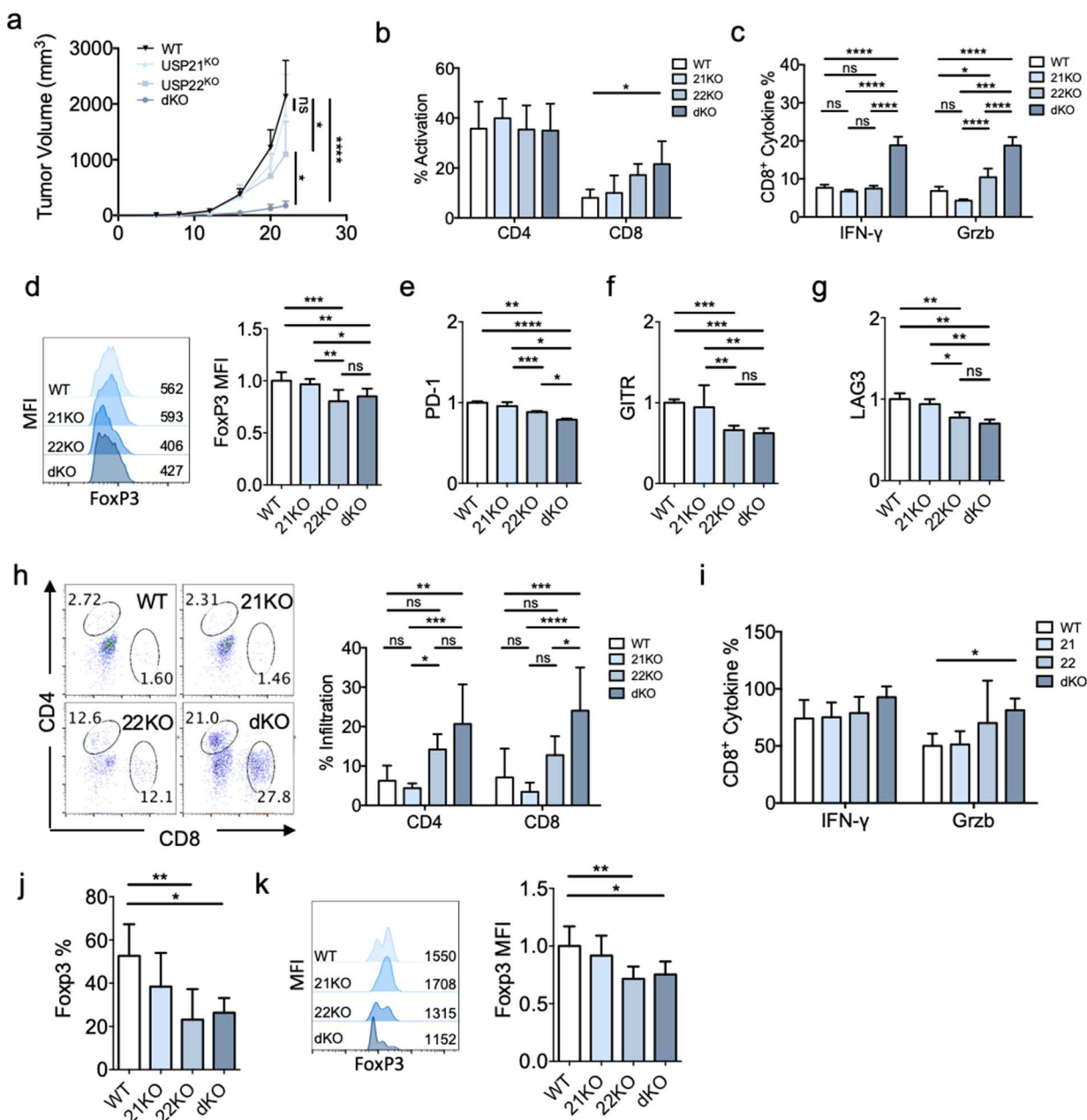


Figure 3.11 Deletion of *Usp21* and *Usp22* in *T_{reg}* cells synergize to enhance antitumor immunity **a**, Tumor growth curve of B16 cells subcutaneously injected in the flank of WT, 21KO, 22KO and dKO mice (n=9). **b**, Percent activation as defined by CD44⁺CD62L^{lo} of CD4⁺ and CD8⁺ T cells in the spleens of B16 challenged mice (n=6). **c**, Percent IFN-gamma and Granzyme B (Grzb) production of peripheral CD8⁺ T cells (n=3). **d**, FOXP3 MFI of peripheral T_{reg} cells relative to WT (n=7-9). **e**, PD-1 MFI of peripheral T_{reg} cells relative to WT (n=3). **f**, GITR MFI of peripheral T_{reg} cells relative to WT (n=6-8). **g**, LAG3 MFI of peripheral T_{reg} cells relative to WT (n=6-8). **h**, Representative flow cytometry plot and graphical representation of % infiltration of CD4⁺ and CD8⁺ T cells within the tumor (n=6). **i**, Percentage IFN-gamma and Granzyme B production of intratumoral CD8⁺ cells (n=5-6). **j**, Representative FOXP3⁺ percentage of CD4⁺ cells in iT_{reg} cells (n=6). **k**, Representative flow plot (left) and quantitative representation of FOXP3 MFI within tumor T_{reg} cells relative to WT (n=4-6). **a-c** and **i-j**, Two-way ANOVA with multiple comparisons between rows was performed to determine statistical significance. All data are presented as mean \pm stdev. NS, not significant. **P* < 0.05, ***P* < 0.01, ****P* < 0.001, *****P* < 0.0001. **d-h** and **k**, One-way ANOVA with multiple comparisons between rows was performed to determine statistical significance. All data are presented as mean \pm stdev. NS, not significant. **P* < 0.05, ***P* < 0.01, ****P* < 0.001, *****P* < 0.0001.

3.2.8 Identification of a Usp22-specific small molecule inhibitors

Identification of a Usp22-specific small molecule inhibitor was done in collaboration with the Sun Lab in the Pharmacology Department at Dalian Medical University.

Although deletion of Usp21 in addition to Usp22 in T_{reg} cells enhances antitumor immunity, Usp22 deletion alone is sufficient in diminishing tumor burden. To assess whether pharmacologic inhibition of Usp22 could modulate T_{reg} function, we aimed to identify Usp22-specific inhibitors. It has been suggested that *in vitro* purified USP22 protein lacks catalytic activity^{206,207}, leading to difficulties for high-throughput screening. Therefore, we used the computer-aided drug design (CADD) to develop a Usp22-specific small molecule inhibitor (**Fig. 3.12**). As Usp22 contains a highly conserved putative catalytic domain (Cys, His, and Asp) from yeast to human, a homology modeling study was performed to obtain a model of human Usp22 for use in structure-based virtual screening (**Fig. 3.12a**). Of three validated structural models of Usp22, the yeast UBP8 structure (PDB code 3MHS) was chosen as a template protein to construct the Usp22 model by Swiss Model (Usp22-m) (**Fig. 3.12b**). In order to obtain conformation at the lowest potential, the structure of Usp22-m was further subjected to molecular dynamics simulation and clustering analysis using Gromacs5.15, and the distance between Cys 185 and His 479 was increased from 3.6 Å to 4.8 Å in the position of catalytic site of USP22 (Usp22-md) (**Fig. 3.12c**). We further compared the predicted amino acid sequence of USP22 with 150 homologous full sequences. The conservation grades are mapped onto the structure and show the Cys domain was highly conserved. This study not only provides basis for the accuracy of homology modeling, but also provides favorable conditions for drug selectivity screening.

We then used both Lipinski's Rule and Veber's Rule to filter through the Specs database and found a total of 240K compounds binding to the catalytic pocket of our Usp22 model. We then filtered the top 100 compounds ranked by docking affinity by MD and MM/PBSA methods and were left with 28 compounds (**Table 1**). This limited number of compounds allowed us for further biological screening. As USP22 suppression leads to dramatic reduction in FOXP3 expression levels, we utilized FOXP3 MFI reduction as a readout for the biological validation of USP22 inhibitory efficacy by each of the 38 chemicals. As indicated in Table S1, the chemical #30 showed strong efficacy in downregulating FOXP3 expression. The compound S30, structure shown in **Fig. 3.14a**, bound stably in the USP22 catalytic domain pocket shown by the RMSD trajectory (**Fig. 3.12d**). Furthermore, analysis of S30 interaction with each residue of Usp22 indicated that the side chain negative residues (Glu, Asp) make a favorable contribution to the binding of the inhibitor and protein, however, the positively charged residues such as Arg and Lys, play a detrimental role (**Fig. 3.12e**). Therefore, future generations of Usp22 inhibitors should take into considerations not only the hydrophobic residues, but also the interaction between the inhibitor and the charged and polar residues on the surface of the binding pocket.

Although deletion of Usp21 in addition to Usp22 in T_{reg} cells enhances antitumor immunity, Usp22 deletion alone is sufficient in diminishing tumor burden. To assess whether pharmacologic inhibition of Usp22 could modulate T_{reg} function, we aimed to identify Usp22-specific inhibitors. It has been suggested that *in vitro* purified USP22 protein lacks catalytic activity^{206,207}, leading to difficulties for high-throughput screening. Therefore, we used the computer-aided drug design (CADD) to develop a Usp22-specific small molecule inhibitor (**Fig. 3.12a**). As Usp22 contains a highly conserved putative catalytic domain (Cys, His, and Asp) from yeast to human, a homology modeling study was performed to obtain a model of human Usp22 for use in structure-based virtual

screening (**Fig. 3.12b**). Of three validated structural models of Usp22, the yeast UBP8 structure (PDB code 3MHS) was chosen as a template protein to construct the Usp22 model by Swiss Model (Usp22-m) (**Fig. 3.12c and d**). In order to obtain conformation at the lowest potential, the structure of Usp22-m was further subjected to molecular dynamics simulation and clustering analysis using Gromacs5.15, and the distance between Cys 185 and His 479 was increased from 3.6 Å to 4.8 Å in the position of catalytic site of USP22 (Usp22-md) (**Fig. 3.12c**). We further compared the predicted amino acid sequence of USP22 with 150 homologous full sequences. The conservation grades are mapped onto the structure and show the Cys domain was highly conserved. This study not only provides basis for the accuracy of homology modeling, but also provides favorable conditions for drug selectivity screening.

We then used both Lipinski's Rule and Veber's Rule to filter through the Specs database and found a total of 240K compounds binding to the catalytic pocket of our Usp22 model. We then filtered the top 100 compounds ranked by docking affinity by MD and MM/PBSA methods and were left with 25 compounds (**Table 1**). This limited number of compounds allowed us for further biological screening. As USP22 suppression leads to dramatic reduction in FOXP3 expression levels, we utilized FOXP3 MFI reduction as a readout for the biological validation of USP22 inhibitory efficacy by each of the 25 chemicals. As indicated in Table S1, the chemical S02 (11-anilino-7,8,9,10-tetrahydrobenzimidazo[1,2-b]isoquinoline-6-carbonitrile) showed strong efficacy in downregulating FOXP3 expression. The compound S02, structure shown in **Fig. 13.4a**, bound stably in the USP22 catalytic domain pocket shown by the RMSD trajectory (**Fig. 3.12e**) with strong binding energies to our USP22-md model (**Fig. 3.12f**). Furthermore, analysis of S02 interaction with each residue of Usp22 indicated that the side chain negative residues (Glu, Asp) make a favorable contribution to the binding of the inhibitor and protein, however, the positively

charged residues such as Arg and Lys, play a detrimental role (**Fig. 3.12g**). Therefore, future generations of Usp22 inhibitors should take into considerations not only the hydrophobic residues, but also the interaction between the inhibitor and the charged and polar residues on the surface of the binding pocket.

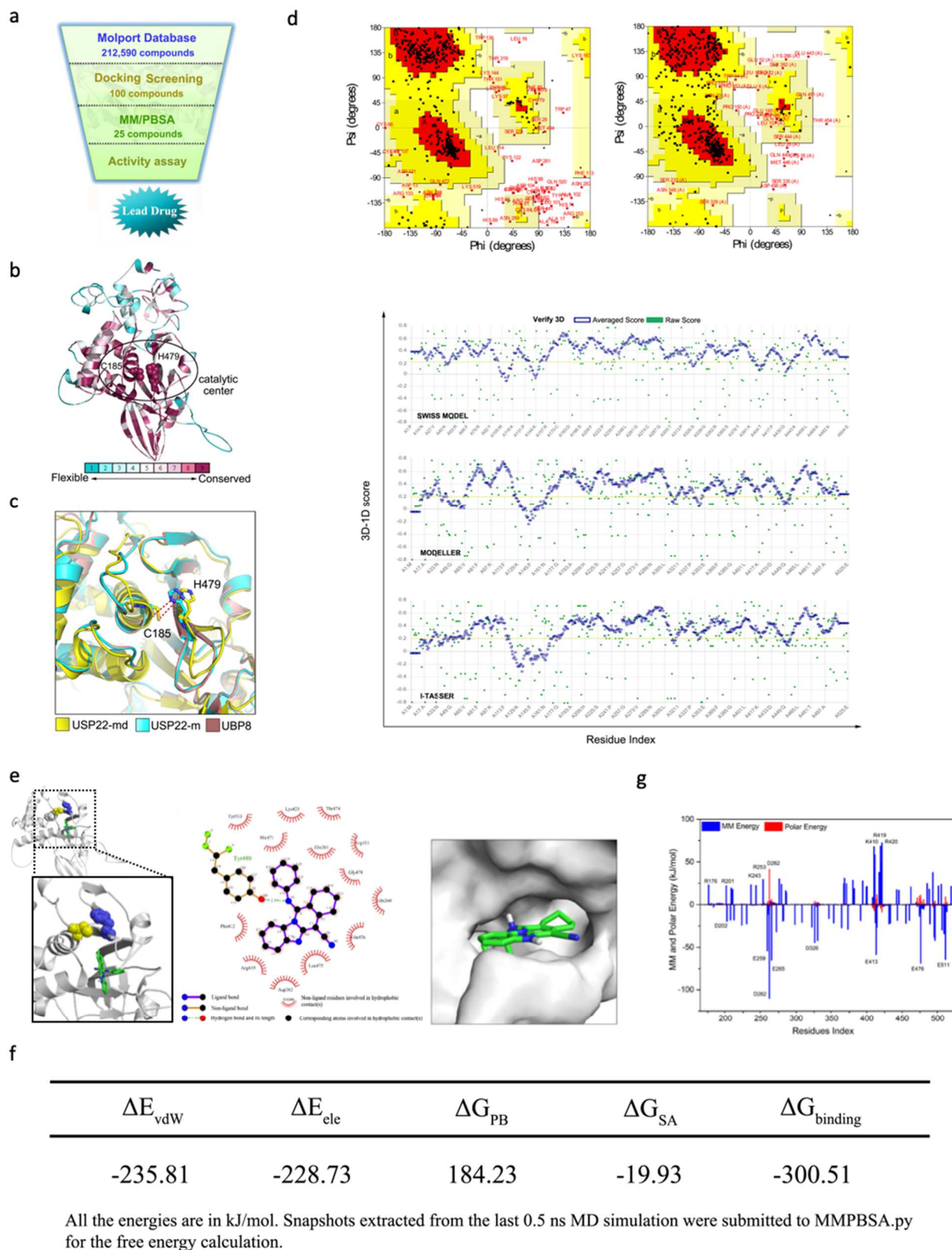


Figure 3.12 Development and validation of *Usp22*-specific inhibitor through structure-based hierarchical virtual screening **a**, Flowchart of structure-based virtual screening. **b**, The overall conformation of USP22-m

(USP22 model generated using SWISS MODEL) is represented by cartoon which are colored by conservation using the color-code bar. Catalytic centre of USP22 was defined as docking position. **c**, Ramachandran plot statistics of USP22-m generated by PROCHEK progress (left). The Displacement of the catalytic centre loop in USP22-md (the MD optimized model) compared to UBP8 (PDB: 3MHS) and USP22-m (right). **d**, S30 displayed in green stick binding in the pocket of USP22-md structure (left). Ligplot showing hydrogen bonding and hydrophobic contacts of S02 with USP22-md (middle). The best ranked position of S30 (shown in green) in the binding pocket of USP22-md is presented, generated by docking. **e**, Individual energy contributions of amino acid residues after MD simulations and PBSA calculations. **f**, The ability of the 38 hits obtained from the drug screening to inhibit PoxP3 MFI was evaluated using flow cytometry assays.

3.2.9 Usp22i-S02 holds great preclinical efficacy in enhancing anti-tumor immunity

The following data was done in collaboration with Ming Yan from the Department of Immunology at the Fourth Military Medical University.

After initial screening, we ran a dose response study on compound S02, now dubbed Usp22i-S02, in both WT and Usp22-null iT_{reg} cells (**Fig. 3.13a-c**). A concentration of $10\mu\text{g/mL}$ showed decreases in Foxp3 MFI and protein level comparable to Usp22-null iT_{reg} cells with little effect on viability, indicating a near complete suppression of Usp22 activity in stabilizing Foxp3. Importantly, Usp22i-S02 administration to human T_{reg} cells significantly decreased Foxp3 MFI, showing the relevance of this inhibitor to human cells (**Fig. 3.13d and e**). In contrast, Usp22i-S02 had minimal effect on Foxp3 levels in murine iT_{reg} cells already lacking Usp22 at $10\mu\text{g/mL}$ (**Fig. 3.13a and f; Fig. 3.14b and c**). If considering the Usp22 genetic deletion a 100% inhibition of Usp22, Usp22i-S02 achieved an 50% suppression of Usp22 function in T_{reg} cells at a concentration of $2.77\ \mu\text{g/mL}$ ($8.2\ \mu\text{M}$) when evaluated using T_{reg} Foxp3 MFI. Functionally, Usp22i-S02 administration had similar effects to Usp22 deletion in iT_{reg} cells, resulting in enhanced FOXP3 degradation in cycloheximide (CHX) treated cells, increased FOXP3 ubiquitination, and decreased Foxp3 transcription (**Fig. 3.13g-j**). Furthermore, Usp22i-S02-mediated FOXP3 degradation was halted by MG132 protease inhibition, indicating that Usp22i-S02 enhances proteasomal-specific

degradation of FOXP3 (**Fig. 3.13k**). Therefore, these results indicate that Usp22i-S02 is a potent USP22-specific small molecule inhibitor that downregulates Foxp3 expression in Tregs.

Administration of Usp22i-S02 to WT mice mimicked a genetic deletion of Usp22 in T_{reg} cells, showing a significant drop in FOXP3 MFI in T_{reg} cells from the spleen and lymph nodes without any alteration in T_{reg} cell frequency (**Fig. 3.14c and d**). To test the functionality of Usp22i-S02 in tumor conditions, we used the LLC1 Lewis lung carcinoma syngeneic tumor model. Upon LLC1-challenge, WT mice administered Usp22i-S02 showed striking tumor rejection compared to untreated mice, as well as a significant increase in CD8⁺ T cell tumor infiltration (**Fig. 3.14e-h**). Further analysis of tumor infiltrating lymphocytes indicated a less exhausted phenotype in CD8⁺ T cells, with an increase in CD44⁺ cells and a decrease in T-bet⁺, Blimp1⁺, and Annexin V⁺ cells (**Fig. 3.14i-l**). Importantly, intratumoral Foxp3⁺ T_{reg} percentage significantly decreased following administration of Usp22i-S02 (**Fig. 3.14m-n**). Together, our data show the critical role of Usp22 in T_{reg} cell stability and adaptation within the TME, and that specifically targeting Usp22 with a small molecule inhibitor enhances antitumor immunity with the potential to complement existing immunotherapies.

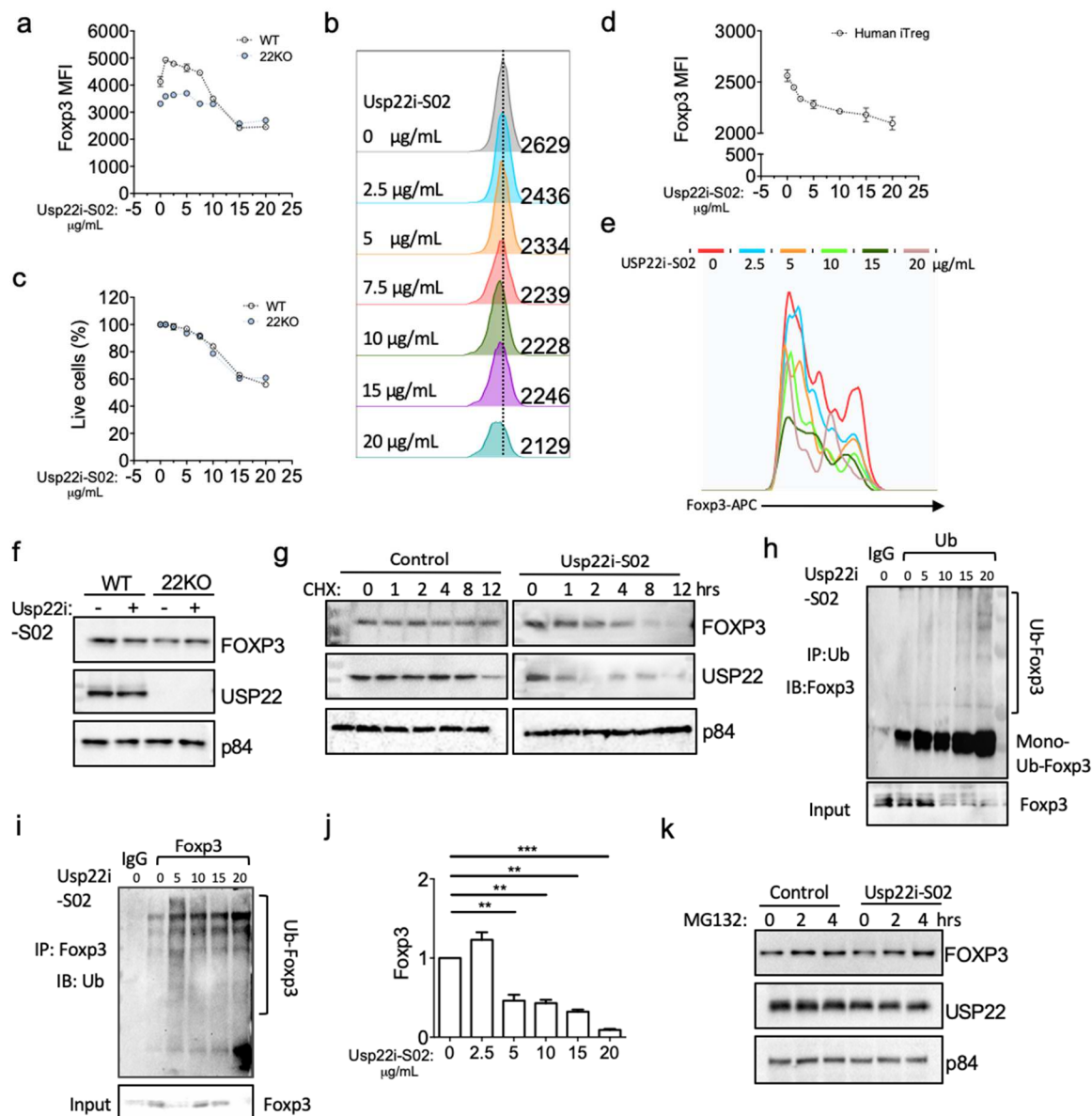


Figure 3.13 *Usp22i-S02* halts in *Usp22*-mediated *Foxp3* deubiquitination. **a**, Graphical representation of FoxP3 MFI change in WT versus 22KO iTreg cells treated with various doses of Usp22i-S02 (n=3). **b**, Representative histogram of Foxp3 MFI level in iTreg cells as Usp22 inhibitor concentration increases from 0-20µg/mL. **c**, Cell survival of iTreg cells treated with various doses of Usp22i-S02 (n=3). **d-e**, Graphical and representative data of Foxp3 MFI of human Treg cells treated with various doses of Usp22i-S02 (n=3). **f**, FOXP3 and USP22 protein level in WT and 22KO mice treated with 10µg/mL Usp22i-S02. **g**, FOXP3 and USP22 protein degradation of cycloheximide (10µg/mL) treated iTreg cells with or without the addition of 10µg/mL of Usp22i-S02. **h-i**, Endogenous DUB assay IP in iTreg cells of USP22 with FOXP3 under increasing concentrations of Usp22i-S02. **j**, Foxp3 mRNA level in iTreg cells as Usp22 inhibitor concentration increases from 0-20µg/mL (n=3). **k**, FOXP3 and USP22 level in WT iTreg cells with or without 20µg/mL Usp22 inhibitor treated with 20µM MG132. **j**, One-way ANOVA with Dunnett's multiple comparisons between rows relative to control was performed to determine statistical All data are presented as mean ± stdev. NS, not significant. *P < 0.05, **P < 0.01, ***P < 0.001, ****P < 0.0001.

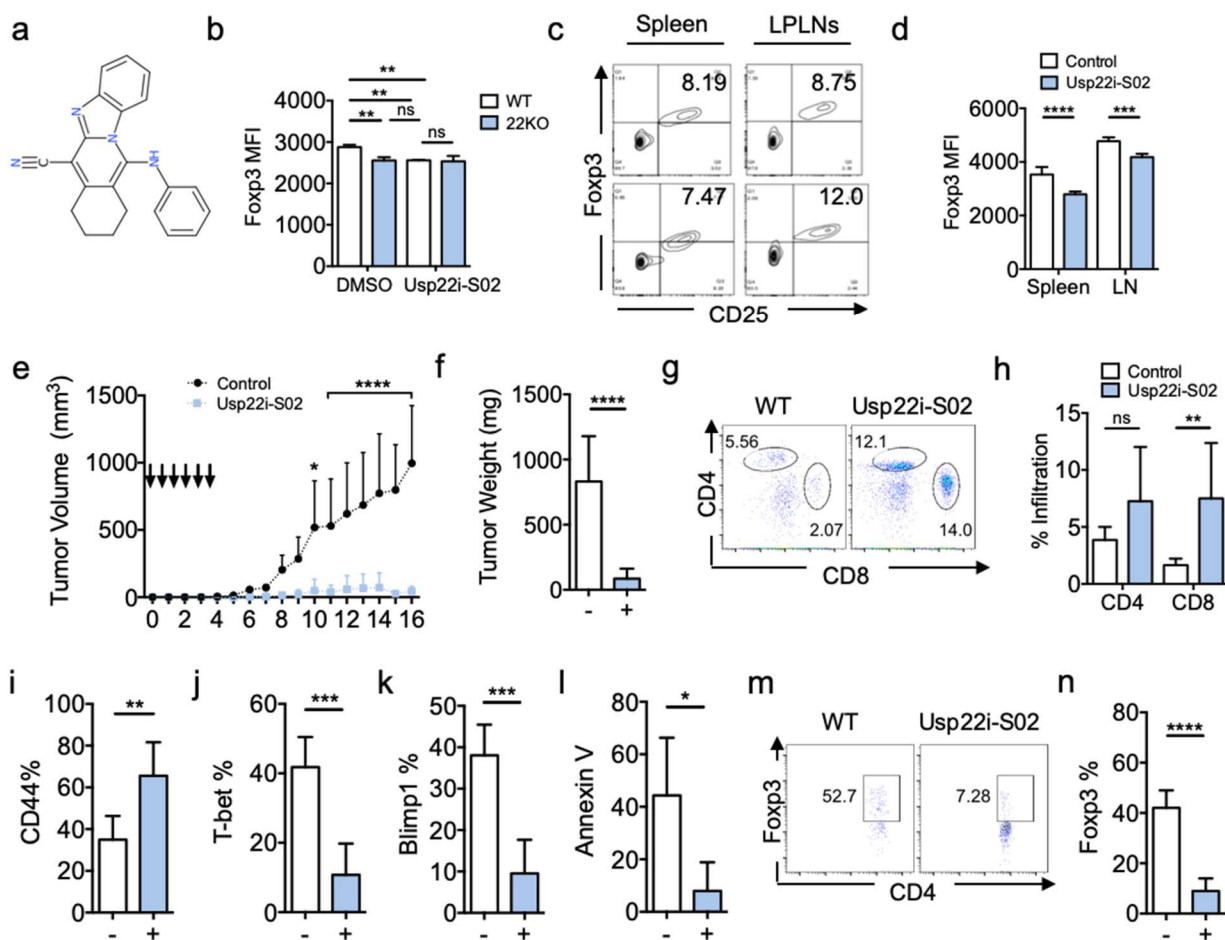


Figure 3.14 *Usp22i-S02* administration enhances antitumor immunity. **a**, Structure of compound CS30 (Usp22i-S02). **b**, FOXP3 MFI in WT and 22KO nT_{reg} cells after treatment with 20 μg/mL of Usp22i-S02 (n=3). **c**, Representative flow cytometry plot of FOXP3+CD25+ MFI of CD4⁺ peripheral cells of mice treated with 20 μg/mL of Usp22i-S02 relative to control (n=5). **d**, Graphical representation of Foxp3 MFI upon Usp22i-S02 administration (n=5). **e**, Tumor growth curve of LLC1 cells subcutaneously injected in the flank of WT mice with or without the addition of 20 mg/kg/time of the Usp22 inhibitor, in 100 μL of oil (n=5-10). **f**, Tumor weight of WT mice treated with 20 μg/mL of Usp22i-S02 (+) relative to control (-) at day 16 (n=10). **g-h** Representative flow cytometry plot and graphical representation of % infiltration of CD4⁺ and CD8⁺ T cells within the tumor (n=5). **i-l**, Percent of activation and exhaustion markers on CD8⁺ intratumoral T cells (n=5). **m-n**, Representative flow cytometry plot and graphical representation of intratumoral Treg percentage in mice treated with 20 μg/mL of Usp22i-S02 relative to control (n=5). **a**, **e**, **h**, Two-way ANOVA with Sidak's multiple comparisons between rows was performed to determine statistical significance. **d**, **f**, **i-l**, **n** Two-tailed unpaired t-test was done to determine statistical significance. All data are presented as mean ± stdev. NS, not significant. **P* < 0.05, ***P* < 0.01, ****P* < 0.001, *****P* < 0.0001.

3.3 Conclusions

Through abnormal vascularization, cytokine production, and nutrient depletion, tumors can create a highly immunosuppressive TME that favors the functionality of immune regulatory programs of T_{reg} cells over anti-tumor effector responses. This TME-specific T_{reg} fitness/adaptation functions through increased Foxp3 expression and suppressive abilities to further diminish the anti-tumor effects of T_{eff} cells. However, the factors and underlying molecular mechanisms by which T_{reg} fitness is induced and maintained remained unknown.

In Chapter 3, we discovered that TME factors including TGF-beta, hypoxia, and metabolic stresses selectively induce Foxp3-targeting deubiquitinases Usp22 and Usp21 to stabilize Foxp3 for T_{reg} adaptation. Usp22 is dramatically elevated in intratumoral T_{reg} cells from multiple syngeneic tumor mouse models as well as in human primary lung cancer. Importantly, Usp22 level is tightly correlated with Foxp3 upregulation in human intratumoral Treg cells. Usp21 levels increase only in certain tumors. The following TME factors are identified to induce the expression of either Usp22 or Usp21 or both, in T_{reg} cells: **(1)** Tumor-secreted TGF-beta enhances Usp22 through Smad-mediated canonical TGF-beta signaling. Subsequently Usp22 functions as a positive feedback through selective deubiquitination and stabilization of SMAD2 and SMAD4. In contrast, TGF-beta induced Usp21 transcription is SMAD-independent. **(2)** Hypoxia induces T_{reg} Usp22 transcription through HIF- α stabilization, and Usp22 is required for maintaining Foxp3 expression in T_{reg} cells under hypoxic conditions. **(3)** Nutrient starvation selectively induces Usp22 and Usp21 in T_{reg} cells through AMPK and mTOR-mediated metabolic reprogramming.

Importantly, T_{reg} -specific deletion of either Usp22 or Usp21 results in marked differences in metabolic and cell cycle pathways, suggesting an importance of these USPs for T_{reg} stability under environmental stress. As a consequence, targeted deletion of both Usp22 and Usp21 in T_{reg} cells

enhanced antitumor immune responses and inhibited tumor growth in mice. Therefore, Usp22 and Usp21 expression is required for T_{reg} fitness in the TME. Indeed, simultaneous Usp22 and Usp21 deletion impairs T_{reg} fitness and consequently improves antitumor immune responses. Finally, as Usp22 inhibition alone is sufficient to illicit antitumor immunity, we developed a Usp22-specific small molecule inhibitor, which resulted in significant anti-tumor effects.

The impact of our findings is multidimensional: **1st**, we have identified a previously unappreciated molecular link between specific TME factors and T_{reg}-mediated suppression, providing a molecular mechanism of how tumors escape from antitumoral immune surveillance through T_{reg} fitness; **2nd**, we have unveiled new mechanisms behind T_{reg} adaptations that conserve their function under environmental stress, which has been an immunological mystery; and more importantly, **3rd**, our studies provide a rationale and method for Usp22-specific targeting in antitumor immune therapy. In particular, while it has been implied that T_{reg} cells are a potential therapeutic target, approaches to specifically inhibiting T_{reg} suppressive functions are yet to be identified. *Our discovery that Usp22 deletion impairs intratumoral Treg suppressive activity without promoting extensive inflammatory response indicate that Usp22 inhibition holds a great therapeutic potential in antitumor immune therapy.* Moreover, our results hold wide-ranging applications to researchers in diverse fields by demonstrating the impact of metabolism, hypoxia, and cytokine secretion in the TME to the preferential stabilization of Treg cells, offering new targets for antitumor therapies.

CHAPTER 4: Discussion

In these studies, I have shown the importance of ubiquitin-specific peptidase in regulating T_{reg} function and adaptability through Foxp3 stability in response to environmental cues.

Emerging data suggests that the TME, which is deprived of nutrients and oxygen, likely offers a metabolic advantage to T_{reg} cells over T_{eff} cells to further promote an immunosuppressive microenvironment. However, the TME-specific factors and their cellular targets that potentiate T_{reg} cell suppressive function and adaptation remain largely unidentified. My thesis illustrates a previously unappreciated role of Foxp3-specific DUBs, Usp22 and Usp21, as environmentally-sensitive factors that enhance Foxp3 stability in the TME. We identified several TME factors that upregulate Usp22 and Usp21, ultimately stabilizing Foxp3: (1) tumor-secreted TGF-beta; (2) hypoxia; (3) glucose-restriction; and (4) amino acid-deprivation (**Fig. 4.1**). Our findings unveil new mechanisms behind the metabolic and functional uniqueness of T_{reg} cells, providing evidence on how these cells adapt in response to environmental cues to support their function.

4.1 Innovation

It is clear that the dynamic nature of Foxp3 expression is pivotal to proper immune regulation. These studies reveal the importance of transcriptional to post-translational modifications to preserving tolerance and T_{reg} function. The breadth of direct DUBs and E3 ligases of FoxP3 suggest a strong need for conditional regulation of T_{reg} suppression. Enlightening both the direct and indirect ubiquitin-mediated pathways that downregulate FoxP3 reveal means to alter T_{reg} functional capabilities. Specifically, the targeting of these regulatory molecules may be an effective way to either elicit or break tolerance in auto-immune or antitumor immune therapies.

4.1.1 Addressing T_{reg} cells in Tumor Immunity

Immunotherapy has revolutionized the landscape of cancer treatments through triggering cell-mediated anti-tumor immunity, resulting in durable and longer-lasting responses in multiple cancer types. However, in specific malignancies, such as bladder cancer and lung cancer, current immunotherapies are proving less efficacious due to the infiltration of particularly suppressive T_{reg} subsets²⁰⁸. Therapeutic targeting of T_{reg} cells is largely restricted due to the lack of T_{reg}-specific cell surface markers. For example, anti-CD25 and anti-CTLA-4 mediated T_{reg} depletion are rather transient, and both markers are upregulated upon conventional T cell activation. As targeting T_{reg} cells through a specific marker has proven challenging, promising new strategies focus on attenuating T_{reg} suppressive function through major transcription factor, Foxp3, regulation.

In Chapter 2, we identified ubiquitin-specific peptidase Usp22 as a transcriptional and post-translational regulator of T_{reg} function through Foxp3 transcription and stability. Particularly, Usp22 transcriptionally regulates Foxp3 through deubiquitinating histone H2B at the Foxp3 locus (**Fig. 2.3-2.4**), and post-translationally stabilizes FOXP3 protein levels through its DUB function (**Fig. 2.5**). Furthermore, Treg-specific deletion of Usp22 (22KO) largely diminishes T_{reg} suppressive function in mice challenged with multiple auto-immune and tumor models. Specifically, 22KO mice develop age-related autoimmune responses (**Fig. 2.6** and **Fig. 2.7a-b**) as well as enhanced MOG-induced autoimmunity (**Fig. 2.7e**). Additionally, T_{reg} cells lacking Usp22 are unable to protect immune-compromised mice in an adoptive transfer model of colitis (**Fig 2.7 c-d**). Importantly, 22KO mice displayed reduced tumor growth and enhanced antitumor immunity against multiple syngeneic tumor models (**Fig. 2.7f-k** and **Fig. 2.8**), defining the role of Usp22 as a previously unappreciated critical deubiquitinase of Foxp3 that maintains T_{reg} stability.

In addition, recent studies have identified Usp22 as a putative cancer stem cell gene, where high expression of Usp22 is tightly correlated with poor prognosis and therapy failure^{170,171,209}. Furthermore, inhibition of Usp22 attenuates tumorigenesis by inducing tumor cell apoptosis and blocking the cell cycle progression during cancer cell proliferation^{171,210,211}. Therefore, targeting on Usp22 could not only inhibit tumorigenesis, but also restrain suppressive activity of T_{reg} cells to boost anti-tumor immune response. In summary, Chapter 2 elucidated the physiological role of Usp22 on Foxp3 expression and Treg suppressive function, expanding our knowledge of Treg biology and immune regulation. Importantly, Chapter 2 set the foundation for Usp22 as an attractive T_{reg}-specific target for immunotherapy.

4.1.2 Importance in Intratumoral T_{reg}-Specific Target

It is well established that an increase in intratumoral (it)T_{reg} cells correlates with poor prognosis, defining itT_{reg} cells as a major hurdle in tumor therapies⁶³. More recent data describes itT_{reg} cells as particularly suppressive, with increased levels of Foxp3 and various suppressive markers^{72,73,127,212}. Chapter 2 and others have shown that diminishing T_{reg} suppressive function results in enhanced anti-tumor immunity^{97,182,213}. Unfortunately, many current checkpoint inhibition tumor therapies, often have severe autoimmune side-effects, which could possibly be exacerbated in T_{reg}-targeting therapies. Despite their negative role in tumor immunity, T_{reg} cells remain an important player in maintaining immune tolerance against autoimmunity. Therefore, the most attractive therapies will be those targeting T_{reg} function specifically within the TME without majorly altering T_{reg} function in the periphery.

In Chapter 3, I describe Usp22 as an ideal immunotherapeutic target for its consistent induction in itT_{reg} cells from various pre-clinical tumor models as well as in human isolated itT_{reg} cells from lung cancer patients (**Fig. 3.2**). Furthermore, Usp22 upregulation is correlated with

higher Foxp3 expression in human lung cancer itT_{reg} cells, suggesting that TME factors selectively induce Usp22 to protect Foxp3 from ubiquitin-mediated degradation while simultaneously promoting Foxp3 transcription (**Fig. 3.2e**). These data suggest a specific importance of Usp22 in Treg cells within the TME. The fact that we observed increased Usp22 in human itT_{reg} cells broadens the relevance of this pathway to human tumor therapies.

In contrast, Usp21 mRNA level was only increased under B16 challenge, suggesting that Usp21 upregulation in T_{reg} cells occurs only under certain TME conditions (**Fig. 3.2a-c**). Furthermore, Usp21 was not increased in human lung tumor $itTreg$ cells nor did it have a significantly positive correlation with Foxp3 (**Fig. 3.2d-e**). This data recapitulates the syngeneic lung cancer model, and suggests that Usp21 is important in itT_{reg} function under certain conditions, but not others.

Although Usp7 in T_{reg} cells is known to control Foxp3 expression and T_{reg} suppressive function in a model of colitis, we did not observe an increase in Usp7 expression in itT_{reg} cells, suggesting Usp7 may primarily regulate T_{reg} function during homeostatic conditions. Furthermore, deletion of Usp7 in T_{reg} cells results in severe autoimmunity in young mice, making targeting Usp7 for cancer therapy problematic¹⁶⁸.

4.2 TME factors and Usps

Our data demonstrates that the upregulation of Usp22 and Usp21 in itT_{reg} cells is not tumor, nor species, specific. Therefore, we wanted to assess the specific factors in the TME that activate USP expression. Determining which factors upregulate these Usps gives us a deeper understanding of TME characteristics and their effects on the immune system.

4.2.1 Tumor-produced TGF-beta

TGF-beta is a major player in iT_{reg} conversion and stability and is broadly secreted by many tumor types. We found that tumor secreted TGF-beta is sufficient in upregulating Usp22 through canonical, Smad-mediated, TGF-beta signaling (**Fig. 3.3-3.5**). Furthermore, Usp22 partakes in a feedback loop to further upregulate itself and Foxp3 through SMAD2 and SMAD4 protein stabilization (**Fig. 3.6**). As TGF-beta is particularly important for T_{reg} cells over T_{eff} cells, tumor-secreted TGF-beta can strengthen T_{reg} suppressive function through Usp22, while potentially skewing T_{eff} to a more regulatory phenotype.

Unlike Smad2 and Smad4 we did not find Smad3 reduction in Usp22- null Treg cells, yet Smad3 was shown to bind to the Usp22 promoter region. This data suggests that, while Smad3 is an important player in Usp22 transcription, Usp22 does not act as a DUB of Smad3 to potentiate signaling. Interestingly, Smad3 is an important component of mTOR-inhibition mediated T_{reg} differentiation. Delgoffe et al. describes that mTOR-null naïve T cells undergoing differentiation are particularly sensitive to TGF-beta , and skew towards the T_{reg} phenotype upon TCR engagement. Specifically, mTOR-deficient T cells displayed significant phosphorylation of Smad3. So, it is possible that, although Smad3 is not decreased upon Usp22 deletion in T_{reg} cells, Smad3 activation through its phosphorylation is significantly decreased. Future experiments determining the levels of phosphorylated SMAD proteins can easily tackle this question.

Although Usp21 was not functioning through the canonical TGF-beta pathway, it is possible that the non-canonical TGF-beta JNK/P38 signaling pathway could be at play²¹⁴. Future research could specifically uncover the mechanism by which Usp21 is upregulated through TGF-beta signaling. However, due to the marginal Usp21 increase, it is possible that this pathway may be secondary to the stability provided by the Usp22-TGF-beta feedback loop. It would be

interesting to see the level of Usp21 under these conditions in T_{reg} cells lacking Usp22, yet it is likely not terribly important for iT_{reg} adaptability to the TME alone.

As TGF-beta is widely implicated in Foxp3 expression and stability, and iT_{reg} function, our data adds a new level of complexity to already known systems^{93,148}. These novel mechanisms potentially function to ensure T_{reg} cell stabilization through alternate pathways, strengthening their ability to maintain their suppressive capacity in diverse microenvironments.

4.2.2 Hypoxia in the TME

As hypoxia is a major hallmark of solid tumors^{32,103}, we investigated how low oxygen conditions influence Usp22 levels in T_{reg} cells. Hypoxia induced Usp22 in a HIF-dependent manner (**Fig. 3.7a-b** and **3.8a-d**). Also, upon Usp22 deletion, nT_{reg} cells under hypoxic stress could not sustain stable FOXP3 expression (**Fig 3.7c-d** and **3.8e-f**). Our findings are in line with previous data that demonstrated heightened proliferation and suppressive capabilities of nT_{reg} cells under hypoxic conditions¹¹⁵. These data, paired with the knowledge of two functioning HIF binding sites along the Usp22 promoter, imply that hypoxia can enhance T_{reg} suppressive function through Usp22-dependent stabilization of FOXP3²⁰⁵.

The field of hypoxia and T_{reg} cells is convoluted, with studies indicating controversial findings on T_{reg} stability and suppressive functions under hypoxic conditions^{115,121,215}. Although nT_{reg} cells cultured in hypoxic conditions became more proliferative and suppressive, suggesting that hypoxia strengthens T_{reg} function, hypoxia is far from an ideal environment for immune cell survival and function. So, rather than considering hypoxia as a potential stimulator of T_{reg} function, Chapter 3 identifies a mechanism for T_{reg} adaptability under hypoxic conditions. As Chapter 2 identifies Usp22 as particularly important for T_{reg} cell function through its Foxp3 inducing and stabilizing roles, the fact that hypoxia can induce Usp22 demonstrates an adaptive advantage over

T_{eff} cells. Specifically, we show that Usp22 induction is through HIF α , which has two functioning HIF binding sites along the Usp22 promoter. This implies that hypoxic stabilization of HIF α induces Usp22 transcription through HIF α binding directly to the Usp22 promoter region, however this assertion is speculative as we do not directly demonstrate it. Ultimately, Chapter 3.2.4 introduces a mechanism for T_{reg} adaptability under hypoxic environments, providing insight to the advantage of T_{reg} over T_{eff} cells within the TME.

4.2.3 AMPK and mTOR: Upstream Signaling

Along with a decrease in oxygen availability, the competition for nutrients that occurs within the TME influences immune cell growth, survival, and function. Classically, T_{reg} cells are thought to have a significantly lower reliance on glycolysis than T_{eff} cells, potentially providing another advantage^{35,126,198}. Our data identifies Usp22 and Usp21 as an important mediator in this process, functioning to stabilize FOXP3 under glucose- and/or amino acid-deprivation.

In part the enhanced stability of FOXP3 appears secondary to AMPK activation, which likely occurs under glucose restriction within the TME. Interestingly, AMPK activation in T_{reg} cells is accompanied by a shift towards oxidative metabolism, which may further enhance T_{reg} survival in the TME¹³⁵. We show that oligomycin-induced AMPK activation is sufficient to upregulate Usp22 and Usp21, implicating their involvement in FOXP3 stabilization for T_{reg} cell function under energy stress (**Fig 3.7d-g** and **Fig. 3.8h-k**). The promotion of AMPK signaling via nutrient deficiency also suppresses mTOR activity within T cells^{36,216}. As the balance of AMPK and mTOR signaling modulates cellular state and metabolism in response nutrient availability, it is possible that AMPK activation primarily increases Usp22 and Usp21 expression thru inhibition of mTOR signaling. Indeed, mTOR inhibition was capable of upregulating Usp22 and Usp21 in T_{reg} cells.

It is widely appreciated that AMPK activation results in mTOR inhibition, however the mechanical underpinnings are not fully defined. Under steady state conditions, ATP is produced by catabolic processes such as the breakdown of glucose. However, under glucose starvation, the ATP:AMP ratio drops, activating AMPK to redirect metabolism towards increased catabolism and decreased anabolism through mTOR inhibition. Although our data shows that both AMPK activation and mTOR inhibition upregulate both Usp22 and Usp21 expression (**Fig. 3.7** and **Fig. 3.8**), the implication that AMPK activation results in mTOR inhibition in this setting is mostly correlative. It is especially important to note that oligomycin, which induces AMPK activation through inhibition of mitochondrial complex V, also independently alters mTOR activity. Future studies can delineate the exact mechanisms behind AMPK-mediated mTOR inhibition as it pertains to Usp22 and Usp21 activation under nutrient restriction.

Recent data identifies RIPK1 as an important facilitator of AMPK-mediated mTOR inhibition through TSC2 phosphorylation²¹⁸. Therefore, it is possible that RIPK1 stabilization within the TME could drive AMPK-mediated mTOR inhibition, ultimately increasing Usp22 and Usp21 levels. Furthermore, another starvation-mediated mechanism has been proposed to activate AMPK, involving fructose-1,6-bisphosphate (FBP)-mediated axin regulation of AMPK activation. In this mechanism, axin-mediated AMPK activation following glucose starvation results in AMPK localization to the lysosome with mTOR, potentially allowing for co-regulation²¹⁷. Specifically, this pathway allows for AMPK activation regardless of the ATP:AMP ratio. As tumor cells are known to secrete fatty acids, and T_{reg} cells have a higher capacity to use fatty acid oxidation (FAO) as an energy source to create ATP, it is possible that their ATP levels do not drop significantly for constitutive AMPK activation. However, as axin-mediated activation of AMPK is ATP:AMP ratio independent, it can allow for T_{reg} cells to use FAO to produce significant ATP for survival while

still activating AMPK. It would be interesting to see the status of AMPK activation in T_{reg} cells within the TME, and if upstream axin-inhibition would diminish the AMPK/mTOR-mediated upregulation of Usp22.

Interestingly, although both glucose and amino acid starvation would result in mTOR inhibition, Usp21 was only upregulated by amino acid starvation while Usp22 was upregulated by both (**Fig 3.7d and f and 3.8h and K**). This implies that distinctive energy starvation signals may be received and transmitted differently within a cell, allowing for more precise regulation for specific environmental cues. Particularly, the v-ATPase-Ragulator-Rag-mTORC1 pathway responsible for mTOR inhibition under amino acid deprivation may be predominant over glucose-starvation-mediated mTOR inhibition in upregulating Usp21. Although this pathway does not directly activate AMPK, and we show AMPK activation is sufficient in upregulating Usp21, amino acid starvation leads to an increase in cytosolic Ca²⁺, which induces AMPK activation through Ca²⁺/calmodulin-dependent kinase kinase-β (CaMKK-β). This activation of AMPK can further inhibit mTOR, potentially explaining how both pathways could be involved in Usp22 and Usp21 activation under amino acid deprivation.

However, when considering the broad importance of these pathways for a T_{reg}, it is logical to consider mTOR as the centerpiece. Specifically, as nutrient starvation shifts cellular metabolism from anabolism to catabolism, it also downregulates protein synthesis. As such, maintenance and stabilization of proteins already in existence, particularly through DUBs like Usp22 and Usp21, becomes pinnacle for a cell's survival. Therefore, it is likely that the environmental signals are ultimately sensed through the mTOR pathway, and Usp22 and Usp21 upregulation is an instrument by which T_{reg} cells can adapt and stabilize their function under metabolic stress.

4.2.4 AMPK and mTOR: Downstream Signaling

Collectively, Chapter 3.2.5 touches on the importance of nutrient sensing in T_{reg} adaptation to the TME through Usp22 and Usp21 upregulation, however our work does not elucidate the downstream mechanisms. As both AMPK activation and mTOR inhibition regulate a plethora of interconnected pathways, it would be incredibly difficult, albeit interesting, to tease out the exact downstream mechanism(s). Possible mechanisms may be found through the many AMPK substrates or through the plethora of mTOR downstream actions.

The most logical place to start would be at the Usp promoter regions, as mTOR inhibition upregulates Usp22 and Usp21 transcription. Although very little is known about Usp22 transcriptional regulation, Xiong *et al.* discovered that specificity protein 1 (SP1) is a transcriptional repressor of Usp22²¹⁶. Interestingly, SP1 is known to be a transcriptional activator of many mTOR signaling gene promoter²¹⁷. Therefore, it is possible that inhibition of mTOR diminishes SP1 activity, and allow for heightened transcription of Usp22. Another possibility is through Smad3 activation. As stated in section 5.2.1, mTOR deficiency showed a remarkable increase in Smad3 phosphorylation. Since we show that Smad3 binds to the Usp22 promoter region in a TGF-beta -dependent manner, it is possible that mTOR-inhibition allows for increased Smad3 phosphorylation to perpetuate Usp22. However, this pathway seems to be more likely in iT_{reg} cells, that are heavily dependent on TGF-beta signaling for their Foxp3 expression and suppressive function.

Unfortunately, not much is known about Usp21 regulation, and without transcription factors to start at, it becomes impossible to determine the exact downstream mechanism without further analysis. Future experiments could focus on proteins inhabiting the Usp21 and Usp22 promoter regions when mTOR signaling is active or inactive through DNA- rather than protein-

mediated chIP. When this technology is widely available, it could give insight into what transcription factors reside on the promoter upon nutrient starvation and mTOR inhibition.

4.3 Usp22 and Usp21 on T_{reg} Stability in the TME

Together, our data indicate that microenvironmental stress within the TME upregulates T_{reg} USP levels, which then function to stabilize FOXP3. Enhanced FOXP3 stability further supports T_{reg} cell adaptation to the TME; thus, identifying Usp22 and Usp21 as important environment-sensitive factors that regulate T_{reg} cell identity, metabolism and function in the TME. Here, I explore the possible mechanisms:

4.3.1 Cell Cycle Progression

The metabolic status of an immune cell is highly important within the TME for their cell survival and function. As T_{reg} cells are able to adapt to low-oxygen, low nutrient environments, this gives them a metabolic advantage compared to T_{eff} cells. Importantly, FOXP3 is essential to this process as it is known to promote oxidative phosphorylation within T_{reg} cells. We show that Usp22- and Usp21-deficient T_{reg} cells have significantly altered expression of metabolic genes and impaired OCR and ECAR. In addition, RNA sequencing analysis demonstrated that loss of Usp22 and Usp21 in T_{reg} cells resulted in the upregulation of multiple pathways associated with cell growth and proliferation. Collectively, these data raise the intriguing possibility that Usp22 and Usp21 work to promote T_{reg} cell quiescence in nutrient-restricted environments in part through modulating T_{reg} cell metabolic programs. Future research could carefully analyze these pathways, such as G₂-M checkpoint and E2F targets in relation to Usp22 and Usp21.

Cell cycle progression is regulated by the association of specific cyclin dependent kinases with cyclin regulatory proteins at the different cell cycle checkpoints. The G₂-M checkpoint is

driven by Cyclin B1 (CCNB1) and cyclin dependent kinase 1 (CDK1) activity, where accumulation of cyclin B aids in CDK1 activation as cells prepare to enter mitosis. E2F proteins, on the other hand, are primarily known to control entry into the S-phase of the cell cycle²¹⁸. Interestingly, Usp22 has been shown to deubiquitinate CCNB1, allowing for cell cycle progression¹⁷³. Furthermore, others have shown that loss of Usp22 decreases cancer growth as well as downregulation of the G₂-M and E2F pathways. Similarly, Usp21 is known to promote cell cycle progression in tumor cells through Foxm1 and MEK2^{219,220}. Our data, however, indicates that loss of Usp22 and Usp21 in T_{reg} cells increases the G₂-M and E2F signaling pathways. This discrepancy could be due to Usp22 and Usp21 having cell-specific functions that are not conserved between tumor cells and T_{reg} cells. Another possibility is Usp22 and Usp21 regulation of cell cycle progression could be indirect and possibly through their regulation of T_{reg} metabolism or autophagy (described below). Ultimately, these data suggest a multifaceted and context-dependent role of Usp22 and Usp21 in cell cycle regulation.

4.3.2 Autophagy

Our data indicates that Usp22 loss results in the upregulation of multiple pathways associated with cell growth and proliferation, suggesting that its role may be more to maintain T_{reg} cells under stress rather than to push them towards proliferation. Interestingly, Usp22 has been implicated in mediating autophagy through the Ras/RAF1/MEK1/2/ERK1/2 pathway²²¹. These data foster the interesting possibility that Usp22 promotes autophagic pathways to sustain T_{reg} cells in stressful environments. Additionally, Usp22-induced autophagy increases resistance to cell starvation in pancreatic tumor cells²²¹, a role that could extend to T_{reg} cells. As selective autophagy can regulate cell cycle progression by removing key cell cycle regulators, Usp22-mediated autophagy may reduce cell cycle progression in Treg cells through potentiating autophagy.

Importantly, autophagy is downregulated by the activation of the PI3K/AKT/mTOR pathway. Although Ras/RAF1/MEK1/2/ERK1/2 and PI3K/AKT/mTOR are parallel pathways, it suggests that inhibition of mTOR and upregulation of Usp22 both function to conserve energy within a cell under stressful conditions.

4.4 Usp22 as the Ideal Antitumor T_{reg} Target

We and others have demonstrated that both Usp22 and Usp21 are upregulated in many cancer types, such as gastric carcinoma, pancreatic cancer and melanoma, and have been correlated with poor prognosis^{170,222}. Usp22 promotes oncogenic c-Myc activation as well as indirectly antagonizes the tumor suppressive function of p53, while Usp21 functions as an oncogene by stabilizing a group of transcription factors including Fra1, FoxM1 and Wnt^{171,222,223}. Importantly, Usp22 and Usp21 also function to maintain Foxp3 expression through DUB function at the transcriptional (Usp22) and post-translational (both) levels. This duality makes Usp22 and Usp21 highly attractive potential therapeutics that can target both tumor cell intrinsic and immunosuppressive pathways simultaneously. Indeed, their combined loss resulted in the most significant impairment in T_{reg} tumor-promoting functions, suggesting that Usp22 and Usp21 play distinct roles in modulating Treg cell adaption and function in the TME.

4.4.1 Usp22 as an ideal Target for itT_{reg} cells

Altogether, this Chapter 3 suggests that Usp22 is the dominant Foxp3-DUB in T_{reg} cells specifically inhabiting the TME, making it an even more attractive target for anti-tumor therapies. Specifically, the loss of Usp22 in T_{reg} cells resulted in enhanced anti-tumor immunity relative to the loss of Usp21, suggesting a dominance of Usp22 in itT_{reg} cells (**Fig 3.11**). Therefore, specifically targeting Usp22 may be sufficient in eliminating the advantage T_{reg} cells have over T_{eff} within the TME. To test this, we developed and tested the first ever Usp22-specific inhibitor.

Administration of the inhibitor resulted in a dramatic decrease in iT_{reg} number, resulting in strong *in vivo* anti-tumor effects. Although Foxp3 MFI levels in iT_{reg} cells did not decrease following Usp22i administration, the significant decrease in iT_{reg} percentage confirms the importance of Usp22 in Treg stability and fitness within the TME. Our data demonstrate that Usp22 is a targetable protein, and that the inhibitor Usp22i has the potential of being incorporated into tumor immune therapies. Furthermore, many current therapeutics focus on promoting T_{eff} cell function, as such the addition of Usp22 inhibition with current therapies could further enhance anti-tumor immunity through synergistic effects without significant hampering to peripheral T_{reg} cells.

CHAPTER 5: Materials and Methods

5.1 Cell Lines, Plasmids, Antibodies, and Reagents

Human embryonic kidney 293 (HEK293) cells were purchased from ATTC and stored in the Fang lab. Platinum-E (Plat-E) Retroviral Packaging cells (Cell Biolabs, Inc., Cat# RV-101) were provided by the Bluestone and Cyster Labs and cultured per the manufacturer's instructions.

EG7 Lymphoma, MC38 colon carcinoma, LLC1-OVA lung carcinoma, and B16-F10 melanoma cell lines were provided by the Zhang laboratory at Northwestern and used for tumor models as previously reported (14). The cells lines were cultured in DMEM with 10% FBS, and were tested for mycoplasma using LookOut Mycoplasma PCR detection kit (Sigma, MP0035-1KT). MYC-USP22, Flag-Smad2, Flag-Smad3, Flag-Smad4, and HA-ubiquitin pCMV expression plasmids and their tagged vectors were constructed by the Fang lab and stored at -20°C. All western blot, co-immunoprecipitation, and flow cytometry antibodies are listed in Table 2. Phorbol 12-myristate 13-acetate (PMA), ionomycin and cycloheximide were purchased from Sigma. Monesin was from eBioscience.

5.2 Animal Models

Usp22 floxed mice were generated and used as recently reported⁴⁷. The Usp22 target mouse embryonic stem cells from C57BL/6 mice were purchased from the Wellcome Trust Sanger Institute. Blastocyst injections resulted in several chimeric mice with the capacity for germline transmission. Breeding of heterozygous mice yielded $Usp22^{+/+}$, $Usp22^{+/targeted}$ but not $Usp22^{targeted/targeted}$ mice due to the obligation of Usp22 expression by the neomycin selection and β -gal reporter cassette, which causes embryonic lethality. We then bred $Usp22^{+/targeted}$ mice with Flp recombinase transgenic mice to delete the selection cassette, leading to the generation of $Usp22^{+/fl}$ mice, further breeding of which produced $Usp22^{+/+}$, $Usp22^{+/fl}$ and $Usp22^{fl/fl}$ mice without phenotypic abnormalities in expected Mendelian ratios. Treg-specific Usp22-null mice were generated by breeding $Usp22^{fl/fl}$ mice with $Foxp3^{YFP-Cre}$ mice. T cell-specific Usp22-null

mice were generated by breeding *Usp22^{fl/fl}* mice with *Lck^{Cre}* mice. Additionally, C57BL/6 Rag^{-/-} mice, SJL CD45.1 congenic mice were purchased from Jackson Laboratories. These mice were maintained and used at the Northwestern University mouse facility under pathogen-free conditions according to institutional guidelines and using animal study proposals approved by the institutional animal care and use committees. Unless stated otherwise, all figures are representative of experiments with healthy 6–8-week-old mice.

Frozen sperm of C57BL/6N-A^{tm1Brd}USP21^{tm1a(EUCOMM)Wtsi/WtsiBait} were purchased from Emma Mouse Repository (EMMA ID: 07280). Blastocyst injections resulted in several chimeric mice with the capacity for germline transmission. T_{reg}-specific *Usp21*-null mice were generated by breeding *Usp21^{fl/fl}* mice with *Foxp3^{YFP-cre}* mice (obtained from The Jackson Laboratory?). USP22^{fl/fl}USP21^{fl/fl}FoxP3^{YFP-Cre} mice were generated by breeding the USP22^{fl/fl}FoxP3^{YFP-Cre} with the USP21^{fl/fl}FoxP3^{YFP-Cre}. This breeding strategy produced the T_{reg}-specific knockout of USP22 (22^{KO}), USP21 (21^{KO}), and a double knockout of both. These mice were maintained and used at the Northwestern University mouse facility under pathogen-free conditions in accordance with institutional guidelines and follow animal study proposals approved by the institutional animal care and use committees. Unless stated otherwise, all figures are representative of experiments with 6- to 8-week-old mice.

B6 *Foxp3^{GFP-Cre}* mice were crossed with B6 *Rosa26^{LSL-RFP}* reporter mice as previously described to generate the Foxp3 fate reporter mice for RNP Validation. These mice were then crossed to B6 constitutive Cas9-expressing mice³⁹ to generate the *Foxp3^{GFP-Cre}Rosa26^{LSL-RFP}Cas9* mice used for the CRISPR screen. For the arrayed validation experiments, B6 *Foxp3^{EGFP}* knock-in mice that were obtained from Jackson Laboratories (Strain No. 006772) were used. These mice were

maintained in the UCSF specific-pathogen-free animal facility in accordance with guidelines established by the Institutional Animal Care and Use Committee and Laboratory Animal Resource Center.

5.3 Pooled sgRNA Library Design, Construction, Pipeline, and Analysis

For the cloning of the targeted library, we followed the custom sgRNA library cloning protocol as previously described. We utilized a MSCV-U6-sgRNA-IRES-Thy1.1 backbone (gifted from the Bluestone Lab). To optimize this plasmid for cloning the library, we first replaced the sgRNA with a 1.9kb stuffer derived from the lentiGuide-Puro plasmid (Addgene, plasmid# 52963) with flanking BsgI cut sites. This stuffer was excised using the BsgI restriction enzyme (NEB, Cat# R0559) and the linear backbone was gel purified (Qiagen, Cat# 28706). We designed a targeted library to include all genes matching Gene Ontology for “Nucleic Acid Binding Transcription Factors”, “Protein Binding Transcription Factors”, “Involved in Chromatin Organization” and “Involved in Epigenetic Regulation.” Genes were then selected based on those that have the highest expression levels across any mouse CD4 T cell subset as defined by Stubbington *et al*⁴². In total, we included 489 targets with 4 guides per gene, GFP and RFP controls with 8 guides for each, and 28 non-targeting controls. Guides were subsetted from the Brie sgRNA library⁶, and the pooled oligo library was ordered from Twist Bioscience (San Francisco, CA) to match the vector backbone. Oligos were PCR amplified and cloned into the modified MSCV backbone by Gibson assembly as described by Joung *et al*. The library was amplified using Endura ElectroCompetent Cells following the manufacturer’s protocol (Endura, Cat# 60242–1). All oligos included in the library and primer sequences are listed in **Table 4**.

Tregs were collected from their culture vessels 8 days after the second transduction and centrifuged for 5 min at 300g. Cells were first stained with a viability dye at a 1:1,000 dilution in 1× PBS for 20 min at 4°C, then washed with EasySep Buffer (1× PBS, 2% FBS, 1 mM EDTA). Cells were then resuspended in the appropriate surface staining antibody cocktail and incubated for 30 min at 4°C, then washed with EasySep Buffer. Cells were then fixed, permeabilized, and stained for transcription factors using the Foxp3 Transcription Factor Staining Buffer Set (eBioscience, Cat# 00-5523-00) according to the manufacturer's instructions. Antibodies used in this study are listed in **Table 2**. For the CRISPR screen, Foxp3^{high} and Foxp3^{low} populations were isolated using fluorescence-activated cell sorting by gating on lymphocytes, live cells, CD4⁺ and gating on the highest 40% of Foxp3-expressing cells (Foxp3^{high}) and lowest 40% of Foxp3-expressing cells (Foxp3^{low}) by endogenous Foxp3 intracellular staining. Over 2 million cells were collected for both sorted populations to maintain a library coverage of at least 1,000 cells per sgRNA (1000x).

5.4 CRISPR Screen

Primary Tregs were isolated from the spleen and lymph nodes of three male Foxp3-GFP-Cre/Rosa26-RFP/Cas9 mice aged 5–7 months old, pooled together, and stimulated for 60 hours. Cells were then retrovirally transduced with the sgRNA library and cultured at a density of 1 million cells/ml continually maintaining a library coverage of at least 1,000 cells per sgRNA. Eight days after the second transduction, cells were sorted based on Foxp3 expression defined by intracellular staining. Genomic DNA was harvested from each population and the sgRNA-encoding regions were then amplified by PCR and sequenced on an Illumina MiniSeq using custom sequencing primers. From this data, we quantified the frequencies of cells expressing different sgRNAs in each in each population (Foxp3^{high} and Foxp3^{low}) and quantified the phenotype

of the sgRNAs, which we have defined as Foxp3 stabilizing (enriched in Foxp3^{high}) or Foxp3 destabilizing (enriched in Foxp3^{low}).

Analysis was performed as previously described⁴⁴. To identify hits from the screen, we used the MAGeCK software to quantify and test for guide enrichment⁷. Abundance of guides was first determined by using the MAGeCK “count” module for the raw fastq files. For the targeted libraries, the constant 5’ trim was automatically detected by MAGeCK. To test for robust guide and gene-level enrichment, the MAGeCK “test” module was used with default parameters. This step included median ratio normalization to account for varying read depths. We used the non-targeting control guides to estimate the size factor for normalization, as well as to build the mean-variance model for null distribution, which was used to find significant guide enrichment. MAGeCK produced guide-level enrichment scores for each direction (i.e. positive and negative) which were then used for alpha-robust rank aggregation (RRA) to obtain gene-level scores. The p-value for each gene was determined by a permutation test, randomizing guide assignments and adjusted for false discovery rates by the Benjamini–Hochberg method. Log2 fold change (LFC) was also calculated for each gene, defined throughout as the median LFC for all guides per gene target. Where indicated, LFC was normalized to have a mean of 0 and standard deviation of 1 to obtain the LFC Z-score.

5.5 Arrayed Cas9 RNP preparation and Electroporation

RNPs were produced by complexing a two-component gRNA to Cas9. In brief, crRNAs and tracrRNAs were chemically synthesized (IDT), and recombinant Cas9-NLS were produced and purified (QB3 Macrolab). Lyophilized RNA was resuspended in Nuclease-free Duplex Buffer (IDT, Cat# 1072570) at a concentration of 160 μ M, and stored in aliquots at -80° C. crRNA and

tracrRNA aliquots were thawed, mixed 1:1 by volume, and annealed by incubation at 37°C for 30 min to form an 80 μ M gRNA solution. Recombinant Cas9 was stored at 40 μ M in 20 mM HEPES-KOH, pH 7.5, 150 mM KCl, 10% glycerol, 1 mM DTT, were then mixed 1:1 by volume with the 80 μ M gRNA (2:1 gRNA to Cas9 molar ratio) at 37°C for 15 min to form an RNP at 20 μ M. RNPs were electroporated immediately after complexing. RNPs were electroporated 3 days after initial stimulation. Tregs were collected from their culture vessels and centrifuged for 5 min at 300g, aspirated, and resuspended in the Lonza electroporation buffer P3 using 20 μ l buffer per 200,000 cells. 200,000 Tregs were electroporated per well using a Lonza 4D 96-well electroporation system with pulse code EO148 (mouse) or EH115 (human). Immediately after electroporation, 80 μ L of pre-warmed media was added to each well and the cells were incubated at 37°C for 15 minutes. The cells were then transferred to a round-bottom 96-well tissue culture plate and cultured in either complete DMEM, 10% FBS, 1% pen/strep + 2000U hIL-2 at 200,000 cells/well in 200 μ l of media (mouse) or X-VIVO 15 media (Lonza, Cat# 04-418Q), supplemented with 5% FBS, 50 μ M 2-mercaptoethanol, 10 μ M N-acetyl L-cysteine and 1% pen/strep with hIL-2 at 300U/mL at 200,000 cells/well in 200 μ l of media (human).

5.6 Retroviral Transduction and Foxp3 Rescue Experiment

Tregs were stimulated as described above for 48–60 hours. Cells were counted and seeded at 3 million cells in 1 mL of media with 2x hIL-2 into each well of a 6 well plate that was coated with 15 μ g/mL of RetroNectin (Takara, Cat# T100A) for 3 hours at room temperature and subsequently washed with 1x PBS. Retrovirus was added at a 1:1 v/v ratio (1 mL) and plates were centrifuged for 1 hour at 2000g at 30°C and placed in the incubator at 37°C overnight. The next day, half (1 mL) of the 1:1 retrovirus to media mixture was removed from the plate and 1 mL of fresh retrovirus

was added. Plates were immediately centrifuged for 1 hour at 2000g at 30°C. After the second spinfection, cells were pelleted, washed, and cultured in fresh media.

CD4⁺ cells were isolated from harvested LN and spleens of 8-week-old *Usp22*^{+/+}*Foxp3*^{YFP-Cre} WT or *Usp22*^{fl/fl}*Foxp3*^{YFP-Cre} KO mice with the Invitrogen CD4⁺ purification kit (ThermoFisher Cat# 11331D). YFP⁺ Tregs were sorted and subsequently stimulated with 3:1 beads to cells using CD3/CD28 dynabeads in complete DMEM with 2000U hIL-2 at a culture density of ~1 million cells/mL in a 24 well plate for 48 hours. After 48h stimulation, cells were transferred to RetroNectin coated 6-well plates at a density of 3 million cells/mL with a 1:1 ratio of virus to media. RetroNectin coating was done at room temperature for 3hr with 1mL of 15ug/mL in PBS in each of the wells in the 6-well plate. The cells were spinfected for 1hr at 2000xg, then left overnight in the plate at 37°C. The following day, 1mL of new virus was added to the cells for a second spinfection for 1hr at 2000xg. Once spinfection was complete, the cells were plated in a 24-well plate at a density of 1million/well in T cell media in complete RPMI 1640 medium containing 10% FBS, 1% penicillin/streptomycin (MediaTech), 50 μM β-mercaptoethanol (Gibco), and 1% L-glutamine (Gibco) for 72 hours. After rest, the cells were sorted for YFP⁺GFP⁺ viral infected Tregs. Naïve CD4⁺CD25⁻ T cells (5×10⁴) labeled with APC CFSE cell proliferation dye were used as responder T cells and cultured in 96-well u-bottom plate for 72h together with increasing ratio of the sorted GFP⁺YFP⁺ Treg cells with anti-CD3 and anti-CD28 (2 μg/ml). The suppressive function of Treg cells was assessed by flow cytometry measurement of the proliferation of activated CD4⁺ effector T cells on the basis of APC CFSE cell proliferation dye dilution.

5.7 Isolation of Genomic DNA from Fixed Cells

After cell sorting and collection, genomic DNA (gDNA) was isolated using a protocol specific for fixed cells. Cell pellets were resuspended in cell lysis buffer (0.5% SDS, 50 mM Tris, pH 8, 10 mM EDTA) with 1:25 v/v of 5M NaCl to reverse crosslinking and incubated at 66°C overnight. RNase A (10 mg/mL) was added at 1:50 v/v and incubated at 37°C for 1 hour. Proteinase K (20 mg/mL) was added at 1:50 v/v and incubated at 45°C for 1 hour. Phenol:Chloroform:Isoamyl Alcohol (25:24:1) was added to the sample 1:1 v/v and transferred to a phase lock gel light tube (QuantaBio, Cat# 2302820), inverted vigorously and centrifuged at 20,000g for 5 mins. The aqueous phase was then transferred to a clean tube and NaAc at 1:10 v/v, 1 µl of GeneElute-LPA (Sigma, Cat# 56575), and isopropanol at 2.5:1 v/v were added. The sample was vortexed, and incubated at -80°C until frozen solid. Then thawed and centrifuged at 20,000g for 30 mins. The cell pellet was washed with 500 µl of 75% EtOH, gently inverted and centrifuged at 20,000g for 5 mins, aspirated, dried, and resuspended in 20 µl TE buffer.

5.8 Preparation of Genomic DNA for Next Generation Sequencing

Amplification and bar-coding of sgRNAs was performed as previously described⁴³ with some modifications. Briefly, after gDNA isolation, sgRNAs were amplified and barcoded with TruSeq Single Indexes using a one-step PCR. TruSeq Adaptor Index 12 (CTTGTA) was used for the Foxp3^{low} population and TrueSeq Adaptor Index 14 (AGTTCC) was used for the Foxp3^{high} population. Each PCR reaction consisted of 50µL of NEBNext Ultra II Q5 Master Mix (NEB, Cat# M0544), 1µg of gDNA, 2.5µL each of the 10µM forward and reverse primers, and water to 100µL total. The PCR cycling conditions were: 3 minutes at 98°C, followed by 10 seconds at 98°C, 10 seconds at 62°C, 25 seconds at 72°C, for 26 cycles; and a final 2 minute extension at 72°C. After the PCR, the samples were purified using Agencourt AMPure XP SPRI beads (Beckman Coulter, Cat #A63880) per the manufacturer's protocol, quantified using the Qubit

ssDNA high sensitivity assay kit (Thermo Fisher Scientific, Cat #Q32854), and then analyzed on the 2100 Bioanalyzer Instrument. Samples were then sequenced on an Illumina MiniSeq using a custom sequencing primer. Primer sequences are listed in **Table 4**.

5.9 *In Vitro* Suppressive Assay

Naïve CD4⁺CD25⁻ T cells (5×10^4) labeled with eFluor 670 cell proliferation dye were used as responder T cells and cultured in 96-well U-bottom plate for 72h together with increasing ratio of sorted YFP⁺ Treg cells from WT or *Usp22^{fl/fl} Foxp3^{YFP-Cre}* mice in the presence of irradiated splenocytes depleted of T cells (5×10^4) plus anti-CD3 (2 µg/ml). The suppressive function of Treg cells was determined by measurement of the proliferation of activated CD4⁺ and CD8⁺ effector T cells on the basis of eFluor 670 cell proliferation dye dilution.

5.10 Tumor Models

Cultured cancer cells were trypsinized and washed once with PBS. EG7 lymphoma and LLC1 lung carcinoma tumor cells were subcutaneously administered to the right flank of 8- to 10-week-old mice at 1×10^6 tumor cells per mouse, and B16 melanoma at 5×10^4 tumor cells per mouse. Tumors were measured every 2–3 days by measuring along 3 orthogonal axes (*x*, *y* and *z*) and tumor volume was calculated as $(xyz)/2$. The tumor size limit agreed by IRB was 2 cm³.

5.11 Adoptive Transfer Model of Colitis

Naïve T cells (CD4⁺CD25⁻CD44^{lo}CD62L^{hi}) were sorted from congenic CD45.1 B6.SJL mice and YFP⁺ Treg cells were sorted from WT or *Usp22^{fl/fl} Foxp3^{YFP-Cre}* mice.

Rag1^{-/-} mice were given intraperitoneal injection of naïve T cells (4×10^5) alone or in combination with WT or *Usp22* KO Treg cells (2×10^5). After T cell reconstitution, mice were weighed weekly

and monitored for clinical signs of disease. Mice were sacrificed when their body weight decreased 20%. At cessation, colons were harvested for measurement and histology and flow cytometry.

5.12 Induced Experimental Autoimmune Encephalomyelitis

8–10-week-old WT or *Usp22^{fl/fl}Foxp3^{YFP-Cre}* mice were subcutaneously injected with 200µg of MOG_{33–55} peptide (Genemed Synthesis). The MOG_{33–55} peptide was emulsified in complete Freund's adjuvant (CFA) which contained 200µg of *Mycobacterium tuberculosis* H37Ra (Difco). The mice were then subsequently intraperitoneally injected with 200 ng of pertussis toxin (List Biological Laboratories) on day 0 and day 2. Clinical signs of EAE were assessed daily. Scores were given as follows: 0, no sign of disease; 2, limp tail, 3, hind leg weakness or limp; 3, partial back limb paralysis; 4, complete hind limb paralysis; 5, total limb paralysis.

5.13 Histology

Mouse tissues were fixed in 10% formalin and embedded in paraffin. 4µm sections were stained with hematoxylin and eosin. The images were viewed on an olympus CX31 microscope and taken with a PixelLink camera.

5.14 Cell Isolation and Flow Cytometry for Analysis of Splenic and Intratumoral T_{reg} Cells

T cells were isolated from mouse spleen using the CD4⁺ T-cell negative isolation kit (Stem Cell Catalog #17952) per the manufacturer's instructions. To isolate murine tumor-infiltrating lymphocytes, subcutaneous tumors were cut into small fragments and digested by collagenase D (Sigma) and DNase (Sigma) for 1h at room temperature prior to isolation with CD45⁺ Positive Selection kit (Stem Cell Catalog # 100-0350). Enriched cells were further sorted for

YFP⁺ (Foxp3⁺) using a FACSAria (BD Bioscience). Purity of sorted cells was >99%. To isolate human tumor-infiltrating lymphocytes, subcutaneous tumors were cut into small fragments and digested by collagenase D (Sigma) and DNase (Sigma) for 1h at room temperature prior to isolation with CD45⁺ Positive Selection kit (Stem Cell Catalog # 100-0350). Enriched cells were further sorted for CD4⁺CD25⁺CD127⁻ cells using a FACSAria (BD Bioscience). Flow cytometry analysis of cells was done using a FACSCanto II. Samples were initially incubated with CD16/32 antibodies to block antibody binding to Fc receptor. Single-cell suspensions were stained with relevant antibodies (**Table 2**) and subsequently washed twice with cold PBS containing 3% FBS. For intracellular staining, cells were fixed, permeabilized, and stained for transcription factors using the Foxp3 Transcription Factor Staining Buffer Set (eBioscience, 00-5523-00) following the manufacturer's instructions. For cytokine staining, cells were first stimulated for 4–5 h with 20 ng/ml PMA plus 0.5 μ M ionomycin in the presence of 10 μ g/ml of monesin before staining. Data were analyzed with FlowJo software.

5.15 RNA Extraction for RNA Sequencing and qPCR

RNA was extracted using the RNeasy Micro Kit (Qiagen, Cat# 74004) from sorted Foxp3⁺ (YFP⁺) Treg cells from mouse organs. qPCR was performed following the manufacturer's protocol using gene-specific primer sets (**Table 3**). Real time PCR data was analyzed using $\Delta\Delta$ Ct method with actin as the housekeeping gene. Gene expression was normalized to WT, untreated Treg cells unless otherwise noted. RNA sequencing was performed by the Northwestern RNA sequencing core. The quality of DNA reads, in fastq format, was evaluated using FastQC. Adapters were trimmed, and reads of poor quality or those aligning to rRNA sequences were filtered. The cleaned reads were aligned to the *Mus musculus* genome (mm10) using STAR (Dobin et al, 2013). Read counts for each gene were calculated using htseq-count (Anders et al, 2015) in conjunction with a

gene annotation file for mm10 obtained from UCSC (University of California Santa Cruz; <http://genome.ucsc.edu>). Differential expression was determined using edgeR (Robinson et al, 2010, McCarthy et al, 2012). The cutoff for determining significantly differentially expressed genes was an FDR-adjusted p-value less than 0.05. Following differential expression analysis, Gene Set Enrichment Analysis (GSEA) was performed using GSEA v4.03 (<https://pubmed.ncbi.nlm.nih.gov/16199517/>). For each separate knockout mouse (Usp21, Usp22, and dKO) an inclusion cutoff of FDR-adjusted p-value < 0.01 was set. Lists of genes, ordered by log₂(fold change), were then run with the GSEA Pre-ranked tool under standard parameters against the Hallmarks MSigDB 7.2 gene sets (<https://www.ncbi.nlm.nih.gov/pmc/articles/PMC4707969/>). Normalized enrichment scores were then plotted for gene sets enriched at an FDR q-val <0.25.

5.16 *In Vitro* iT_{reg} Cell Generation

Splenic CD4⁺CD25⁻CD44⁺CD62L⁺ naïve T cells were isolated using mouse naïve CD4 isolation kit (Stem Cell Catalog #19765) and cultured in 24-well plates at 5 x 10⁵ cells per well for 3 days. Cells cultured in T cell medium made of complete RPMI 1640 medium containing 10% FBS, 1% penicillin/streptomycin (MediaTech), 50 µM β-mercaptoethanol (Gibco), and 1% L-glutamine (Gibco). Wells were coated in 3 µg/ml anti-CD3 and 5 µg/ml anti-CD28 antibodies. Culture media was supplemented with IL-2 (5ng/ml), anti-IFN-g (2µg/ml), anti-IL-4 (2ug/ml) and TGF-b (5ng/ml) all purchased from Peprotech.

5.17 ChIP-qPCR Sample Preparation

iT_{reg} cells (as described above) were used for immunoprecipitation to allow for ample cell number. Three million iT_{reg} cells per immunoprecipitation were fixed in 37% formaldehyde for 10 minutes at 37°C. Glycine was then added to a final concentration of 0.125M and the samples were incubated

for an additional 5 minutes at room temperature. The cells were subsequently washed with ice-cold phosphate-buffered saline with 1x Protease Inhibitor cocktail (Roche, Cat# 36363600). The ChIP assay was done using the Millipore ChIP Assay Kit (Lot 3154126) following the protocol as described previously (14).

5.18 ChIP-Seq Sample Preparation and Analysis

Treg cells were collected and either cross-linked in 1% formaldehyde for ten minutes or cross-linked first in 3mM disuccinimidyl glutarate (DSG) in 1X PBS for thirty minutes then in 1% formaldehyde for another ten minutes, both at room temperature. After quenching the excess formaldehyde with a final concentration of 125 mM glycine, the fixed cells were washed in 1X PBS, pelleted, flash-frozen in liquid nitrogen, and stored at -80°C . The cells were thawed on ice and incubated in lysis solution (50 mM HEPES-KOH pH 8, 140 mM NaCl, 1 mM EDTA, 10% glycerol, 0.5% NP40, 0.25% Triton X-100) for ten minutes. The isolated nuclei were washed with wash solution (10 mM Tris-HCl pH 8, 1 mM EDTA, 0.5 mM EGTA, 200 mM NaCl) and shearing buffer (0.1% SDS, 1 mM EDTA, 10 mM Tris-HCl pH 8) then sheared in a Covaris E229 sonicator for ten minutes to generate DNA fragments between ~ 200 –1000 base pairs (bp). After clarification of insoluble material by centrifugation, the chromatin was immunoprecipitated overnight at 4°C with antibodies against Usp22 (1:100 v/v), Rnf20 (1:100 v/v), H2BK120Ub (1:100 v/v), and H2AK119Ub (1:100 v/v). The next day, the antibody bound DNA was incubated with Protein A+G Dynabeads (Invitrogen) in ChIP buffer (50 mM HEPES-KOH pH 7.5, 300 mM NaCl, 1 mM EDTA, 1% Triton X-100, 0.1% DOC, 0.1% SDS), washed and treated with Proteinase K and RNase A. Cross-linking was reversed by incubation at 65°C overnight. Purified ChIP DNA was used for library generation (NuGen Ovation Ultralow Library System V2) according to manufacturer's instructions for subsequent sequencing. ChIP-seq samples were performed with at

least 2 biological replicates; with the exception of Usp22 ChIP which has 1 biological replicate with 2 technical replicates (due to poor IP efficiency in the second biological replicate) and H2AK119Ub ChIP performed on Rnf20-RNP cells which has only 1 biological replicate (due to limiting cell number, H2BK120Ub ChIP was prioritized).

Single-end 50 base pair (bp) or paired-end 42 bp reads were aligned to mouse genome mm10 using STAR alignment tool (V2.5). ChIP-seq peaks were called using findPeaks within HOMER using parameters for histone (-style histone) or transcription factor (-style factor) (Christopher Benner, HOMER, <http://homer.ucsd.edu/homer/index.html>, 2018). Peaks were called when enriched > four-fold over input and > four-fold over local tag counts, with Benjamin-Hochberg false discovery rate (FDR) 0.001. For histone ChIP, peaks within a 1000 bp range were stitched together to form regions. ChIP-Seq peaks or regions were annotated by mapping to the nearest TSS using the annotatePeaks.pl command. Differential ChIP peaks were found by merging peaks from control and experiment groups and called using getDiffExpression.pl with fold change ≥ 1.5 or ≤ -1.5 , Poisson p value < 0.0001 . Significance of peak overlap was determined by calculating the number of peaks co-occurring across the entire genome using the HOMER mergePeaks program. For the heatmaps of ChIP-seq read densities at sites bound by Foxp3, publicly available Foxp3 ChIP-seq data was used. For enhancer enrichment analysis, we defined the different enhancer classes using publicly available Treg ChIP-seq data for histone modifications H3K4me, H3K4me3, and H3K27ac. All enhancers were called by identifying all H3K4me-positive regions that are at least 1 kb away from the nearest TSS or H3K4me3 mark. These were sub-divided as either active (H3K27ac-positive) or poised (H3K27ac-negative). To call super enhancers, we used the findPeaks program in HOMER with the style option super. This was performed with the two

H3K27ac ChIP-seq replicates and the sites common between the two were used for further analysis. H2BK120Ub ChIP-seq read density histograms at Treg super enhancers were generated by partitioning each super enhancer into 20 bins and also considering 20 kb upstream and downstream, which were also binned similarly. The number of peaks per kb per bin was calculated and averaged across all super enhancers in the genome. To compare across samples with different number of peaks, the final averaged values were normalized by the number of peaks in each data set. Genome browser tracks for H2BK120Ub ChIP-seq data were generated by combining the tag directories from replicate experiments and using the makeBigWig command in HOMER.

5.19 Ubiquitination Assay

Flag–Smad proteins and HA–ubiquitin plasmids were co-transfected into HEK293 cells using Turbofect Transfection Reagent (Thermo Fisher, R0532) along with either Myc empty vector or Myc-Usp22). After 24 hours, the cells were collected and immunoprecipitated with anti-Flag to pull down the relevant SMAD antibody, and immunoblotted for HA–ubiquitin to assess SMAD protein ubiquitination in the presence or absence of functional Usp22. Whole-cell lysate controls were immunoblotted with HRP-conjugated Myc and HRP-conjugated Flag to show transfection efficiency.

5.20 *Ex-Vivo* nT_{reg} Cell Culture Conditions

nT_{reg} cells were isolated from mouse spleens using the CD4⁺ T-cell negative isolation kit (Stem Cell Catalog #17952) followed by YFP⁺ flow cytometry sorting on the FACS Aria (BD Bioscience) at 99% efficiency. Cells were then plated in a 96-well plate at 1×10^5 cells per well with 2000U of IL-2 and CD3/CD28 beads (from Treg Expansion kit Miltenyi Biotec Catalog #130-095-925) added to T cell medium following the manufacturer's instructions.

5.21 *In Vitro* T_{reg} Cell Hypoxia Culture

nT_{reg} cells were isolated as described above and cultured at 37°C in either normoxic (21% O₂) or in hypoxic conditions (1%O₂) for 24 hours. Hypoxia was induced using (Name of hypoxia chamber and company). T cell medium was incubated at 37°C at normoxia or hypoxia for 3 hours prior to usage. Cells were then collected and RNA was extracted as described above. For iT_{reg} cells, cells were isolated and polarized as described above. Subsequently, cells were rested in optiMEM overnight and then plated in optiMEM containing 5ng/ml IL-2 in either normoxic or hypoxic conditions. optiMEM media was incubated at 37°C at normoxia or hypoxia overnight prior to usage. Hypoxia stability assay was conducted as described above but cells were cultured in normoxia or hypoxia for 72 hours, then collected and stained for FOXP3 for flow cytometry.

5.22 Glucose and Amino Acid Restriction Assays

nT_{reg} cells were isolated as described above and cultured in either normal T cell medium, T cell medium lacking glucose (Thermo Fisher Catalog# 11879020), or T cell medium lacking amino acids including glutamine (US Biological Catalog# R9010-02) substituted with dialyzed FBS (GIBCO Catalog# A3382001) for 24 hours at 1 x 10⁵ cells per well. T cell media included with 2000U of IL-2 and CD3/CD28 beads as described above. iT_{reg} cells were isolated and polarized as described above for 3 days. Following polarization, iT_{reg} cells were cultured in normal T cell media or T cell media lacking glucose or amino acids for 24 hours. Both nT_{reg} and iT_{reg} cells were then collected and RNA was extracted as described above. For stability assays, cells were cultured as described above for 48 hours, then collected and stained for FOXP3 for flow cytometry.

5.23 *In Vitro* Inhibitor Assays

All nT_{reg} and iT_{reg} cells were plated as described above DMOG (Sigma Catalog #D3695) was administered to the cells in relevant experiments at 1mM for 24 hours. Oligomycin (Sigma Catalog# 75351) was administered at 1μM to the media of the cells in relevant experiments for 24 hours. Torin 1 (Millipore Catalog #475991) was administered to the relevant cells at 250 nM for 24 hours. FOXP3 protein level was assessed via flow cytometry following 48 hours of treatment of inhibitors described above.

5.24 Assessment of Cellular Metabolism

The rates of mitochondrial oxygen consumption and glycolysis were measured using the Seahorse XF-96 analyzer (Agilent). 250,000 splenic T_{reg} cells (YFP+) were isolated by flow sorting and adhered to XF96 cell culture plates using Cell-tak (Corning) per the manufacturer's instructions. Cells were plated in XF RPMI Medium (Agilent) supplemented with 1% FBS, 11mM glucose, 2mM glutamine and 1mM pyruvate to match normal concentrations of those metabolites in base RPMI. The basal mitochondrial oxygen consumption rate (OCR) was determined by subtracting the Antimycin A and Piericidin A sensitive oxygen consumption from the basal mitochondrial oxygen consumption. The basal glycolytic rate was calculated by subtracting the 2-deoxyglucose sensitive extracellular acidification rate (ECAR) from the basal ECAR. Antimycin A and Piericidin A purchased from Sigma where both used at a final concentration of 1μM. 2-deoxyglucose purchased from Sigma was used at a final concentration of 25mM.

5.25 Homology Modeling of Human USP22

The amino acid sequence of human USP22 was retrieved from the sequence database of UniProt (<https://www.uniprot.org/uniprot/>; Uniprot ID: Q9UPT9). *UBP8 structure (PDB code 3MHS)* was chosen as a template protein to construct the human USP22 model. The homology modeling

of the *human USP22 model* was performed by three different homology modeling programs including SWISS MODEL, I-TASSER and MODELLER. Subsequently, the quality of the USP22 models was checked with structure validation programs including PROCHECK and Verify_3D programs. Finally, the best model was subjected to energy minimization for removing clashes between side chains using GROMACS 5.1.5 and subsequently applied in structure-based virtual screening.

5.26 Virtual Screening

Specs (www.specs.net) database containing 212,558 compounds was first filtered by lead like properties ($180 < \text{MW} < 480$, $-0.5 < \text{ClogP} < 5.5$, $\text{PSA} < 140 \text{Å}$, $0 < \text{rotational bonds} < 10$, $0 < \text{donor and acceptor} < 13$) and led to a total of 102 442 compounds using DruLiTo software. The 3D geometry of the ligands was optimized, minimized and prepared using Open Babel. The virtual screening was performed using AutoDock Vina program. The docking grid was created with the grid points 16, 18, 16 and defined as coordinates of the center of binding site with 37.64, 11.33, 70.33 for x, y and z dimensions, respectively. The Genetic Algorithms were selected to perform the molecular docking and keeping other docking parameters in default. The top 100 compounds ranked by docking affinity were selected for further study. Moreover, residual interactions at the protein-drug interface were evaluated using LigPlot.

5.27 Molecular Docking Mechanism

Molecular docking result showed that Compound S02 stably binds in the USP22 catalytic domain pocket, mainly in the hydrophobic effect provided by the amino acid residues His471, Gln261, Gly478, Glu476, Leu475, Asp262, Arg419, Tyr480 and Phe412. It is worth noting that the benzene ring on compound S02 not only forms a hydrophobic interaction with the Tyr480 residue, but also

the hydrogen atom on the anilino group of ligand acts as hydrogen donor to form a hydrogen bond with the hydrogen acceptor on the Tyr480 residue. Binding stability indicates that the anilino functional group may play an important role in the inhibitory activity of USP22.

5.28 Molecular Dynamics Simulation

The conformation of the complexes formed between ligands and USP22 receptor protein were predicted using AutoDock Vina program, and all of the molecular dynamics (MD) simulations were performed by Gromacs 5.1.5 with Amber99sb force field. After MD simulation, the molecular mechanics energies combined with the Molecular Mechanics/Poisson Boltzmann Surface Area (MM/PBSA) methods were employed to calculate the binding free energy of *ligands* with USP22 *receptor* protein. Structural stability of complexes was compared by analyzing RMSD and the hydrogen-bonding interactions throughout the trajectory.

5.29 Statistics and Data Availability

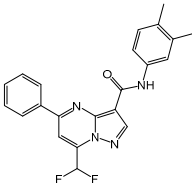
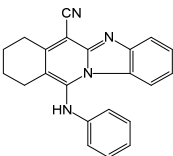
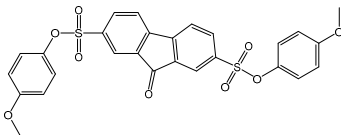
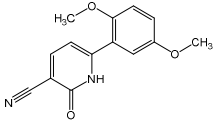
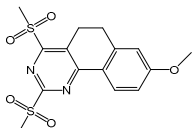
No statistical methods were used to predetermine sample size. The experiments were not randomized. The investigators were not blinded to allocation during experiments and outcome assessment. All statistical analyses were computed with GraphPad and tests used for each experiment are listed in the figure legends. ANOVAs with multiple comparisons between rows were corrected with Tukey's test to determine statistical significance. Two-tailed unpaired t tests were performed with Welch's correction. All the raw data underlying figures in the manuscript are available upon request.

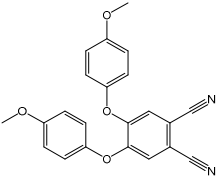
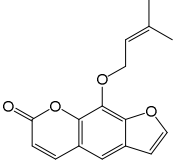
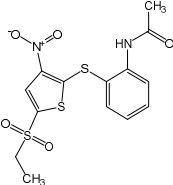
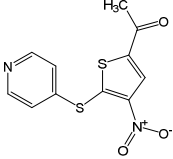
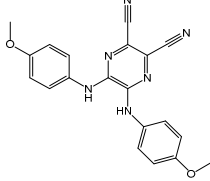
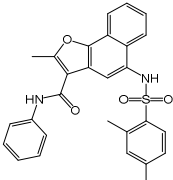
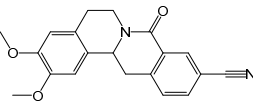
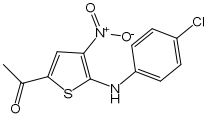
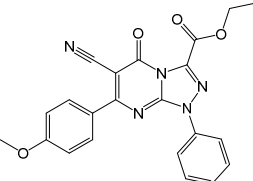
ChIP-seq data that support the findings of this study have been deposited in the Gene Expression Omnibus under the accession

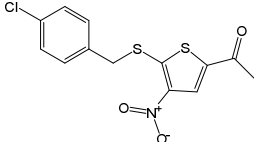
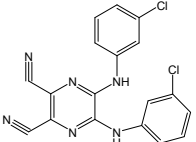
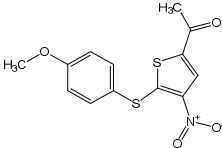
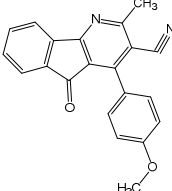
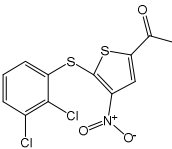
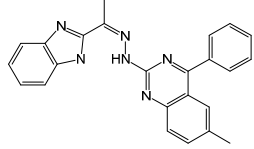
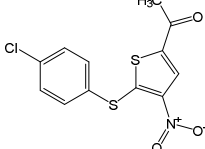
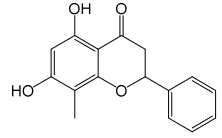
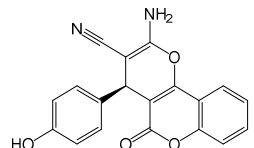
code [GSE140102](https://www.ncbi.nlm.nih.gov/geo/query/acc.cgi?acc=GSE140102) [https://www.ncbi.nlm.nih.gov/geo/query/acc.cgi?acc=GSE140102]. Publicly available ChIP-seq and ATAC-seq data were downloaded from the indicated repositories and processed using HOMER v4.8 (Christopher Benner, HOMER, <http://homer.ucsd.edu/homer/index.html>, 2018). Foxp3 ChIP-seq GEO accession code [GSE40684](https://www.ncbi.nlm.nih.gov/geo/query/acc.cgi?acc=GSE40684); ATAC-seq and ChIP-seq for H3K4me, H3K27ac, H3K4me3 SRA accession number DRP003376.

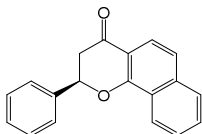
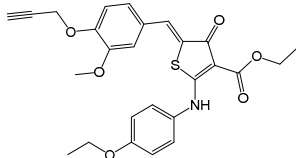
5.30 Tables

5.30.1 Table 1: Structure and Chemical Names of Usp22 Inhibitors

Chemical number	Chemical name	MM/PBSA Binding Free Energy(kJ/mol)	Chemical structure	Efficacy in USP22 inhibition
S01	7-(difluoromethyl)-N-(3,4-dimethylphenyl)-5-phenylpyrazolo[1,5-a]pyrimidine-3-carboxamide	-342.23		-
S02	11-anilino-7,8,9,10-tetrahydrobenzimidazo[1,2-b]isoquinoline-6-carbonitrile	-300.51		+
S03	2,7-bis(4-methoxyphenyl) 9-oxo-9H-fluorene-2,7-disulfonate	-201.50		-
S04	6-(2,5-dimethoxyphenyl)-2-oxo-1,2-dihydropyridine-3-carbonitrile	-190.83		-
S05	2,4-dimethanesulfonyl-8-methoxy-5H,6H-benzo[h]quinazoline	-187.88		-

S06	4,5-bis(4-methoxyphenoxy)benzene-1,2-dicarbonitrile	-175.87		-
S07	9-[(3-methylbut-2-en-1-yl)oxy]-7H-furo[3,2-g]chromen-7-one	-164.09		-
S08	N-(2-[[5-(ethanesulfonyl)-3-nitrothiophen-2-yl]sulfonyl]phenyl)acetamide	-147.32		-
S09	1-[4-nitro-5-(pyridin-4-ylsulfonyl)thiophen-2-yl]ethan-1-one	-141.38		-
S10	bis[(4-methoxyphenyl)amino]pyrazine-2,3-dicarbonitrile	-139.07		-
S11	5-[[[(2,4-dimethylphenyl)sulfonyl]amino]-2-methyl-N-phenylnaphtho[1,2-b]furan-3-carboxamide	-134.24		-
S12	8-Oxotetrahydropalmatine	-133.44		-
S13	1-[5-[(4-chlorophenyl)amino]-4-nitrothiophen-2-yl]ethan-1-one	-121.93		-
S14	ethyl 6-cyano-7-(4-methoxyphenyl)-5-oxo-1-phenyl-1,5-dihydro[1,2,4]triazolo[4,3-a]pyrimidine-3-carboxylate	-119.36		-

S15	1-(5-[(4-chlorophenyl)methyl]sulfanyl)-4-nitrothiophen-2-yl)ethan-1-one	-118.92		-
S16	bis[(3-chlorophenyl)amino]pyrazine-2,3-dicarbonitrile	-117.91		-
S17	1-{5-[(4-methoxyphenyl)sulfanyl]-4-nitrothiophen-2-yl}ethan-1-one	-115.11		-
S18	4-(4-methoxyphenyl)-2-methyl-5-oxo-5H-indeno[1,2-b]pyridine-3-carbonitrile	-112.41		-
S19	1-{5-[(2,3-dichlorophenyl)sulfanyl]-4-nitrothiophen-2-yl}ethan-1-one	-112.36		-
S20	1-(1H-benzimidazol-2-yl)ethanone (6-methyl-4-phenyl-2-quinazoliny)hydrazone	-109.21		-
S21	1-{5-[(4-chlorophenyl)sulfanyl]-4-nitrothiophen-2-yl}ethan-1-one	-109.19		-
S22	Cryptochrysin	-108.43		-
S23	2-amino-4-(4-hydroxyphenyl)-5-oxo-4H,5H-pyrano[3,2-c]chromene-3-carbonitrile	-105.05		-

S24	alpha-naphthoflavanone	-104.67		-
S25	ethyl 2-(4-ethoxyanilino)-5-[3-methoxy-4-(2-propynyloxy)benzylidene]-4-oxo-4,5-dihydro-3-thiophenecarboxylate	-103.73		-

5.30.2 Table 2: FACS Antibodies

<u>Application</u>	<u>Target</u>	<u>Clone</u>	<u>Fluorophore</u>	<u>Vendor</u>	<u>Catalog Number</u>
Flow Cytometry Antibodies					
Viability Dye	dead cells	N/A	Brilliant Violet 450	Tonbo	13-0863-T100
Viability Dye	dead cells	N/A	Brilliant Violet 510	Tonbo	13-0870-T100
Viability Dye	dead cells	N/A	Alexa Fluor 506	eBioscience	65-0866-14
Mouse T Cell Surface Staining	CD90.1 (Thy1.1)	HIS51	APC	eBioscience	17-0900-82
Mouse T Cell Surface Staining	CD3e	145-2C11	PE	BioLegend	100307
Mouse T Cell Surface Staining	CD3e	17A2	PE-Cy7	BioLegend	100219
Mouse T Cell Surface Staining	CD3e	145-2C11	APC	BioLegend	100311
Mouse T Cell Surface Staining	CD4	V4	BV785	BioLegend	100453
Mouse T Cell Surface Staining	CD4	GK1.5	Pacific Blue	BioLegend	100428
Mouse T Cell Surface Staining	CD4	GK1.5	PerCP-Cy5.5	BioLegend	100433
Mouse T Cell Surface Staining	CD4	GK1.5	APC Cy7	BioLegend	100413
Mouse T Cell Surface Staining	CD4	GK1.5	PE-Cy7	BioLegend	100421
Mouse T Cell Surface Staining	CD8a	53-6.7	BV510	BioLegend	100751
Mouse T Cell Surface Staining	CD8a	53-6.7	BV650	BioLegend	100741
Mouse T Cell Surface Staining	CD8a	53-6.7	Pacific Blue	BioLegend	100725
Mouse T Cell Surface Staining	CD25	PC61	APC	BioLegend	102012
Mouse T Cell Surface Staining	CD25	PC61	PECF594	BioLegend	102047
Mouse T Cell Surface Staining	CD25	PC61	PE-Cy7	BioLegend	102016
Mouse T Cell Surface Staining	CD25	PC61	PE	BioLegend	102008
Mouse T Cell Surface Staining	CD44	IM7	PE-Cy7	BioLegend	103030
Mouse T Cell Surface Staining	CD44	IM7	APC	BioLegend	103011
Mouse T Cell Surface Staining	CD44	IM7	APC Cy7	BioLegend	103027
Mouse T Cell Surface Staining	CD45.2	104	PerCP-Cy5.5	BioLegend	109827
Mouse T Cell Surface Staining	CD62L	MEL-14	APC	BioLegend	104412
Mouse T Cell Surface Staining	CD62L	MEL-14	PE	eBioscience	12-0621-82
Mouse T Cell Surface Staining	CD62L	MEL-14	PE-Cy7	BioLegend	134517
Mouse T Cell Surface Staining	CD357 (GITR)	DTA-1	PerCP-Cy5.5	BioLegend	126315
Mouse T Cell Surface Staining	CD357 (GITR)	DTA-1	PE	BioLegend	126309
Mouse T Cell Surface Staining	CD128 (ICOS)	7E.17G9	PE	eBioscience	12-9942-81
Mouse T Cell Surface Staining	CD279 (PD-1)	29F.IA12	PE	BioLegend	135205
Mouse T Cell Surface Staining	CD279 (PD-1)	29F.IA12	BV510	BioLegend	135241
Mouse T Cell Surface Staining	CD274 (PD-L1)	10F.9G2	PE	BioLegend	124308
Mouse T Cell Surface Staining	CD103	2E7	PE	eBioscience	12-1031-82
Mouse T Cell Surface Staining	Ki67	SOA15	APC Cy7	eBioscience	47-5698-82
Mouse T Cell Intracellular Staining	Foxp3	FJK-16s	FITC	eBioscience	11-5773-82
Mouse T Cell Intracellular Staining	Foxp3	FJK-16s	PE	eBioscience	12-5773-82
Mouse T Cell Intracellular Staining	Usp22	C-3	Alexa Fluor 647	Santa Cruz Bio	sc-390585
Mouse T Cell Intracellular Staining	IL-2	JES6-5H4	APC	eBioscience	17-7021-81
Mouse T Cell Intracellular Staining	IFN-γ	XMG1.2	FITC	BioLegend	505806
Mouse T Cell Intracellular Staining	IFN-γ	XMG1.2	PE-Cy7	BioLegend	505806
Mouse T Cell Intracellular Staining	IL-4	11B11	APC	BioLegend	505826
Mouse T Cell Intracellular Staining	IL-17A	TC11-18H10.1	APC	BioLegend	506915
Mouse T Cell Intracellular Staining	Granzyme B	GB11	APC	BioLegend	515405
Mouse T Cell Intracellular Staining	Granzyme B	GB11	FITC	BioLegend	515403
Mouse T Cell Intracellular Staining	Helios	22F6	APC	BioLegend	137221
Mouse T Cell Intracellular Staining	CD152 (CTLA-4)	UC10-4B9	APC	BioLegend	106309
Mouse T Cell Intracellular Staining	CD152 (CTLA-4)	UC10-4B9	PE-Cy7	BioLegend	106313
Mouse T Cell Intracellular Staining	CD304 (Nrp-1)	3E12	APC	BioLegend	145205
Human T Cell Surface Staining	CD4	SK3	PerCP	Tonbo	67-0047-T500
Human T Cell Surface Staining	CD25	BC96	APC	Tonbo	20-0259-T100
Human T Cell Surface Staining	CD127	hIL-7R-M21	PE	BD	557938
Human T Cell Surface Staining	CD25	M-A251	PE-Cy7	BD	557741
Human T Cell Intracellular Staining	FOXP3	206D	Alexa Fluor 488	BioLegend	320112
Human T Cell Intracellular Staining	CD152 (CTLA4)	L3D10	APC	BioLegend	349908
Human T Cell Intracellular Staining	IFN-γ	B27	V450	BD	560371
Human T Cell Intracellular Staining	Helios	22F6	PerCP/Cy5.5	BioLegend	137230
Human T Cell Intracellular Staining	IL-2	MQ1-17H12	Brilliant Violet 650	BioLegend	500334
Human T Cell Intracellular Staining	IL-4	MP4-25D2	APC/Cy7	BioLegend	5000834
Human T Cell Intracellular Staining	IL-10	JES3-9D7	PE	BD	554498
Human T Cell Intracellular Staining	IL-17A	BL168	Alexa Fluor 700	BioLegend	512318

5.30.3 Table 3: Western Antibodies

Western Blot Antibodies
HRP-conjugated Myc (Santa Cruz, Cat# 2040S)
HRP-conjugated HA (Santa Cruz, Cat# 14031S)
HRP-conjugated FLAG (Sigma, Cat# A8592)
anti-GAPDH (Sigma, Cat# G9545)
anti-Usp22 (Santa Cruz, Cat# sc-390585)
anti-Foxp3 (eBioscience, Cat# 11-5773-82)
anti-Usp21 (ThermoFisher, Cat# PA5-12024)
anti-USP7 (Invitrogen, Cat# MA5-15585)
anti-Actin (Sigma, Cat# A2103)
anti-Smad2 (ABCAM, Cat# ab71109)
anti-smad3 (ABCAM, Cat# ab28379)
anti-Smad4 (Santa Cruz, Cat# 38454S)
p-84 (GeneTex, Cat# GTX70220)
Vinculin (Cell Signaling, Cat# 13901T)
mono-Ub (Cell Signaling, Cat#43124S)
anti-Usp22 (Novus Biologicals, Cat# NBP1-49644)
rabbit anti-IgG (Cell Signaling, Cat# 2729)
rabbit anti-USP22 (Abcam, ab195289)

5.30.4 Table 4: Primers

Primer Name	Sequence >> 5' to 3'	Usage
USP22Chp1F	TGTATTCTTGCCACGCCCAA	Smad ChIP
USP22Chp1R	TCCTAGTGTGGGCGTTTCTG	
USP22Chp2F	ATTGCGGTACCCAACACAGT	
USP22Chp2R	GCGTCTGCGAGTTCTCTGAA	
USP22Chp3F	TTCAGAGAACTCGCAGACGC	
USP22Chp3R	GCGTGCTGAGGATTGGGTAA	
USP22Chp4F	TTACCCAATCCTCAGCACGC	
USP22Chp4R	ATTGGTGGTTTGCCGGTCTA	
USP22Chp5F	CTTAGACCGGCAAACCACCA	
USP22 Chp5R	GGCTCCAGAGAAAAGCCGAA	
USP22Chp6F	TCTTAGACCGGCAAACCACC	
USP22 Chp6R	TGTCCGCGGGAAAGGATAAC	
USP22Chp7F	TCCCACCTGTGTTGGATTGC	
USP22Chp7R	GGGCTTCCAAGACAATGACT	
USP22Chp8F	TAAGCCAAGGGCTTCCAAG	
USP22Chp8R	ACTCAGGGCATATTGTGAGGG	
USP22Chp9F	TGTCGGCAATTTTTCTCGGC	
USP22Chp9R	CCCATGATGTGGAGCAGTGA	
USP21Pro1F	TGCATCGGCTAGGAATGGTC	
USP21Pro1R	ACCAATCAGGTCACCAAGCC	
USP21Pro2F	AGGCTTGGTGACCTGATTGG	
USP21Pro2R	GCTTGTTCCGAGATTCCAC	
USP21Pro3F	AGCTCTCCTCTGTCAAGCCT	
USP21Pro3R	AACGTAGAGCAGCCTCTTGG	
USP21Pro4F	AGTGGAAGTCCCGATCTGA	
USP21Pro4R	GGCGTAGTCCTTCATTGGCT	
USP21Pro5F	AGCCAATGAAGGACTACGCC	
USP21Pro5R	CCTCCAGGGCTCTACTTGGA	
USP21Pro6F	CCTGGTAGCCTGTGGTTCTC	
USP21Pro6R	CTCCGCGTTTTGCTTGTTC	
USP21Pro7F	GGATCTCCCCACCCTTAGGT	
USP21Pro7R	GGAAGCAAGAGGGATGCAGT	
Usp7F	AAGTCTCAAGGTTATAGGGACGG	murine qPCR
Usp7R	CCATGCTTGTCTGGGTATAGTGT	
USP21F	Tgcatgaagaacctgagttga	
USP21R	acaggtccacaatcttgctgt	
USP22ex2_1F	gcttcaagtgagacaactgg	
USP22ex2_1R	acatggcagacacaggactt	Human intratumoral qPCR
hUSP22F_1	GGAAAATGCAAGGCGTTGGAG	
hUSP22R_1	GTGCAGTTCGAGGTGATCTTT	
hUSP22F_2	CTGGGACATCAGCTTGGATCT	
hUSP22R_2	CTTTCCCGTTTACCACGTTG	
hUSP21F_1	GCCACCACTTTGAGACGTAG	
hUSP21R_1	TCCGTATGCTGAACAGGGTAG	
hUSP7F	CCCTCCGTGTTTTGTGCGA	
hUSP7R	AGACCATGACGTGGAATCAGA	
h18S_F	GAG GAT GAG GTG GAA CGT GT	
h18S_R	AGA AGT GAC GCA GCC CTC TA	

References

1. BURNET, M. IMMUNOLOGICAL FACTORS IN THE PROCESS OF CARCINOGENESIS. *Brit Med Bull* **20**, 154–158 (1964).
2. Dunn, G. P., Old, L. J. & Schreiber, R. D. The Immunobiology of Cancer Immunosurveillance and Immunoediting. *Immunity* **21**, 137–148 (2004).
3. Kyburz, D. *et al.* T cell immunity after a viral infection versus T cell tolerance induced by soluble viral peptides. *Eur J Immunol* **23**, 1956–1962 (1993).
4. Bonilla, F. A. & Oettgen, H. C. Adaptive immunity. *J Allergy Clin Immun* **125**, S33–S40 (2010).
5. Mosmann, T. R., Cherwinski, H., Bond, M. W., Giedlin, M. A. & Coffman, R. L. Two types of murine helper T cell clone. I. Definition according to profiles of lymphokine activities and secreted proteins. *J Immunol Baltim Md 1950* **136**, 2348–57 (1986).
6. Steinman, L. A brief history of TH17, the first major revision in the TH1/TH2 hypothesis of T cell-mediated tissue damage. *Nat Med* **13**, 139–145 (2007).
7. Netea, M. G., Schlitzer, A., Placek, K., Joosten, L. A. B. & Schultze, J. L. Innate and Adaptive Immune Memory: an Evolutionary Continuum in the Host's Response to Pathogens. *Cell Host Microbe* **25**, 13–26 (2019).
8. Iwasaki, A. & Medzhitov, R. Control of adaptive immunity by the innate immune system. *Nat Immunol* **16**, 343–353 (2015).
9. Göschl, L., Scheinecker, C. & Bonelli, M. Treg cells in autoimmunity: from identification to Treg-based therapies. *Semin Immunopathol* **41**, 301–314 (2019).
10. Plitas, G. & Rudensky, A. Y. Regulatory T Cells: Differentiation and Function. *Cancer Immunol Res* **4**, 721–725 (2016).
11. Horwitz, D. A., Zheng, S. G. & Gray, J. D. Natural and TGF- β -induced Foxp3⁺CD4⁺CD25⁺ regulatory T cells are not mirror images of each other. *Trends Immunol* **29**, 429–435 (2008).
12. Zheng, S. G., Wang, J. H., Gray, J. D., Soucier, H. & Horwitz, D. A. Natural and Induced CD4⁺CD25⁺ Cells Educate CD4⁺CD25⁻ Cells to Develop Suppressive Activity: The Role of IL-2, TGF- β , and IL-10. *J Immunol* **172**, 5213–5221 (2004).
13. Corthay, A. How do Regulatory T Cells Work? *Scand J Immunol* **70**, 326–336 (2009).
14. Homann, D. *et al.* Autoreactive CD4⁺ T Cells Protect from Autoimmune Diabetes via Bystander Suppression Using the IL-4/Stat6 Pathway. *Immunity* **11**, 463–472 (1999).

15. Mahajan, D. *et al.* CD4+CD25+ Regulatory T Cells Protect against Injury in an Innate Murine Model of Chronic Kidney Disease. *J Am Soc Nephrol* **17**, 2731–2741 (2006).
16. Pacholczyk, R. *et al.* NonselF-Antigens Are the Cognate Specificities of Foxp3+ Regulatory T Cells. *Immunity* **27**, 493–504 (2007).
17. Tang, Q. *et al.* Visualizing regulatory T cell control of autoimmune responses in nonobese diabetic mice. *Nat Immunol* **7**, 83–92 (2006).
18. Read, S., Malmström, V. & Powrie, F. Cytotoxic T Lymphocyte–Associated Antigen 4 Plays an Essential Role in the Function of Cd25+Cd4+ Regulatory Cells That Control Intestinal Inflammation. *J Exp Medicine* **192**, 295–302 (2000).
19. Walunas, T. L. *et al.* CTLA-4 can function as a negative regulator of T cell activation. *Immunity* **1**, 405–413 (1994).
20. Vibhakar, R., Juan, G., Traganos, F., Darzynkiewicz, Z. & Finger, L. R. Activation-Induced Expression of Human Programmed Death-1 Gene in T-Lymphocytes. *Exp Cell Res* **232**, 25–28 (1997).
21. Vignali, D. A. A., Collison, L. W. & Workman, C. J. How regulatory T cells work. *Nat Rev Immunol* **8**, 523–532 (2008).
22. Sakaguchi, S., Sakaguchi, N., Asano, M., Itoh, M. & Toda, M. Immunologic self-tolerance maintained by activated T cells expressing IL-2 receptor alpha-chains (CD25). Breakdown of a single mechanism of self-tolerance causes various autoimmune diseases. *J Immunol Baltim Md 1950* **155**, 1151–64 (1995).
23. Ronchetti, S. *et al.* Frontline: GITR, a member of the TNF receptor superfamily, is costimulatory to mouse T lymphocyte subpopulations. *Eur J Immunol* **34**, 613–622 (2004).
24. Ito, T. *et al.* Two Functional Subsets of FOXP3+ Regulatory T Cells in Human Thymus and Periphery. *Immunity* **28**, 870–880 (2008).
25. Robb, R., Munck, A. & Smith, K. T cell growth factor receptors. Quantitation, specificity, and biological relevance. *J Exp Medicine* **154**, 1455–1474 (1981).
26. Fontenot, J. D., Gavin, M. A. & Rudensky, A. Y. Foxp3 programs the development and function of CD4+CD25+ regulatory T cells. *Nat Immunol* **4**, 330–336 (2003).
27. Curiel, T. J. *et al.* Specific recruitment of regulatory T cells in ovarian carcinoma fosters immune privilege and predicts reduced survival. *Nat Med* **10**, 942–949 (2004).
28. Zhou, X. *et al.* Instability of the transcription factor Foxp3 leads to the generation of pathogenic memory T cells in vivo. *Nat Immunol* **10**, 1000–1007 (2009).

29. Bacchetta, R., Barzaghi, F. & Roncarolo, M. From IPEX syndrome to FOXP3 mutation: a lesson on immune dysregulation. *Ann Ny Acad Sci* **1417**, 5–22 (2018).
30. Tanaka, A. & Sakaguchi, S. Targeting Treg cells in cancer immunotherapy. *Eur J Immunol* **49**, 1140–1146 (2019).
31. Bennett, C. L. *et al.* The immune dysregulation, polyendocrinopathy, enteropathy, X-linked syndrome (IPEX) is caused by mutations of FOXP3. *Nat Genet* **27**, 20–21 (2001).
32. Hanahan, D. & Weinberg, R. Hallmarks of Cancer: The Next Generation. *Cell* **144**, 646–674 (2011).
33. Shankaran, V. *et al.* IFN-gamma and lymphocytes prevent primary tumour development and shape tumour immunogenicity. *Nature* **410**, 1107–1111 (2001).
34. Dunn, G. P., Bruce, A. T., Ikeda, H., Old, L. J. & Schreiber, R. D. Cancer immunoediting: from immunosurveillance to tumor escape. *Nat Immunol* **3**, 991–998 (2002).
35. Angelin, A. *et al.* Foxp3 Reprograms T Cell Metabolism to Function in Low-Glucose, High-Lactate Environments. *Cell Metab* **25**, 1282–1293.e7 (2017).
36. Chang, C.-H. *et al.* Metabolic Competition in the Tumor Microenvironment Is a Driver of Cancer Progression. *Cell* **162**, 1229–1241 (2015).
37. Farkona, S., Diamandis, E. P. & Blasutig, I. M. Cancer immunotherapy: the beginning of the end of cancer? *Bmc Med* **14**, 73 (2016).
38. Mellman, I., Coukos, G. & Dranoff, G. Cancer immunotherapy comes of age. *Nature* **480**, 480–489 (2011).
39. Walsh, S. R. *et al.* Endogenous T cells prevent tumor immune escape following adoptive T cell therapy. *J Clin Invest* **129**, 5400–5410 (2019).
40. Hinrichs, C. S. & Rosenberg, S. A. Exploiting the curative potential of adoptive T-cell therapy for cancer. *Immunol Rev* **257**, 56–71 (2014).
41. Dudley, M. E. *et al.* Cancer Regression and Autoimmunity in Patients After Clonal Repopulation with Antitumor Lymphocytes. *Science* **298**, 850–854 (2002).
42. Yee, C. Adoptive T-Cell Therapy for Cancer: Boutique Therapy or Treatment Modality? *Clin Cancer Res* **19**, 4550–4552 (2013).
43. Charoentong, P. *et al.* Pan-cancer Immunogenomic Analyses Reveal Genotype-Immunophenotype Relationships and Predictors of Response to Checkpoint Blockade. *Cell Reports* **18**, 248–262 (2017).

44. Gross, G., Waks, T. & Eshhar, Z. Expression of immunoglobulin-T-cell receptor chimeric molecules as functional receptors with antibody-type specificity. *Proc National Acad Sci* **86**, 10024–10028 (1989).
45. Turtle, C. J. *et al.* CD19 CAR–T cells of defined CD4+:CD8+ composition in adult B cell ALL patients. *J Clin Invest* **126**, 2123–2138 (2016).
46. Maude, S. L. *et al.* Chimeric Antigen Receptor T Cells for Sustained Remissions in Leukemia. *New Engl J Medicine* **371**, 1507–1517 (2014).
47. Fecci, P. E. *et al.* Systemic CTLA-4 Blockade Ameliorates Glioma-Induced Changes to the CD4+ T Cell Compartment without Affecting Regulatory T-Cell Function. *Clin Cancer Res* **13**, 2158–2167 (2007).
48. Kvistborg, P. *et al.* Anti–CTLA-4 therapy broadens the melanoma-reactive CD8+ T cell response. *Sci Transl Med* **6**, 254ra128-254ra128 (2014).
49. Yang, Y. F. *et al.* Enhanced induction of antitumor T-cell responses by cytotoxic T lymphocyte-associated molecule-4 blockade: the effect is manifested only at the restricted tumor-bearing stages. *Cancer Res* **57**, 4036–41 (1997).
50. Hodi, F. S. *et al.* Improved Survival with Ipilimumab in Patients with Metastatic Melanoma. *New Engl J Medicine* **363**, 711–723 (2010).
51. Downey, S. G. *et al.* Prognostic Factors Related to Clinical Response in Patients with Metastatic Melanoma Treated by CTL-Associated Antigen-4 Blockade. *Clin Cancer Res* **13**, 6681–6688 (2007).
52. Garon, E. B. *et al.* Pembrolizumab for the Treatment of Non–Small-Cell Lung Cancer. *New Engl J Medicine* **372**, 2018–2028 (2015).
53. Hamanishi, J. *et al.* Safety and Antitumor Activity of Anti–PD-1 Antibody, Nivolumab, in Patients With Platinum-Resistant Ovarian Cancer. *J Clin Oncol* **33**, 4015–4022 (2015).
54. Robert, C. *et al.* Nivolumab in Previously Untreated Melanoma without BRAF Mutation. *New Engl J Medicine* **372**, 320–330 (2015).
55. Wang, C. *et al.* In Vitro Characterization of the Anti-PD-1 Antibody Nivolumab, BMS-936558, and In Vivo Toxicology in Non-Human Primates. *Cancer Immunol Res* **2**, 846–856 (2014).
56. Brahmer, J. R. *et al.* Phase I Study of Single-Agent Anti–Programmed Death-1 (MDX-1106) in Refractory Solid Tumors: Safety, Clinical Activity, Pharmacodynamics, and Immunologic Correlates. *J Clin Oncol* **28**, 3167–3175 (2010).

57. Brahmer, J. R. *et al.* Safety and Activity of Anti-PD-L1 Antibody in Patients with Advanced Cancer. *New Engl J Medicine* **366**, 2455–2465 (2012).
58. Robert, C. *et al.* Pembrolizumab versus Ipilimumab in Advanced Melanoma. *New Engl J Medicine* **372**, 2521–2532 (2015).
59. Curran, M. A., Montalvo, W., Yagita, H. & Allison, J. P. PD-1 and CTLA-4 combination blockade expands infiltrating T cells and reduces regulatory T and myeloid cells within B16 melanoma tumors. *Proc National Acad Sci* **107**, 4275–4280 (2010).
60. Wolchok, J. D. *et al.* Nivolumab plus Ipilimumab in Advanced Melanoma. *New Engl J Medicine* **369**, 122–133 (2013).
61. Larkin, J. *et al.* Combined Nivolumab and Ipilimumab or Monotherapy in Untreated Melanoma. *New Engl J Medicine* **373**, 23–34 (2015).
62. Gao, X. & McDermott, D. F. Ipilimumab in combination with nivolumab for the treatment of renal cell carcinoma. *Expert Opin Biol Ther* **18**, 947–957 (2018).
63. Tanaka, A. & Sakaguchi, S. Regulatory T cells in cancer immunotherapy. *Cell Res* **27**, 109–118 (2017).
64. Bates, G. J. *et al.* Quantification of Regulatory T Cells Enables the Identification of High-Risk Breast Cancer Patients and Those at Risk of Late Relapse. *J Clin Oncol* **24**, 5373–5380 (2006).
65. Shang, B., Liu, Y., Jiang, S. & Liu, Y. Prognostic value of tumor-infiltrating FoxP3+ regulatory T cells in cancers: a systematic review and meta-analysis. *Sci Rep-uk* **5**, 15179 (2015).
66. Xu, L., Xu, W., Qiu, S. & Xiong, S. Enrichment of CCR6+Foxp3+ regulatory T cells in the tumor mass correlates with impaired CD8+ T cell function and poor prognosis of breast cancer. *Clin Immunol* **135**, 466–475 (2010).
67. Li, Y.-Q. *et al.* Tumor Secretion of CCL22 Activates Intratumoral Treg Infiltration and Is Independent Prognostic Predictor of Breast Cancer. *Plos One* **8**, e76379 (2013).
68. Wolf, D. *et al.* The Expression of the Regulatory T Cell-Specific Forkhead Box Transcription Factor FoxP3 Is Associated with Poor Prognosis in Ovarian Cancer. *Clin Cancer Res* **11**, 8326–8331 (2005).
69. Deng, G. Tumor-infiltrating regulatory T cells: origins and features. *Am J Clin Exp Immunol* **7**, 81–87 (2018).
70. Attia, P., Maker, A. V., Haworth, L. R., Rogers-Freezer, L. & Rosenberg, S. A. Inability of a Fusion Protein of IL-2 and Diphtheria Toxin (Denileukin Diftitox, DAB389IL-2, ONTAK) to

- Eliminate Regulatory T Lymphocytes in Patients With Melanoma. *J Immunother* **28**, 582–592 (2005).
71. Nishikawa, H. & Sakaguchi, S. Regulatory T cells in tumor immunity. *Int J Cancer* **127**, 759–767 (2010).
72. Plitas, G. *et al.* Regulatory T Cells Exhibit Distinct Features in Human Breast Cancer. *Immunity* **45**, 1122–1134 (2016).
73. Mao, F. *et al.* Increased tumor-infiltrating CD45RA–CCR7– regulatory T-cell subset with immunosuppressive properties foster gastric cancer progress. *Cell Death Dis* **8**, e3002–e3002 (2017).
74. Paluskievicz, C. M. *et al.* T Regulatory Cells and Priming the Suppressive Tumor Microenvironment. *Front Immunol* **10**, 2453 (2019).
75. Crane, C. A., Ahn, B. J., Han, S. J. & Parsa, A. T. Soluble factors secreted by glioblastoma cell lines facilitate recruitment, survival, and expansion of regulatory T cells: implications for immunotherapy. *Neuro-oncology* **14**, 584–595 (2012).
76. Mizukami, Y. *et al.* CCL17 and CCL22 chemokines within tumor microenvironment are related to accumulation of Foxp3+ regulatory T cells in gastric cancer. *Int J Cancer* **122**, 2286–2293 (2008).
77. Maruyama, T. *et al.* CCL17 and CCL22 chemokines within tumor microenvironment are related to infiltration of regulatory T cells in esophageal squamous cell carcinoma. *Dis Esophagus* **23**, 422–429 (2010).
78. Qin, X.-J. *et al.* CCL22 Recruits CD4-positive CD25-positive Regulatory T Cells into Malignant Pleural Effusion. *Clin Cancer Res* **15**, 2231–2237 (2009).
79. Molinaro, R. *et al.* CCR4 Controls the Suppressive Effects of Regulatory T Cells on Early and Late Events during Severe Sepsis. *Plos One* **10**, e0133227 (2015).
80. Tan, M. C. B. *et al.* Disruption of CCR5-Dependent Homing of Regulatory T Cells Inhibits Tumor Growth in a Murine Model of Pancreatic Cancer. *J Immunol* **182**, 1746–1755 (2009).
81. Velasco-Velázquez, M., Xolalpa, W. & Pestell, R. G. The potential to target CCL5/CCR5 in breast cancer. *Expert Opin Ther Tar* **18**, 1265–1275 (2014).
82. Chang, L.-Y. *et al.* Tumor-Derived Chemokine CCL5 Enhances TGF- β -Mediated Killing of CD8+ T Cells in Colon Cancer by T-Regulatory Cells. *Cancer Res* **72**, 1092–1102 (2012).
83. Susek, K. H., Karvouni, M., Alici, E. & Lundqvist, A. The Role of CXC Chemokine Receptors 1–4 on Immune Cells in the Tumor Microenvironment. *Front Immunol* **9**, 2159 (2018).

84. Jordan, J. T. *et al.* Preferential migration of regulatory T cells mediated by glioma-secreted chemokines can be blocked with chemotherapy. *Cancer Immunol Immunother* **57**, 123–131 (2007).
85. Reynders, N. *et al.* The Distinct Roles of CXCR3 Variants and Their Ligands in the Tumor Microenvironment. *Cells* **8**, 613 (2019).
86. Priceman, S. J. *et al.* S1PR1 Is Crucial for Accumulation of Regulatory T Cells in Tumors via STAT3. *Cell Reports* **6**, 992–999 (2014).
87. Schlecker, E. *et al.* Tumor-Infiltrating Monocytic Myeloid-Derived Suppressor Cells Mediate CCR5-Dependent Recruitment of Regulatory T Cells Favoring Tumor Growth. *J Immunol* **189**, 5602–5611 (2012).
88. Han, Y. *et al.* Malignant B Cells Induce the Conversion of CD4⁺CD25⁻ T Cells to Regulatory T Cells in B-Cell Non-Hodgkin Lymphoma. *Plos One* **6**, e28649 (2011).
89. Ai, W. Z. *et al.* Follicular lymphoma B cells induce the conversion of conventional CD4⁺ T cells to T-regulatory cells. *Int J Cancer* **124**, 239–244 (2009).
90. Curti, A. *et al.* Modulation of tryptophan catabolism by human leukemic cells results in the conversion of CD25⁻ into CD25⁺ T regulatory cells. *Blood* **109**, 2871–2877 (2006).
91. Zheng, S. G. *et al.* TGF- β Requires CTLA-4 Early after T Cell Activation to Induce FoxP3 and Generate Adaptive CD4⁺CD25⁺ Regulatory Cells. *J Immunol* **176**, 3321–3329 (2006).
92. Downs-Canner, S. *et al.* Suppressive IL-17A⁺Foxp3⁺ and ex-Th17 IL-17AnegFoxp3⁺ Treg cells are a source of tumour-associated Treg cells. *Nat Commun* **8**, 14649 (2017).
93. Fu, S. *et al.* TGF-beta Induces Foxp3 + T-Regulatory Cells from CD4 + CD25 - Precursors. *Am J Transplant* **4**, 1614–1627 (2004).
94. Hsu, P. *et al.* IL-10 Potentiates Differentiation of Human Induced Regulatory T Cells via STAT3 and Foxo1. *J Immunol* **195**, 3665–3674 (2015).
95. Sato, T. *et al.* Interleukin 10 in the tumor microenvironment: a target for anticancer immunotherapy. *Immunol Res* **51**, 170–182 (2011).
96. Neel, J.-C., Humbert, L. & Lebrun, J.-J. The Dual Role of TGF β in Human Cancer: From Tumor Suppression to Cancer Metastasis. *Isrn Mol Biology* **2012**, 1–28 (2012).
97. Schaer, D. A. *et al.* GITR Pathway Activation Abrogates Tumor Immune Suppression through Loss of Regulatory T-cell Lineage Stability. *Cancer Immunol Res* **1**, 320–331 (2013).
98. Overacre-Delgoffe, A. E. *et al.* Interferon- γ Drives Treg Fragility to Promote Anti-tumor Immunity. *Cell* **169**, 1130-1141.e11 (2017).

99. Nakagawa, H. *et al.* Instability of Helios-deficient Tregs is associated with conversion to a T-effector phenotype and enhanced antitumor immunity. *Proc National Acad Sci* **113**, 6248–6253 (2016).
100. De Simone, M. *et al.* Transcriptional Landscape of Human Tissue Lymphocytes Unveils Uniqueness of Tumor-Infiltrating T Regulatory Cells. *Immunity* **45**, 1135–1147 (2016).
101. Scharping, N. E. *et al.* The Tumor Microenvironment Represses T Cell Mitochondrial Biogenesis to Drive Intratumoral T Cell Metabolic Insufficiency and Dysfunction. *Immunity* **45**, 374–388 (2016).
102. De Simone, M. *et al.* Transcriptional Landscape of Human Tissue Lymphocytes Unveils Uniqueness of Tumor-Infiltrating T Regulatory Cells. *Immunity* **45**, 1135–1147 (2016).
103. Chouaib, S., Noman, M. Z., Kosmatopoulos, K. & Curran, M. A. Hypoxic stress: obstacles and opportunities for innovative immunotherapy of cancer. *Oncogene* **36**, 439–445 (2017).
104. Kahlert, U. D. *et al.* Resistance to Hypoxia-Induced, BNIP3-Mediated Cell Death Contributes to an Increase in a CD133-Positive Cell Population in Human Glioblastomas In Vitro. *J Neuropathology Exp Neurology* **71**, 1086–1099 (2012).
105. Li, J. *et al.* Cbx4 Governs HIF-1 α to Potentiate Angiogenesis of Hepatocellular Carcinoma by Its SUMO E3 Ligase Activity. *Cancer Cell* **25**, 118–131 (2014).
106. Semenza, G. L. Targeting HIF-1 for cancer therapy. *Nat Rev Cancer* **3**, 721–732 (2003).
107. Bertout, J. A., Patel, S. A. & Simon, M. C. The impact of O₂ availability on human cancer. *Nat Rev Cancer* **8**, 967–975 (2008).
108. Clever, D. *et al.* Oxygen Sensing by T Cells Establishes an Immunologically Tolerant Metastatic Niche. *Cell* **166**, 1117–1131.e14 (2016).
109. Jaakkola, P. *et al.* Targeting of HIF- α to the von Hippel-Lindau Ubiquitylation Complex by O₂-Regulated Prolyl Hydroxylation. *Science* **292**, 468–472 (2001).
110. Scholz, C. C. & Taylor, C. T. Targeting the HIF pathway in inflammation and immunity. *Curr Opin Pharmacol* **13**, 646–653 (2013).
111. Keith, B., Johnson, R. S. & Simon, M. C. HIF1 α and HIF2 α : sibling rivalry in hypoxic tumour growth and progression. *Nat Rev Cancer* **12**, 9–22 (2012).
112. Michiels, C. Physiological and Pathological Responses to Hypoxia. *Am J Pathology* **164**, 1875–1882 (2004).
113. Kumar, V. & Gabrilovich, D. I. Hypoxia-inducible factors in regulation of immune responses in tumour microenvironment. *Immunology* **143**, 512–519 (2014).

114. Shi, L. Z. *et al.* HIF1 α -dependent glycolytic pathway orchestrates a metabolic checkpoint for the differentiation of TH17 and Treg cells. A metabolic checkpoint in T cell differentiation. *J Exp Medicine* **208**, 1367–1376 (2011).
115. Westendorf, A. M. *et al.* Hypoxia Enhances Immunosuppression by Inhibiting CD4+ Effector T Cell Function and Promoting Treg Activity. *Cell Physiol Biochem* **41**, 1271–1284 (2017).
116. Clambey, E. T. *et al.* Hypoxia-inducible factor-1 α -dependent induction of FoxP3 drives regulatory T-cell abundance and function during inflammatory hypoxia of the mucosa. *Proc National Acad Sci* **109**, E2784–E2793 (2012).
117. Guan, S.-Y. *et al.* Hypoxia-inducible factor-1 α : a promising therapeutic target for autoimmune diseases. *Expert Opinion on Therapeutic Targets* **21**, 715–723 (2017).
118. Ivashkiv, L. B. The hypoxia–lactate axis tempers inflammation. *Nat Rev Immunol* 1–2 (2019) doi:10.1038/s41577-019-0259-8.
119. Facciabene, A. *et al.* Tumour hypoxia promotes tolerance and angiogenesis via CCL28 and Treg cells. *Nature* **475**, 226–230 (2011).
120. Neumann, A. K. *et al.* Hypoxia inducible factor 1 regulates T cell receptor signal transduction. *Proc National Acad Sci* **102**, 17071–17076 (2005).
121. Dang, E. V. *et al.* Control of TH17/Treg Balance by Hypoxia-Inducible Factor 1. *Cell* **146**, 772–784 (2011).
122. Hsiao, H.-W. *et al.* Deltex1 antagonizes HIF-1 α and sustains the stability of regulatory T cells in vivo. *Nat Commun* **6**, 6353 (2015).
123. Fallarino, F. *et al.* T cell apoptosis by tryptophan catabolism. *Cell Death Differ* **9**, 1069–1077 (2002).
124. Ho, P.-C. *et al.* Phosphoenolpyruvate Is a Metabolic Checkpoint of Anti-tumor T Cell Responses. *Cell* **162**, 1217–1228 (2015).
125. Michalek, R. D. *et al.* Cutting Edge: Distinct Glycolytic and Lipid Oxidative Metabolic Programs Are Essential for Effector and Regulatory CD4+ T Cell Subsets. *J Immunol* **186**, 3299–3303 (2011).
126. Weinberg, S. E. *et al.* Mitochondrial complex III is essential for suppressive function of regulatory T cells. *Nature* **565**, 495–499 (2019).
127. Wu, H. *et al.* Intratumoral regulatory T cells with higher prevalence and more suppressive activity in hepatocellular carcinoma patients. *J Gastroen Hepatol* **28**, 1555–1564 (2013).

128. Nakaya, M. *et al.* Inflammatory T Cell Responses Rely on Amino Acid Transporter ASCT2 Facilitation of Glutamine Uptake and mTORC1 Kinase Activation. *Immunity* **40**, 692–705 (2014).
129. Cobbold, S. P. *et al.* Infectious tolerance via the consumption of essential amino acids and mTOR signaling. *Proc National Acad Sci* **106**, 12055–12060 (2009).
130. Cluxton, D., Petrasca, A., Moran, B. & Fletcher, J. M. Differential Regulation of Human Treg and Th17 Cells by Fatty Acid Synthesis and Glycolysis. *Front Immunol* **10**, 115 (2019).
131. Long, Y. *et al.* Dysregulation of Glutamate Transport Enhances Treg Function That Promotes VEGF Blockade Resistance in Glioblastoma. *Cancer Res* **80**, 499–509 (2020).
132. Warburg, O., Wind, F. & Negelein, E. THE METABOLISM OF TUMORS IN THE BODY. *J Gen Physiology* **8**, 519–530 (1927).
133. Fischer, K. *et al.* Inhibitory effect of tumor cell–derived lactic acid on human T cells. *Blood* **109**, 3812–3819 (2007).
134. O’Neill, L. A. J. & Hardie, D. G. Metabolism of inflammation limited by AMPK and pseudo-starvation. *Nature* **493**, 346–355 (2013).
135. Gualdoni, G. A. *et al.* The AMP analog AICAR modulates the Treg/Th17 axis through enhancement of fatty acid oxidation. *Faseb J* **30**, 3800–3809 (2016).
136. Zheng, Y. *et al.* A Role for Mammalian Target of Rapamycin in Regulating T Cell Activation versus Anergy. *J Immunol* **178**, 2163–2170 (2007).
137. Delgoffe, G. M. *et al.* The mTOR Kinase Differentially Regulates Effector and Regulatory T Cell Lineage Commitment. *Immunity* **30**, 832–844 (2009).
138. Pavlova, N. N. & Thompson, C. B. The Emerging Hallmarks of Cancer Metabolism. *Cell Metab* **23**, 27–47 (2016).
139. Bohn, T. *et al.* Tumor immunoevasion via acidosis-dependent induction of regulatory tumor-associated macrophages. *Nat Immunol* **19**, 1319–1329 (2018).
140. Wellenstein, M. D. & Visser, K. E. de. Cancer-Cell-Intrinsic Mechanisms Shaping the Tumor Immune Landscape. *Immunity* **48**, 399–416 (2018).
141. Davies, M. *et al.* Overexpression of autocrine TGF- β 1 suppresses the growth of spindle epithelial cells in vitro and in vivo in the rat 4NQO model of oral carcinogenesis. *Int J Cancer* **73**, 68–74 (1997).

142. Kim, I. Y. *et al.* Loss of expression of transforming growth factor-beta receptors is associated with poor prognosis in prostate cancer patients. *Clin Cancer Res Official J Am Assoc Cancer Res* **4**, 1625–30 (1998).
143. Yang, Z. *et al.* Notch1 signaling in melanoma cells promoted tumor-induced immunosuppression via upregulation of TGF- β 1. *J Exp Clin Canc Res* **37**, 1 (2018).
144. Visser, K. de & Kast, W. Effects of TGF- β on the immune system: implications for cancer immunotherapy. *Leukemia* **13**, 1188–1199 (1999).
145. Nickerson, N. K., Mill, C. P., Wu, H.-J., Riese, D. J. & Foley, J. Autocrine-Derived Epidermal Growth Factor Receptor Ligands Contribute to Recruitment of Tumor-Associated Macrophage and Growth of Basal Breast Cancer Cells In Vivo. *Oncol Res Featur Preclin Clin Cancer Ther* **20**, 303–317 (2013).
146. Lohr, J. *et al.* Effector T-Cell Infiltration Positively Impacts Survival of Glioblastoma Patients and Is Impaired by Tumor-Derived TGF- β . *Clin Cancer Res* **17**, 4296–4308 (2011).
147. Wallace, A. *et al.* Transforming Growth Factor- β Receptor Blockade Augments the Effectiveness of Adoptive T-Cell Therapy of Established Solid Cancers. *Clin Cancer Res* **14**, 3966–3974 (2008).
148. Budhu, S. *et al.* Blockade of surface-bound TGF- β on regulatory T cells abrogates suppression of effector T cell function in the tumor microenvironment. *Sci Signal* **10**, eaak9702 (2017).
149. Chen, M.-L. *et al.* Regulatory T cells suppress tumor-specific CD8 T cell cytotoxicity through TGF- β signals in vivo. *P Natl Acad Sci Usa* **102**, 419–424 (2005).
150. Shen, E., Zhao, K., Wu, C. & Yang, B. The suppressive effect of CD25+Treg cells on Th1 differentiation requires cell—cell contact partially via TGF- β production. *Cell Biol Int* **35**, 705–712 (2011).
151. Ciechanover, A., Elias, S., Heller, H. & Hershko, A. “Covalent affinity” purification of ubiquitin-activating enzyme. *J Biological Chem* **257**, 2537–42 (1982).
152. Ciechanover, A., Hod, Y. & Hershko, A. A heat-stable polypeptide component of an ATP-dependent proteolytic system from reticulocytes. *Biochem Bioph Res Co* **81**, 1100–1105 (1978).
153. Kirisako, T. *et al.* A ubiquitin ligase complex assembles linear polyubiquitin chains. *Embo J* **25**, 4877–4887 (2006).
154. Xu, P. *et al.* Quantitative Proteomics Reveals the Function of Unconventional Ubiquitin Chains in Proteasomal Degradation. *Cell* **137**, 133–145 (2009).

155. Johnson, E. S., Ma, P. C. M., Ota, I. M. & Varshavsky, A. A Proteolytic Pathway That Recognizes Ubiquitin as a Degradation Signal. *J Biol Chem* **270**, 17442–17456 (1995).
156. Peng, J. *et al.* A proteomics approach to understanding protein ubiquitination. *Nat Biotechnol* **21**, 921–926 (2003).
157. van Loosdregt, J. *et al.* Stabilization of the Transcription Factor Foxp3 by the Deubiquitinase USP7 Increases Treg-Cell-Suppressive Capacity. *Immunity* **39**, 259–271 (2013).
158. Kim, H. T. *et al.* Certain Pairs of Ubiquitin-conjugating Enzymes (E2s) and Ubiquitin-Protein Ligases (E3s) Synthesize Nondegradable Forked Ubiquitin Chains Containing All Possible Isopeptide Linkages. *J Biol Chem* **282**, 17375–17386 (2007).
159. Tenno, T. *et al.* Structural basis for distinct roles of Lys63- and Lys48-linked polyubiquitin chains. *Genes Cells* **9**, 865–875 (2004).
160. Hanna, J., Leggett, D. S. & Finley, D. Ubiquitin Depletion as a Key Mediator of Toxicity by Translational Inhibitors. *Mol Cell Biol* **23**, 9251–9261 (2003).
161. Wilkinson, K. D. Regulation of ubiquitin-dependent processes by deubiquitinating enzymes. *Faseb J* **11**, 1245–1256 (1997).
162. Suresh, B., Lee, J., Kim, H. & Ramakrishna, S. Regulation of pluripotency and differentiation by deubiquitinating enzymes. *Cell Death Differ* **23**, 1257–1264 (2016).
163. Fraile, J. M., Quesada, V., Rodríguez, D., Freije, J. M. P. & López-Otín, C. Deubiquitinases in cancer: new functions and therapeutic options. *Oncogene* **31**, 2373–88 (2011).
164. Loosdregt, J. van *et al.* Regulation of Treg functionality by acetylation-mediated Foxp3 protein stabilization. *Blood* **115**, 965–74 (2009).
165. Loosdregt, J. van *et al.* Rapid Temporal Control of Foxp3 Protein Degradation by Sirtuin-1. *Plos One* **6**, e19047 (2011).
166. Cortez, J. T. *et al.* CRISPR screen in regulatory T cells reveals modulators of Foxp3. *Nature* **582**, 416–420 (2020).
167. Li, Y. *et al.* USP21 prevents the generation of T-helper-1-like Treg cells. *Nat Commun* **7**, 13559 (2016).
168. Wang, L. *et al.* Ubiquitin-specific Protease-7 Inhibition Impairs Tip60-dependent Foxp3+ T-regulatory Cell Function and Promotes Antitumor Immunity. *Ebiomedicine* **13**, 99–112 (2016).

169. Zhang, X.-Y. *et al.* The putative cancer stem cell marker USP22 is a subunit of the human SAGA complex required for activated transcription and cell-cycle progression. *Mol Cell* **29**, 102–11 (2008).
170. Glinsky, G. V., Berezovska, O. & Glinskii, A. B. Microarray analysis identifies a death-from-cancer signature predicting therapy failure in patients with multiple types of cancer. *J Clin Invest* **115**, 1503–1521 (2005).
171. Lin, Z. *et al.* USP22 Antagonizes p53 Transcriptional Activation by Deubiquitinating Sirt1 to Suppress Cell Apoptosis and Is Required for Mouse Embryonic Development. *Mol Cell* **46**, 484–494 (2012).
172. Li, L. *et al.* SIRT1 activation by a c-MYC oncogenic network promotes the maintenance and drug resistance of human FLT3-ITD acute myeloid leukemia stem cells. *Cell Stem Cell* **15**, 431–46 (2014).
173. Lin, Z. *et al.* Ubiquitin-specific protease 22 is a deubiquitinase of CCNB1. *Cell Discov* **1**, 15028 (2015).
174. Gong, L., Kamitani, T., Millas, S. & Yeh, E. T. H. Identification of a Novel Isopeptidase with Dual Specificity for Ubiquitin- and NEDD8-conjugated Proteins. *J Biol Chem* **275**, 14212–14216 (2000).
175. Zhang, J. *et al.* Identification of the E3 Deubiquitinase Ubiquitin-specific Peptidase 21 (USP21) as a Positive Regulator of the Transcription Factor GATA3. *J Biol Chem* **288**, 9373–9382 (2013).
176. Wang, Y., Su, M. A. & Wan, Y. Y. An essential role of the transcription factor GATA-3 for the function of regulatory T cells. *Immunity* **35**, 337–48 (2011).
177. Wohlfert, E. A. *et al.* GATA3 controls Foxp3⁺ regulatory T cell fate during inflammation in mice. *J Clin Invest* **121**, 4503–4515 (2011).
178. Chauhan, D. *et al.* A Small Molecule Inhibitor of Ubiquitin-Specific Protease-7 Induces Apoptosis in Multiple Myeloma Cells and Overcomes Bortezomib Resistance. *Cancer Cell* **22**, 345–358 (2012).
179. Zugazagoitia, J. *et al.* Current Challenges in Cancer Treatment. *Clin Ther* **38**, 1551–1566 (2016).
180. Perez, S. A. *et al.* CD4⁺CD25⁺ Regulatory T-Cell Frequency in HER-2/neu (HER)-Positive and HER-Negative Advanced-Stage Breast Cancer Patients. *Clin Cancer Res* **13**, 2714–2721 (2007).
181. Najafi, M., Farhood, B. & Mortezaee, K. Contribution of regulatory T cells to cancer: A review. *J Cell Physiol* **234**, 7983–7993 (2019).

182. Marabelle, A. *et al.* Depleting tumor-specific Tregs at a single site eradicates disseminated tumors. *J Clin Invest* **123**, 2447–2463 (2013).
183. Rech, A. J. *et al.* CD25 Blockade Depletes and Selectively Reprograms Regulatory T Cells in Concert with Immunotherapy in Cancer Patients. *Sci Transl Med* **4**, 134ra62-134ra62 (2012).
184. Vazquez-Lombardi, R. *et al.* Potent antitumour activity of interleukin-2-Fc fusion proteins requires Fc-mediated depletion of regulatory T-cells. *Nat Commun* **8**, 15373 (2017).
185. Maruyama, T., Konkol, J. E., Zamarron, B. F. & Chen, W. The molecular mechanisms of Foxp3 gene regulation. *Semin Immunol* **23**, 418–423 (2011).
186. Kitoh, A. *et al.* Indispensable Role of the Runx1-Cbfb Transcription Complex for In Vivo-Suppressive Function of FoxP3+ Regulatory T Cells. *Immunity* **31**, 609–620 (2009).
187. Yao, Z. *et al.* Nonredundant roles for Stat5a/b in directly regulating Foxp3. *Blood* **109**, 4368–4375 (2007).
188. Beyer, M. *et al.* Repression of the genome organizer SATB1 in regulatory T cells is required for suppressive function and inhibition of effector differentiation. *Nat Immunol* **12**, 898–907 (2011).
189. Schumann, K. *et al.* Generation of knock-in primary human T cells using Cas9 ribonucleoproteins. *Proc National Acad Sci* **112**, 10437–10442 (2015).
190. Li, X., Liang, Y., LeBlanc, M., Benner, C. & Zheng, Y. Function of a Foxp3 cis-Element in Protecting Regulatory T Cell Identity. *Cell* **158**, 734–748 (2014).
191. Zheng, Y. *et al.* Role of conserved non-coding DNA elements in the Foxp3 gene in regulatory T-cell fate. *Nature* **463**, 808–812 (2010).
192. DuPage, M. *et al.* The Chromatin-Modifying Enzyme Ezh2 Is Critical for the Maintenance of Regulatory T Cell Identity after Activation. *Immunity* **42**, 227–238 (2015).
193. Zhang, Y. *et al.* Cimetidine down-regulates stability of Foxp3 protein via Stub1 in Treg cells. *Hum Vacc Immunother* **12**, 00–00 (2016).
194. Loosdregt, J. van & Coffey, P. J. Post-translational modification networks regulating FOXP3 function. *Trends Immunol* **35**, 368–378 (2014).
195. Montauti, E. & Fang, D. Regulation of Treg Functions by the Ubiquitin Pathway. *Adv Exp Med Biol* **1278**, 47–62 (2020).
196. Melo-Cardenas, J., Zhang, Y., Zhang, D. D. & Fang, D. Ubiquitin-specific peptidase 22 functions and its involvement in disease. *Oncotarget* **7**, 44848–44856 (2016).

197. Wu, Y., Guo, B. & Ghosh, G. Differential Effects of Tumor Secreted Factors on Mechanosensitivity, Capillary Branching, and Drug Responsiveness in PEG Hydrogels. *Ann Biomed Eng* **43**, 2279–2290 (2015).
198. Beckermann, K. E., Dudzinski, S. O. & Rathmell, J. C. Dysfunctional T cell metabolism in the tumor microenvironment. *Cytokine Growth F R* **35**, 7–14 (2017).
199. Busk, M. *et al.* Inhibition of tumor lactate oxidation: Consequences for the tumor microenvironment. *Radiother Oncol* **99**, 404–411 (2011).
200. Wang, X. *et al.* Cancer-FOXP3 directly activated CCL5 to recruit FOXP3+Treg cells in pancreatic ductal adenocarcinoma. *Oncogene* **36**, 3048–3058 (2017).
201. Barbi, J., Pardoll, D. M. & Pan, F. Ubiquitin-dependent regulation of Foxp3 and Treg function. *Immunol Rev* **266**, 27–45 (2015).
202. Takimoto, T. *et al.* Smad2 and Smad3 Are Redundantly Essential for the TGF- β -Mediated Regulation of Regulatory T Plasticity and Th1 Development. *J Immunol* **185**, 842–855 (2010).
203. Lu, L. *et al.* Synergistic effect of TGF- β superfamily members on the induction of Foxp3+Treg. *Eur J Immunol* **40**, 142–152 (2010).
204. Dennler, S., Huet, S. & Gauthier, J.-M. A short amino-acid sequence in MH1 domain is responsible for functional differences between Smad2 and Smad3. *Oncogene* **18**, 1643–1648 (1999).
205. Kim, T. H. *et al.* G α 12 ablation exacerbates liver steatosis and obesity by suppressing USP22/SIRT1-regulated mitochondrial respiration. *J Clin Invest* **128**, 5587–5602 (2018).
206. Köhler, A., Zimmerman, E., Schneider, M., Hurt, E. & Zheng, N. Structural Basis for Assembly and Activation of the Heterotetrameric SAGA Histone H2B Deubiquitinase Module. *Cell* **141**, 606–617 (2010).
207. Morgan, M. T. *et al.* Structural basis for histone H2B deubiquitination by the SAGA DUB module. *Science* **351**, 725–728 (2016).
208. Oh, D. Y. *et al.* Intratumoral CD4+ T Cells Mediate Anti-tumor Cytotoxicity in Human Bladder Cancer. *Cell* **181**, 1612–1625.e13 (2020).
209. He, Y. *et al.* Ubiquitin-specific peptidase 22 overexpression may promote cancer progression and poor prognosis in human gastric carcinoma. *Transl Res* **165**, 407–416 (2015).
210. Liu, Y.-L. *et al.* USP22 Acts as an Oncogene by the Activation of BMI-1-Mediated INK4a/ARF Pathway and Akt Pathway. *Cell Biochem Biophys* **62**, 229–235 (2012).

211. Lv, L. *et al.* Silencing USP22 by asymmetric structure of interfering RNA inhibits proliferation and induces cell cycle arrest in bladder cancer cells. *Mol Cell Biochem* **346**, 11–21 (2011).
212. Akimova, T. *et al.* Human lung tumor FOXP⁺ Tregs upregulate four “Treg-locking” transcription factors. *Jci Insight* **2**, e94075 (2017).
213. Wang, H. *et al.* CD36-mediated metabolic adaptation supports regulatory T cell survival and function in tumors. *Nat Immunol* **21**, 298–308 (2020).
214. Engel, M. E., McDonnell, M. A., Law, B. K. & Moses, H. L. Interdependent SMAD and JNK Signaling in Transforming Growth Factor- β -mediated Transcription. *J Biol Chem* **274**, 37413–37420 (1999).
215. Lee, J. H., Elly, C., Park, Y. & Liu, Y.-C. E3 Ubiquitin Ligase VHL Regulates Hypoxia-Inducible Factor-1 α to Maintain Regulatory T Cell Stability and Suppressive Capacity. *Immunity* **42**, 1062–1074 (2015).
216. Xiong, J. *et al.* Cloning and Characterization of the Human USP22 Gene Promoter. *Plos One* **7**, e52716 (2012).
217. Ravi, V. *et al.* SIRT6 transcriptionally regulates global protein synthesis through transcription factor Sp1 independent of its deacetylase activity. *Nucleic Acids Res* **47**, 9115–9131 (2019).
218. Dimova, D. K. & Dyson, N. J. The E2F transcriptional network: old acquaintances with new faces. *Oncogene* **24**, 2810–2826 (2005).
219. Li, W., Cui, K., Prochownik, E. V. & Li, Y. The deubiquitinase USP21 stabilizes MEK2 to promote tumor growth. *Cell Death Dis* **9**, 482 (2018).
220. Arceci, A. *et al.* FOXM1 Deubiquitination by USP21 Regulates Cell Cycle Progression and Paclitaxel Sensitivity in Basal-like Breast Cancer. *Cell Reports* **26**, 3076-3086.e6 (2019).
221. LIANG, J.-X. *et al.* Ubiquitin-specific protease 22-induced autophagy is correlated with poor prognosis of pancreatic cancer. *Oncol Rep* **32**, 2726–2734 (2014).
222. Hou, P. *et al.* USP21 deubiquitinase promotes pancreas cancer cell stemness via Wnt pathway activation. *Gene Dev* **33**, 1361–1366 (2019).
223. Peng, L. *et al.* Ubiquitin specific protease 21 upregulation in breast cancer promotes cell tumorigenic capability and is associated with the NOD-like receptor signaling pathway. *Oncol Lett* **12**, 4531–4537 (2016).